Evolutionary divergence of drug-binding sites in ribosomes

Chinenye Loveth, Ekemezie

A thesis submitted in partial fulfilment of the requirements for the degree of

Doctor of Philosophy

Newcastle University

Biosciences institute

Faculty of Medical Sciences

March 2025

Declaration

The work presented in this thesis is the work of the author and has not been submitted in whole or part for another degree.

Collaboration contribution declaration:

Lewis I. Chan – Evolution of drug-binding residues in eukaryotic ribosomes

The computation part of this thesis is part of two manuscripts currently under review in Cell reports.

Abstract

Ribosome-targeting drugs are widely used in medicine, research, and agriculture. However, most of our knowledge about how these drugs work comes from studying a few model organisms—such as *Escherichia coli* and *Thermus thermophilus* (for bacteria), and yeast and humans (for eukaryotes). As a result, it is often assumed that drug-binding sites are the same across all organisms. However, emerging evidence suggests otherwise. We aimed to understand how drug-binding sites in ribosomes vary across different organisms and how many organisms in nature bear rRNA substitutions in the drug-binding sites of their ribosomes. To answer this, we developed a novel approach to address issues such as data bias, sequencing errors, pseudogenes, and chimeric sequences. Using this method, we systematically analysed drug-binding sites in eukaryotic ribosomes and identified lineages bearing rRNA substitutions in the drug-binding sites of their ribosomes compared to humans and yeast. We then extended our analysis to bacterial species, comparing the conservation of the drug-binding sites of their ribosomes to that of the common model bacterium *E. coli*. Our findings suggest that the diversification of ribosomal drug-binding sites in bacteria began long before separation of the some of the earliest bacterial phyla, indicating that these variations are ancient. By using *Streptomyces* ribosomes—which have a modified drug-binding site—as a model, we explored how natural rRNA substitutions affect the orthosomycin family of drugs. Our analysis showed that while some substitutions may change how drug binds to the ribosome, others have little or no effect. Overall, this study offers a detailed understanding of how rRNA changes in the drug-binding site influence drug interactions. This knowledge can guide the precise use of these drugs and support the development of drugs targeting specific organisms.

Dedication

This work is dedicated to my dear mother, Mrs Esther Ekemezie, whom I fondly call '*nne di ora mma*.'

Acknowledgement

Words are not enough to express my gratitude to my mentor and PhD supervisor, Dr Sergey Melnikov, for his unwavering guidance and support throughout my PhD. You provided me with a platform that allowed me to grow both academically and personally, nurturing my skills and giving me the confidence to tackle complex challenges. My time in the Melnikov lab was very transformative—a period of immense learning, discovery, and development. Beyond scientific training, you taught me the importance of personal development, maintaining high-quality standards, setting clear goals, and adopting a proactive approach in both research and life. Your mentorship extended beyond the lab, inspiring me to pursue excellence and continuously seek new learning opportunities. For all the lessons, encouragement, and countless moments of support, I am deeply thankful. The experiences and wisdom I have gained under your guidance will remain invaluable as I move forward in my career.

I am deeply thankful to my academic panel, Prof Health Murray, Dr Katarzyna Mickiewicz and Prof Waldemar Vollmer, for their constructive feedback, encouragement and valuable insights that enriched my work.

I would like to extend a heartfelt thank you to the entire Melnikov lab team both past and present (Lewis I. Chan, Charlotte R. Brown, Karla Helena-Bueno, Charlotte Dingwell, and Jess Clark), for their support, which was essential to the successful completion of my PhD. A special thank you to Lewis Chan (the great)—you are an amazing collaborator and made analysing over half a million sequence data both easy and fun. Charlotte Brown, I am grateful for your support during the early stages when I was still learning the basics of python scripting. Dr Tonnie, thank you for your contribution—those three python tutorials you taught me helped me advance beyond the beginner's level. Thank you, Karla, for always sharing your thoughts on cryo-EM data processing. To everyone else, I deeply appreciate your invaluable supports.

I will not fail to recognize the impact of Dr Chris Hill of the University of York to my training. Thank you for giving me the opportunity to work as a visiting associate in your lab and for allowing me to learn more about cryo-EM sample preparation and data processing.

I am grateful to the Medical Research Council DiMeN DTP for financially supporting my research and providing additional training opportunities. This work would not have been possible without your generous support.

To my friends—Ugochi, Cyril, and Uche—thank you for always being there. Having to talk to you consistently meant that I pulled through this in one piece. To my Church (City of God Newcastle), I could not have done it without your prayers, for that I say thank you..

To my beloved parents, Mr John Ekemezie and Mrs Esther Ekemezie, and my sibliings—Somtochukwu, Nnaemeka, Chioma, Chinonso and Odinaka—thank you for your constant support and for always believing in me. Your unconditional love, encouragement and faith in me gave me the strength to keep going, especially during the challenging times. I am deeply grateful. To the next generation of Ekemezies—my nephews and nieces (Chimebuka, Chimdimma, Chinenye Jnr and Chinedu)—you are my greatest joys. Your little voices gave me the motivation to keep pushing forward and I love you to the moon and back.

Table of Contents

List of Tables

List of Figures

Chapter 1. Introduction

1.1 Ribosomes: what are they and why should we study them?

Ribosomes are indispensable components of virtually every living cell on our planet. They were first discovered in 1955 by George E. Palade when he was investigating the inner structure of eukaryotic cells using electron microscopy. He identified what we now call ribosomes as small particles, approximately 20 nanometres (nm) in diameter, that were predominantly associated with the membranes of the endoplasmic reticulum, while also being freely distributed throughout the cytoplasm (1).

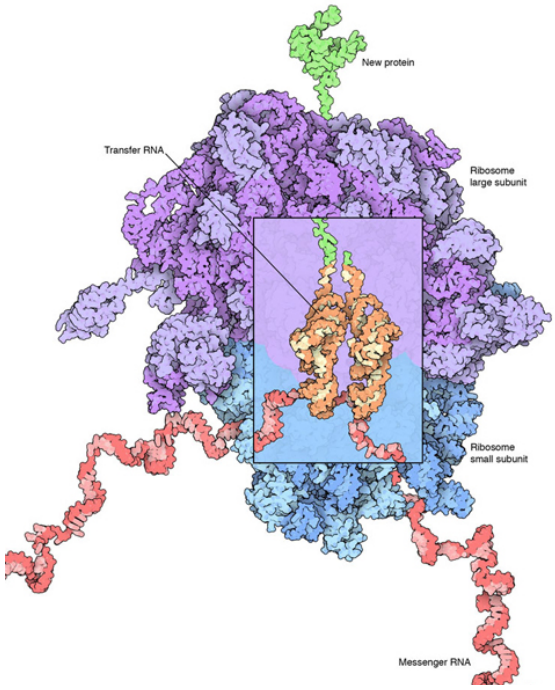

Figure 1.1 | Schematic structure of the ribosome bound with its ligands: mRNA and tRNAs. The ribosome is an enzyme made of three rRNAs (5S, 16S and 23S rRNAs) and over 50 ribosomal proteins. These individual components of the ribosome are organised into two unequal subunits, including the small subunit (also known as the 30S in bacteria) and the large subunit (or the 50S subunit in bacteria). Together, these subunits form the 70S ribosome. Each ribosomal subunit has a dedicated role in protein synthesis. The 30S subunit acts as a "reader" of the genetic code, decoding the mRNA codons by recruiting cognate tRNAs in the ribosomal A site and its decoding centre. The 50S subunit fulfils the catalytic function of the ribosome: it creates chemical bonds between amino acids in the peptidyl transferase centre, forming a growing nascent peptide chain that exits through the nascent peptide exit tunnel in the 50S subunit. The figure is adapted from (2,3).

Because of their rounded shape, small size, high electron density, and granular appearance, Palade described these structures as "small granular components" of the cytoplasm. Initially, he referred to them as *microsomes*, a term then commonly used to describe small granules that

were recently found in the cytoplasm of eukaryotic cells by Albert Claude, a PhD advisor of George Palade and the pioneer of using electron microscopy to define the constitution of living cells (4).

However, the term *microsomes* was ambiguous and lacked specificity because it was used to describe several types of small particles in the cellular cytosol. To address this issue, in 1958, these microsomes or "Palade granules" were renamed "*ribosomes"* by Howard Dintzis (5), who introduced the term to distinguish them from other cytoplasmic "microsomes." Today, ribosomes are recognized as essential macromolecular ribonucleoprotein complexes responsible for protein synthesis in all living cells (6).

1.2 Ribosomes are evolutionary diverged across species, which allows their species-specific drug targeting.

Ribosomes found in modern-day organisms are believed to have emerged around 4 billion years ago, in the last universal common ancestor (LUCA) (7). As organisms began to diverge into the two distinctive lineages of bacteria and archaea-eukaryotes, likely around 3.9 billion years ago (8), ribosomes were retained in both lineages because of their indispensable requirement for gene expression through protein synthesis (**Figure 1.2**).

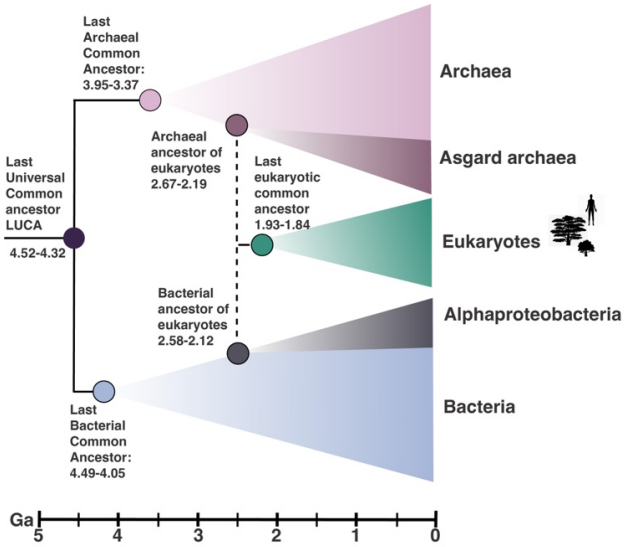

Figure 1.2 | Apparent timeline of the origin of major domains of life.
The evolution of life from the last universal common ancestor (LUCA) to extant species had likely involved three key events. The first event was the emergence of bacteria about 4 billion years ago, followed by that of archaeo-eukaryotes and their separation into archaea and eukaryotes. Because bacteria and eukaryotes have likely been independently evolving for approximately 4 billion years, this resulted in the gradual diversification of ribosomes across these species. The figure is adapted from (8).

However, ancient ribosomes did not remain unchanged. Over billions of years, the ribosomes of bacterial and archaeo-eukaryotic lineages evolved by acquiring new components, such as new ribosomal proteins, or changing the existing ones, which possibly helped adapt ribosomes to the specific needs of different life forms (**Figure 1.3**) (7–15).

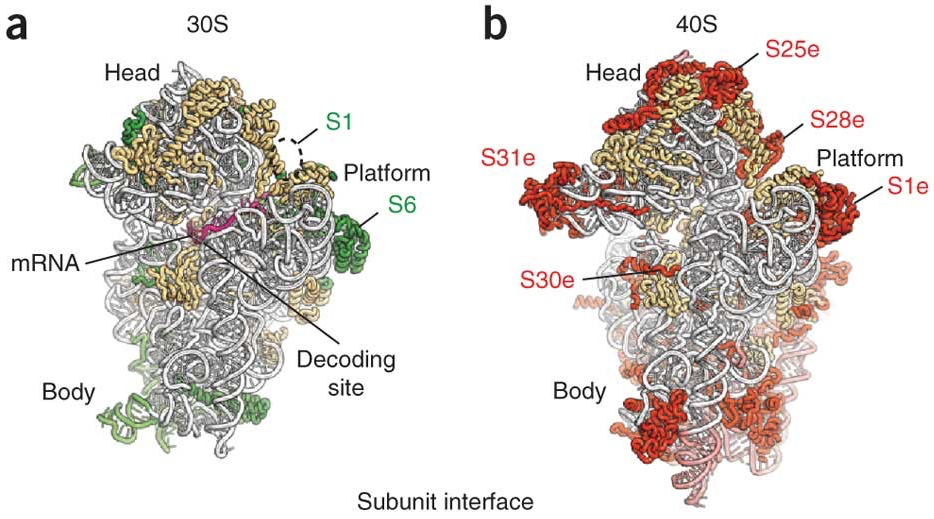

Figure 1.3 | Species have diversified the structure and composition of their ribosomes. Comparison of the small ribosomal subunits from bacteria (*Thermus thermophilus*) and eukaryotes (*Saccharomyces cerevisiae*) illustrates structurally conserved segments of rRNA and ribosomal proteins (in white and yellow, respectively), as well as bacteria-specific features (in green) and eukaryote-specific features (in red) of the small ribosomal subunit. The figure is adapted from (16).

The most noticeable changes occurred in rRNA, where extensions (additional rRNA helices) emerged in both bacterial and eukaryotic species (**Figure 1.3**). Also, ribosomes from bacteria and eukaryotes have acquired several domain-specific ribosomal proteins (**Figure 1.3**). These modifications gave rise to differences in the molecular weights of ribosomes from the three domains of life, including ~2.5 MDa in bacteria and ~3.1–4.5 MDa in eukaryotes (16).

Since cells depend on protein synthesis for growth, inhibiting the ribosome can disrupt cellular growth, making the ribosome an excellent drug target (17). In fact, there are currently over 42 ribosome-targeting drugs available, including small molecules and peptides of both natural and synthetic origin (18). Furthermore, 10 of them are included in the World Health Organisation's list of the most essential medicines for treating bacterial infections (19).

Ribosome-targeting drugs work by binding to the active sites of the ribosome, the very same sites where canonical protein synthesis ligands such as tRNAs and mRNAs bind (20). By doing so, these drugs can inhibit the ribosome function by preventing its association with its ligands.

What is more, some of the drug-binding sites of the ribosome have different sequences of rRNA and ribosomal proteins, leading to species-specific (or, more precisely, domain-specific) targeting of ribosomes with drugs (21). This selectivity is a crucial advantage in medical treatment for bacterial infections.

1.3 The discovery of ribosome-targeting drugs was inspired by the penicillin discovery.

In 1928, Alexander Fleming accidentally discovered penicillin, the first natural antibiotic, when he observed that mould contamination inhibited the growth of *Staphylococcus aureus* in a culture (22). However, it was not until 1940—over a decade later—that penicillin was successfully isolated by scientists at Oxford University (23). The first clinical use of penicillin to treat an infection occurred in 1941 (24). These breakthroughs inspired Dr Selman Waksman, who had been studying antagonistic behaviour in soil microorganisms for over two decades, to shift his focus to antibiotics (25–27).

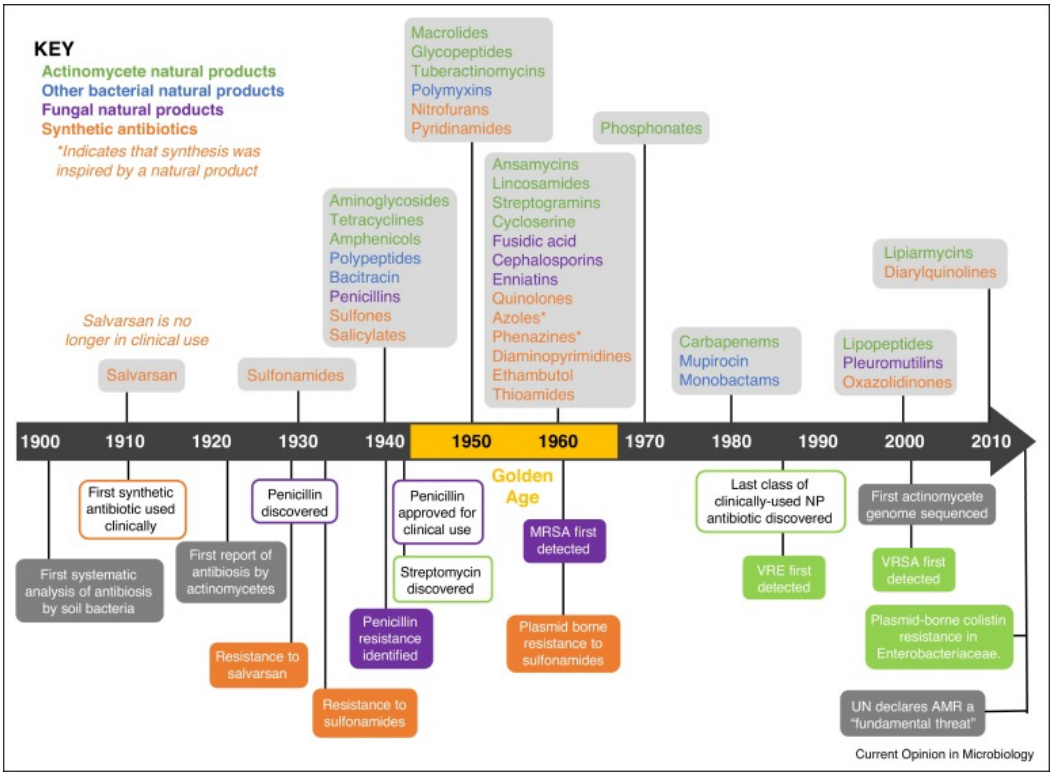

Figure 1.4 | Discovery of major families of antibiotics, including ribosome-targeting drugs. Timelines illustrating major milestones in antibiotic discovery. The discovery of streptomycin, the first ribosome-targeting drug to be identified, was inspired by the penicillin discovery. Streptomycin discovery gave way to the discovery of drugs in other families of ribosome targeting drugs between the 1940s to 2000s when the last family oxazolidinones was introduced into human medicine. This figure was adapted from (28).

Following this, in 1939, Waksman's group began to systematically screen the soil bacteria, actinomycetes, for antibiotics (27). They quickly identified several compounds, including actinomycin, streptothricin, fumigacin, and clavacin (29–31), but all were found to be toxic to animals. In 1943, Waksman's student Albert Schatz discovered streptomycin (32), which was later confirmed by researchers at the Mayo Clinic not only to be effective against tuberculosis but also non-toxic to animals (33). This discovery marked a pivotal moment, leading to a surge in research on natural antibiotics from microorganisms over the next 20 years. During this period, numerous ribosome-targeting drugs (**Figure 1.4**) were discovered and introduced into medicine.

1.4 Ribosome-targeting drugs interfere with protein synthesis in growing cells.

Decades of biochemical and structural studies have provided a detailed understanding of the mechanisms by which major families of ribosome-targeting drugs function (20). They revealed that ribosome-targeting drugs typically bind to the active centres of the ribosomes, including the messenger RNA (mRNA) channel, decoding centre, and peptidyl transferase centre (**Figure 1.5**) (21).

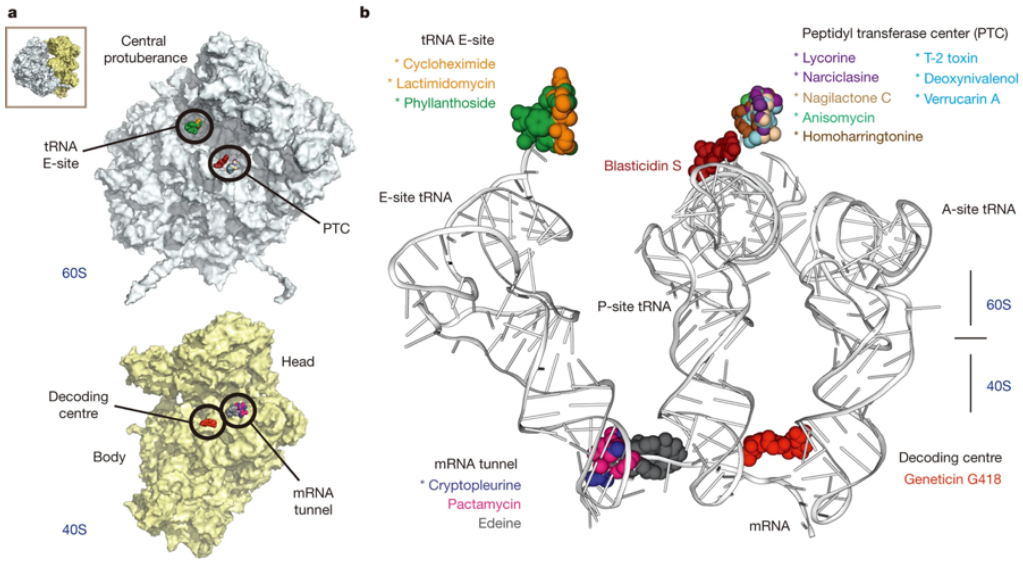

Figure 1.5 | Ribosome-targeting drugs obstruct the active centres of the ribosome.
(a) Structure of the two subunits of eukaryotic ribosomes from yeasts *Saccharomyces cerevisiae*, including large subunit (grey) and the small subunit (golden) (both subunits are shown as surface). Ribosome-targeting drugs (shown as colourful blobs) cluster at four major distinct sites namely: decoding centre and mRNA tunnel in the 40S subunit, as well as the E site and peptidyl transferase centre in the 60S subunit. **(b)** Superposition of the ribosomal ligands—tRNAs and mRNA, —with ribosome-targeting drugs. This superposition suggests that when drugs bind to ribosomes, they prevent either association or dissociation of ligands from the ribosome. This figure is adapted from (21).

Previous studies revealed that drug targeting of the active sites of the ribosome interferes with at least one of the four key steps of protein synthesis—initiation, elongation, termination, or recycling (9,17,34–36). Because of this, ribosome-targeting drugs are usually classified into 4 groups based on the specific step of protein synthesis they inhibit (**Figure 1.6**).

The first group includes the inhibitors of protein synthesis initiation, such as edeine and kasugamycin. These drugs act by preventing the formation of the translation initiation complex that helps ribosomes bind to a mRNA and initiate protein synthesis (36–38). Structural studies of one of these drugs, the natural aminoglycoside kasugamycin, revealed its binding site within the mRNA channel of the 30S subunit between the universally conserved A794 and G926 16S rRNA residues (39). There, kasugamycin introduces structural changes that prevent the association of the 30S ribosomal subunit with its ligand, the fMet-tRNA, thereby preventing the 30S subunit from initiating protein synthesis (39–41).

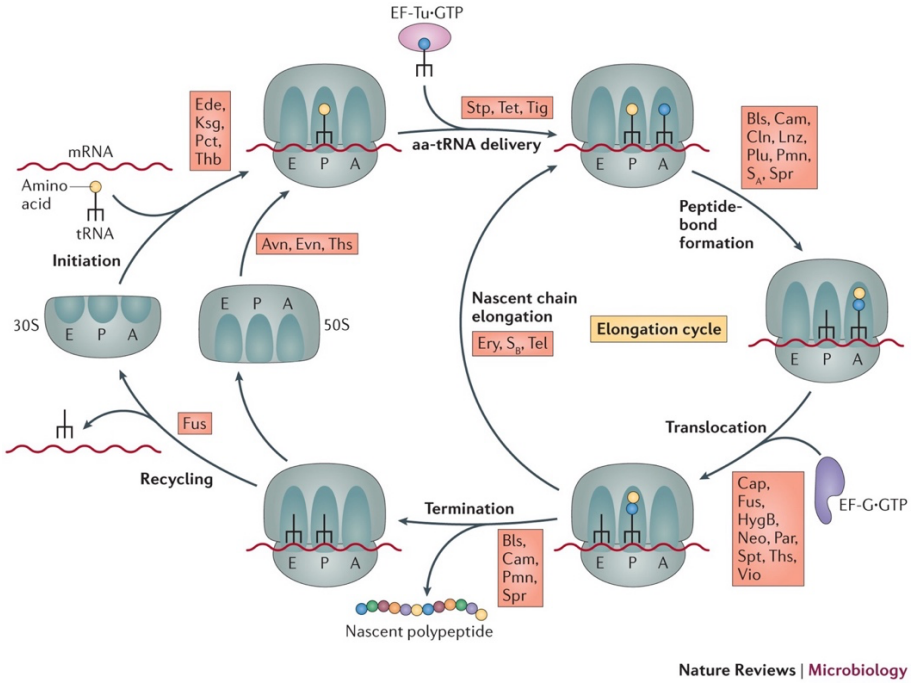

Figure 1.6 | Ribosome-targeting drugs can interfere with each major step of protein synthesis. The cycle of protein synthesis includes initiation, elongation, termination to recycling. Different ribosome-targeting drugs are able to target either one or more of these steps. In combination, these drugs disrupt ribosome function by either arresting the ribosome activity or making the ribosome error prone. This figure is adapted from (20).

The second group includes most ribosome-targeting drugs: the drugs that inhibit the elongation step of protein synthesis (**Figure 1.6**). These peptide elongation inhibitors can act through 3 possible mechanisms (36). For example, the broad spectrum natural antibiotic, tetracycline,

binds between h31 and h34 at the A site of the 30S subunit where it overlaps with the binding site of the anticodon stem-loop of the aminoacyl-tRNA (42). By doing so, tetracycline prevents the binding of aminoacyl-tRNA to the ribosome which is required for protein synthesis. Similarly, the synthetic antibiotic, linezolid, binds to the catalytic site of the ribosome known as the peptidyl transferase centre and arrests the catalytic activity of the ribosome (43). The macrolide family of drugs binds in the nascent peptide exit tunnel, where they restrict movement of the elongating nascent peptide chain, eventually causing its premature release from the ribosome. Other drugs, such as sparsomycin and aminoglycosides (including neomycin), interfere with the translocation of tRNAs and the mRNA, which is essential for protein synthesis (20).

The third group of inhibitors includes the natural antibiotic thermorubin, which can arrest the terminal stage of protein synthesis called termination (44). This drug binds at the interface between the ribosomal subunits, specifically at the intersubunit bridge B2a, where it interacts with h44 of the 16S rRNA and H69 of the 23S rRNA (45). By binding at this interface between the 30S and 50S subunits, thermorubin is able to interfere with multiple steps of protein synthesis, including elongation and also termination of protein synthesis (44). Specifically, the superposition of the ribosome structure bound to thermorubin and the ribosome structure bound to bacterial release factor 1 shows that thermorubin alters the conformation of the 23S rRNA residue C1914, causing a steric clash with release factor 1 at the A site (44).

Finally, the fourth group of inhibitors, target the stage known as recycling. For ribosomes to initiate the next cycle of protein synthesis, they must pass through the post termination complex state. In this state, the ribosome is bound to both deacylated P-site tRNA and mRNA. Here, the complex must be disassembled so that the released ribosomal subunits can engage in a new round of protein synthesis (46). This recycling process is mediated by the elongation factor G (EF-G) in bacteria (47). The anti-ribosome drug, fusidic acid, inhibits ribosome recycling by preventing EF-G from dissociating from the ribosome (46).

Recent studies showed that some ribosome-targeting drugs can target only a small subset of cellular ribosomes in a context-specific manner (41,48–51). For example, the peptide bond formation inhibitors, such as linezolid and chloramphenicol, selectively inhibit protein synthesis only when the active centre of the ribosome is occupied by the peptidyl-tRNA usually with a specific sequence of the nascent peptide (49,51). Specifically, these antibiotics arrest

protein synthesis when the penultimate residue of the peptidyl-tRNA is represented by an alanine (49,51).

1.5 Certain ribosome-targeting drugs act in a lineage-specific fashion.

Importantly, some of the evolutionary changes in ribosomes from different species occurred within the rRNA sequences near or at the active site of the ribosome, giving rise to domain-specific features of the ribosomal active sites (**Figure 1.7**) (21). As a result, eukaryotic ribosomes have acquired unique structural and functional features that make them structurally dissimilar from bacterial ribosomes and, therefore, less susceptible to many clinically available ribosome targeting antibiotics (52). This is why we can use many ribosome-targeting antibiotics to suppress bacterial infection without harming to a human body.

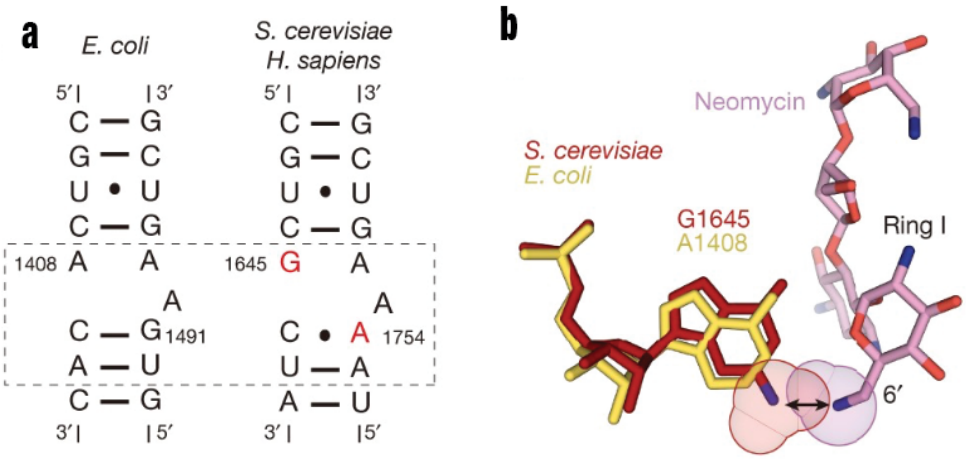

Figure 1.7 | Ribosomal drug-binding sites are different in bacteria compared to eukaryotes.
(a) Secondary structure of one of the drug-binding sites in bacterial (*Escherichia coli*), yeast (*Saccharomyces cerevisiae*) and human (*Homo sapiens*) ribosomes, showing domain-specific features of bacterial and eukaryotic ribosomes at this site. This region corresponds to one of the active sites of the ribosome called the decoding centre (surrounded with the dashed line) where aminoglycoside antibiotics such as neomycin bind. The two residues, G1645 and A1754 (shown in red) in eukaryotic ribosomes corresponds to residues A1408 and G1491 respectively in bacteria ribosomes, illustrating the evolutionary variation in rRNA sequence present at this site in ribosomes from these two domains of life. **(b)** A zoomed-in view of showing that the conformation of G1645 in yeast ribosomes prevents the accommodation of the clinical antibiotic, neomycin. Specifically, the protruding nitrogen atom of G1645 clashes with the NH6' group of neomycin. This observed conformation is different from that of A1408 in the *E. coli* model. This single nucleotide change at this site forms the basis of domain-specific mode of action of drugs such as neomycin.

1.6 Why do ribosome-targeting drugs sometimes fail to inhibit protein synthesis?

Ribosome-targeting drugs sometimes fail to inhibit protein synthesis because of either intrinsic or acquired drug-resistance (20,35). In bacteria, eight different mechanisms of drug-resistance have been characterized to date (20). Specifically, certain bacterial groups, including mycobacteria, have special features outside their cell wall called the outer cell membrane which can impair the transport of drugs into their cells (20). Some bacteria instantly get rid of drugs inside their cells through efflux pumps that expel these drugs out of the cell before they can reach the concentration that is harmful to the cells (20). Mutations of the drug-target means that drugs can no longer recognise their substrate thereby eliminating the effect of the drug in the cell (20). Similarly, the modification of drug target by special enzymes also means that drugs fail to recognise their substrate thereby rendering drugs ineffective (20). Sometimes, certain bacterial strains possess the ability to produce mimics of the drug-target which can trick the drug into binding to the fake targets (20). Some proteins, called factor-associated protection proteins, can reversibly bind to the drug-target and protect it from the drugs (20). Certain enzymes can modify drugs from their active to inactive forms in bacterial cells. Some bacterial strains can produce enzymes that are capable of degrading drugs in the cell thereby rendering drugs ineffective (**Figure 1.8**).

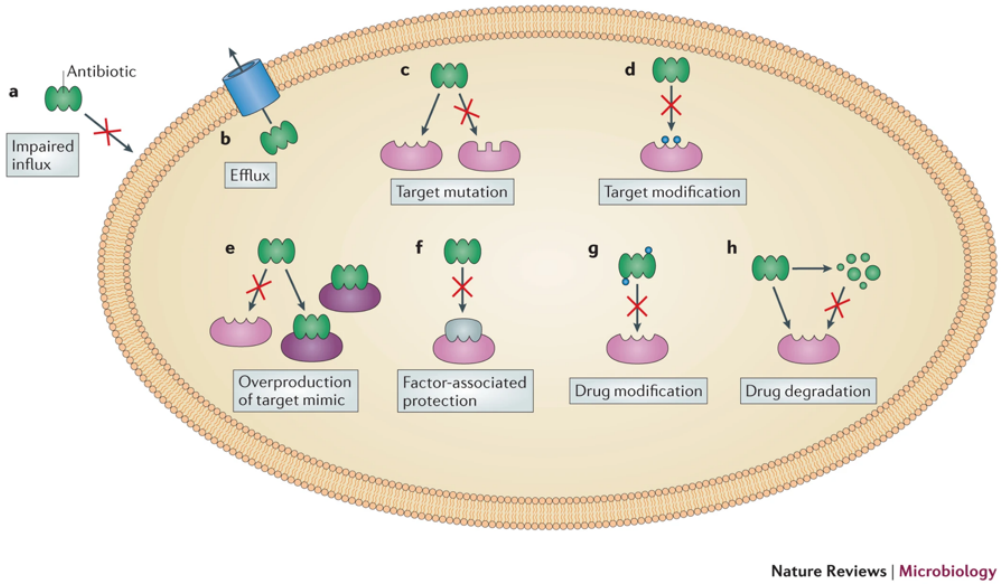

Figure 1.8 | Organisms can develop resistance to ribosome-targeting drugs through one or more ways.
This figure shows 8 drug-resistant mechanisms commonly found in bacteria. Of these 8, 7 **(a-d, f-h)** are mainly used by bacterial to express resistance against ribosome-targeting drugs. Despite these plethora of drug-resistant mechanisms, target mutation **(c)** remains the primary mechanism of acquired resistance to most drugs that target bacterial ribosomes (20). This was adapted from (20).

1.7 *Streptomyces*: antibiotic-producing bacteria with intrinsic resistance to ribosome-targeting drugs.

As mentioned above, some species are intrinsically resistant to ribosome-targeting drugs. This can be exemplified by *Streptomyces*, which is the largest genus of antibiotic-producing bacteria from the Actinobacteria phylum (53). The last common ancestor of these species is estimated to have emerged approximately 382 million years ago when *Streptomyces* diverged from their closest relatives, *Kitasatospora* species (54). Since then, the *Streptomyces* genus gave rise to over 1,500 species (55).

Members of this genus are Gram-positive, filamentous, and spore-forming bacteria that predominantly inhabit soil ecosystems (56). *Streptomyces* are characterized by a unique and complex morphology, which initially led scientists to confuse them with fungi (57,58). Unlike most bacterial species, *Streptomyces* grow as multicellular structures called mycelia (**Figure 1.9**). Their growth begins with the germination of their spores into vegetative hyphae that penetrate their medium, followed by the development of aerial hyphae that precede spore formation. This distinctive growth pattern is a hallmark of their biology (59).

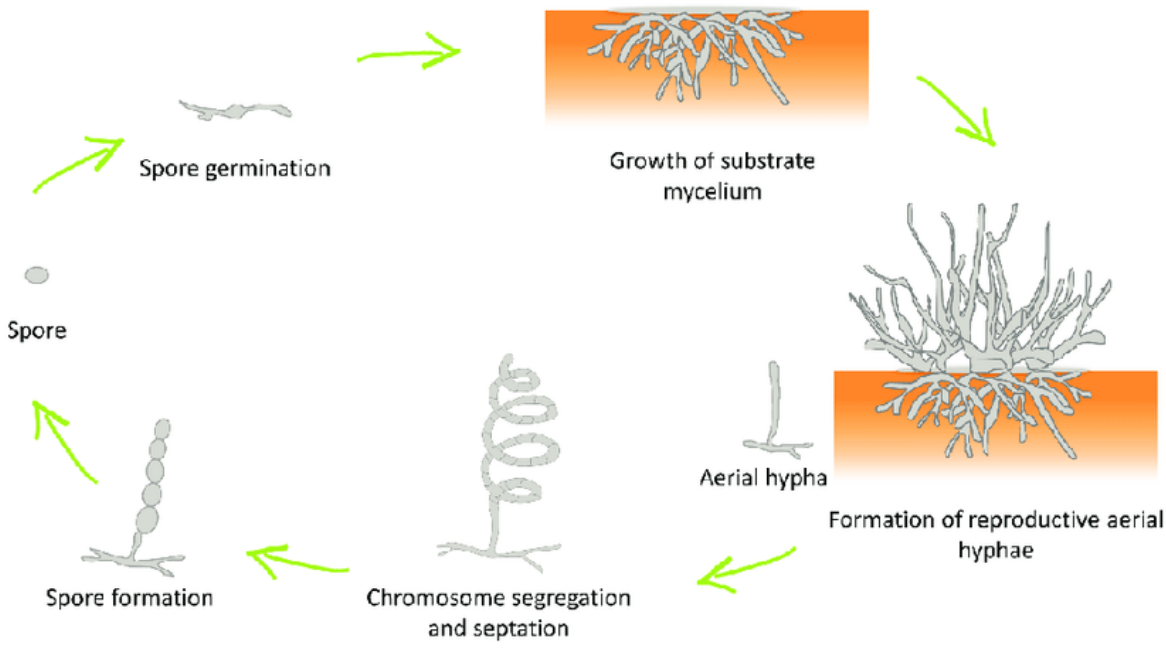

Figure 1.9 | *Streptomyces* have a complex lifecycle different from other bacterial species on solid medium.
Streptomyces are renowned for their complex lifecycle that involves six major stages that involve germination of spores into vegetative hyphae characterized by growth into the medium, and the subsequent aerial mycelial growth and then sporulation. Adapted from (59).

The most remarkable aspect of *Streptomyces* is its ability to produce a vast array of secondary metabolites, which include antibiotics, antifungals, and other bioactive compounds (60). Specifically, approximately two-thirds of all known natural antibiotics are derived from species of this genus, thereby making them the cornerstone of antibiotic discovery and development (61).

Two species of *Streptomyces* were previously characterized as natural producers of ribosome-targeting antibiotics(62,63). Specifically, *Streptomyces griseus* is a natural producer of the ribosome-targeting anti-tuberculosis antibiotic streptomycin (62), while *Streptomyces fradiae* is a natural producer of neomycin (63). To avoid the self-targeting with ribosome-antibiotics, both of these species have evolved self-immunity. In *S. griseus*, this self-immunity was shown to originate from streptomycin inactivation by a special enzyme, streptomycin 6-phosphotransferase, encoded by one of the genes in the streptomycin gene cluster. Through phosphorylation of the streptomycin molecule, this enzyme is able to produce inactive forms of streptomycin (64,65). Similarly, in *S. fradiae*, the mechanism of self-immunity involves two enzymes namely: aminoglycoside phosphotransferase (66) and aminoglycoside *N*-acetyltransferase (67), both of which are found in the neomycin biosynthetic gene cluster (68).

1.8 Mycobacteria species exemplify bacterial ribosomes with structurally diverged drug-binding sites.

Studies of ribosomes from different organisms revealed that certain bacterial species bear sequence alterations in rRNA and ribosomal proteins that render their drug-binding sites dissimilar to those of *E. coli* (69). This can be exemplified by mycobacteria. Mycobacteria are members of Actinobacteria, distantly related to *Streptomyces* (70) (**Figure 1.10**).

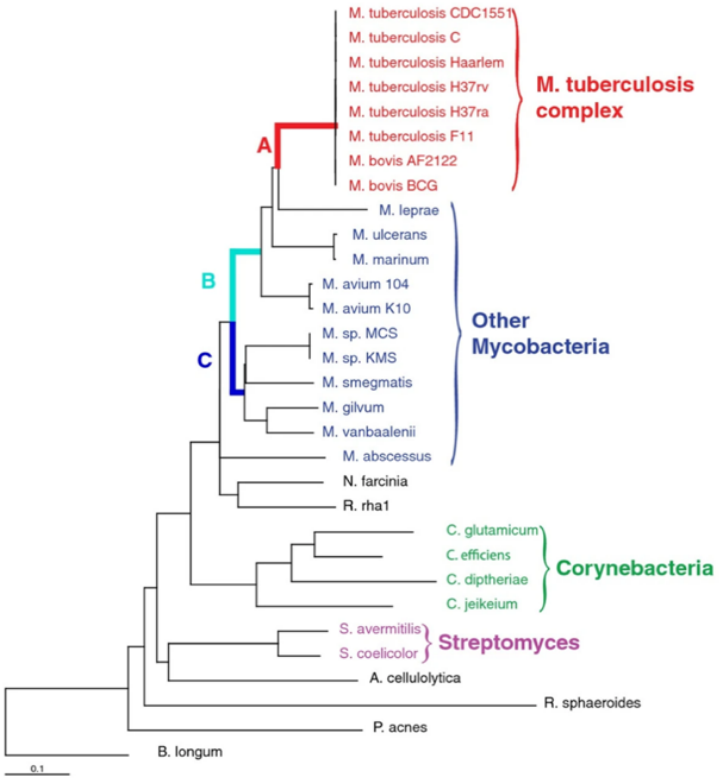

Figure 1.10 | The Actinobacteria tree shows the evolutionary relationship between *Streptomyces* and mycobacterial species.
A simplified phylogenetic tree of Actinobacteria, showing only few species from the phylum, reveals that the *Streptomyces* and *Mycobacterium* branches are distantly related. The *Streptomyces* group appears to have emerged earlier, while the *Mycobacterium* group is relatively more recent. This figure was adapted from (71)

These species have a characteristic rod-like morphology with a thick cell wall that is covered by complex outer layers of arabinogalactan and long-chain mycolic acids (72). Many species of mycobacteria exhibit a slow growth rate, with the division time ranging from 10 to 24 hours (73). The genus, *Mycobacterium,* encompasses over 195 validly published species, including the important human pathogens *Mycobacterium tuberculosis* and *Mycobacterium leprae* (74).

Sequencing of rRNA genes from various bacteria species, including mycobacteria revealed that one of the drug-binding sites of the ribosome—the aminoglycoside-binding site—bears rRNA substitutions in the direct vicinity of the drug-binding pocket (**Figure 1.11**). Specifically, Propionibacteria bear the G1491U natural mutation in their 16S rRNA. This very same mutation showed approximately 512-fold decrease in ribosome inhibition by the aminoglycoside paromomycin in laboratory engineered strains of *Mycobacterium smegmatis* (75). This study revealed that the drug-binding sites of the ribosome are not strictly conserved across bacterial

species, potentially leading to dissimilar sensitivity of bacterial species to ribosome-targeting drugs.

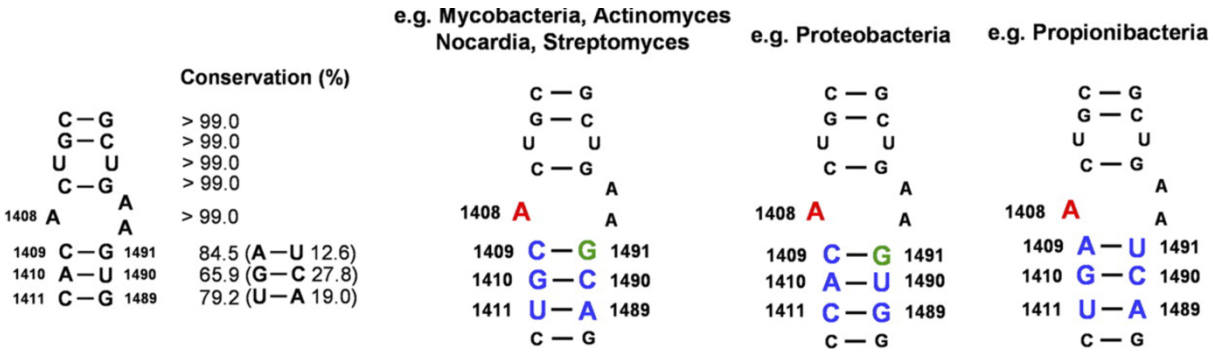

Figure 1.11 | Certain bacterial species bear rRNA variations in their ribosomal drug-binding sites.
Secondary structures of the ribosomal A site showing the lineage specific variation in the drug-binding site of 6 bacterial groups including *Mycobacterium*, *Actinomyces*, *Nocardia*, *Streptomyces*, Proteobacteria and *Propionibacteria*. This site which corresponds to the binding site of such drug families as the aminoglycosides. Adapted from (76).

More recently, structural studies of mycobacterial ribosomes (from *Mycobacterium smegmatis*) revealed remarkable architectural differences when compared to ribosomes from other bacteria, such as *E.* coli (77–79). These differences are primarily found in the 23S rRNA, where unique helical stem-loop extensions give rise to helices H15, H16a, H31a, and H54a (**Figure 1.12**). Among these, the more than 100 nucleotides long H54a stands out as a prominent feature on the solvent side of mycobacterial ribosome where it forms a new inter-subunit bridge 'B9' through its interaction with ribosomal protein uS6 of the small subunit (80). H54a also interacts with bS21 in hibernating mycobacterial ribosomes (78). Interestingly, while helices H15, H16a, and H54a are present in other Actinobacteria, while H31a appears to be unique to mycobacteria (77,79). These structural adaptations underscore the distinct evolutionary features ribosomes of members of the actinobacterial phylum.

Most of the ribosomal proteins in mycobacteria are homologous to those found in *E. coli*, with one key exception: protein S21, which is absent in mycobacteria (79). However, the mycobacteria homologs are larger than their *E. coli* counterparts because of expansions in their N-terminal, C-terminal or both termini (77,79). For example, the ribosomal proteins (bL17, bL22, bL29) found within the vicinity of the peptide exit tunnel are significantly larger than their *E. coli* homologs (81). These structural differences while subtle, are likely to influence the function—and possibly drug targeting—of the mycobacterial ribosome.

Another distinctive feature of the mycobacterial ribosome is the presence of two additional proteins—bL37 and bS22—in the mycobacterial 70S ribosome model (77). The 24-amino-acid-long bL37 is located near the peptidyl transferase centre in the 50S subunit, where it interacts with the tip of the 5S rRNA as well as helices H39, H40, H72, and H89 of the 23S rRNA (77). Meanwhile, bS22, a 33-amino-acid-long protein, resides beneath the mRNA channel, in proximity to helices h27, h44, and h45 (77). The presence of these mycobacteria-specific ribosomal proteins may indicate a species-specific translation landscape that is unique to organisms within the mycobacterial group.

Beyond structural differences, mycobacteria exhibit an extraordinary ability to reprogram their ribosomal protein composition in response to environmental challenges (82). For example, during zinc starvation, species of mycobacteria such as *M. smegmatis* and *M. tuberculosis* produce isoforms of some ribosomal proteins including uS14, bS18, bL28, bL31, bL33, bL36 lacking the zinc binding 'CXXC' motif (77,82,83). The incorporation of the non-zinc binding forms of these proteins into the ribosome resulted in a population of ribosomes that are structurally different those formed under zinc-rich conditions (82). This capacity to adapt ribosomal structure underscores the resilience and flexibility of mycobacterial ribosomes, enabling them to thrive under diverse and often harsh conditions.

Overall, the unique structural features and adaptability of mycobacterial ribosomes reflect their distinct evolutionary trajectory and functional specialization. These differences not only offer insights into ribosome biology but also present potential opportunities for targeted therapeutic interventions against mycobacterial infections.

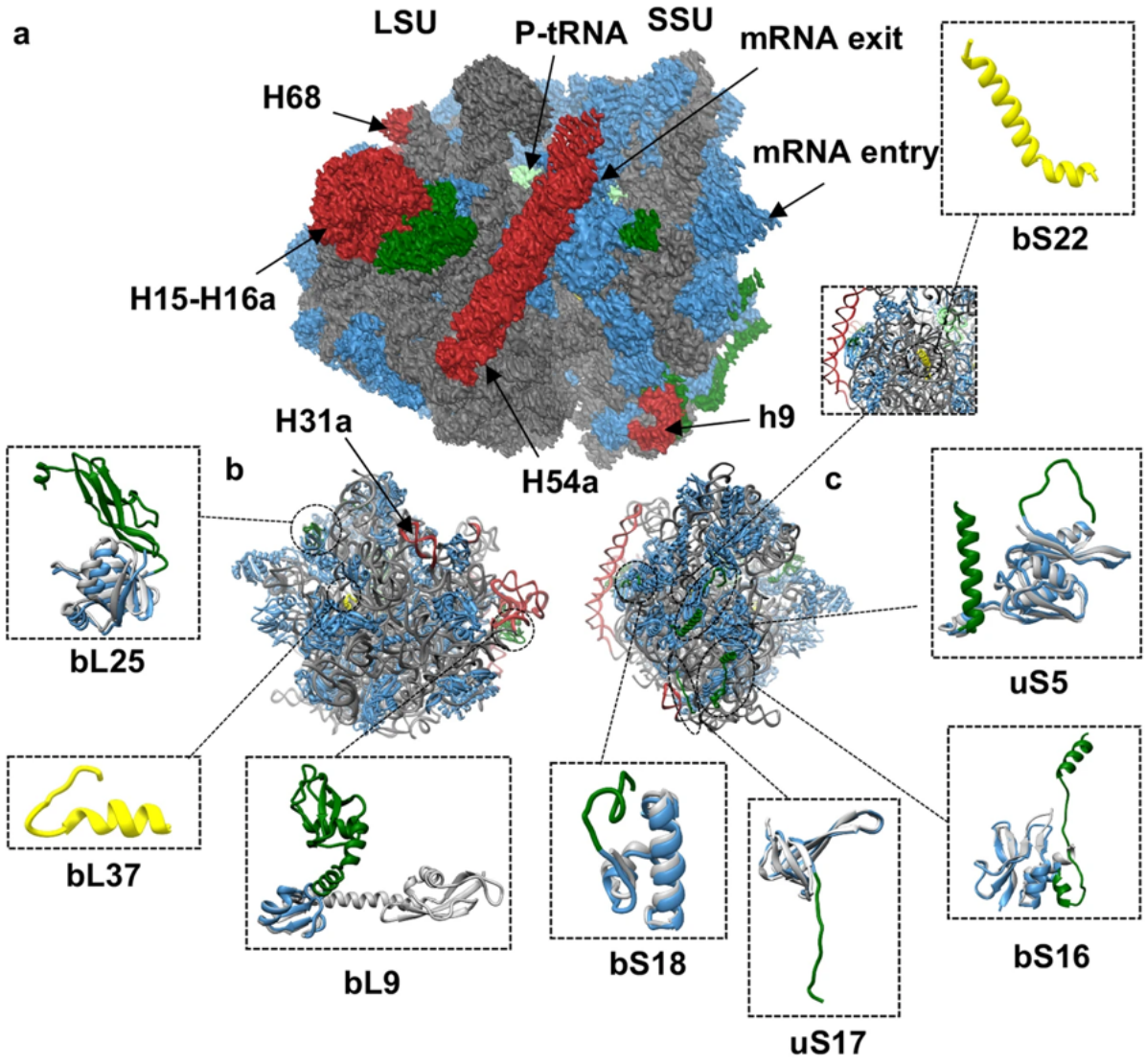

Figure 1.12 | Substitutions in rRNA are not the only species-specific features of *Mycobacterium* ribosome.
(a) Overview of the structure of mycobacterial ribosome highlight its unique features including rRNA extensions (red) and ribosomal protein expansion (green). (b) Model of the mycobacterial 50S subunit showing rRNA extension (red), a new mycobacterial specific ribosomal protein bL37 (yellow) with zoomed in view of the superposition of the extended bL25 (green) with its *E. coli* homolog (grey). (c) Model of the mycobacterial 30S subunit with zoomed in view of the new mycobacterial specific ribosomal protein bS22 (yellow) and superposition of the extended proteins uS5, bS16, uS17 and bS18 with their *E. coli* homologs (grey). This figure was adapted from (78).

1.9 Project aims

Previously, model organisms such as *E. coli*, yeasts and humans have been used as main model organisms to provide understanding of how ribosomes are recognized by drugs. However, using these model organisms left unanswered the following fundamental questions:

- To what extent can we extrapolate the findings made for *E. coli*, yeast, and human ribosomes to ribosomes from other bacterial and eukaryotic species?
- In other words, how many species on the tree of life share conserved sequences of the ribosomal drug-binding residues with those of the model organisms, and how many species differ from model organisms in this regard?
- And, most importantly, does natural variation in the sequence of ribosomal drug-binding residues result in intrinsic resistance or hypersensitivity of certain species to ribosome-targeting drugs?

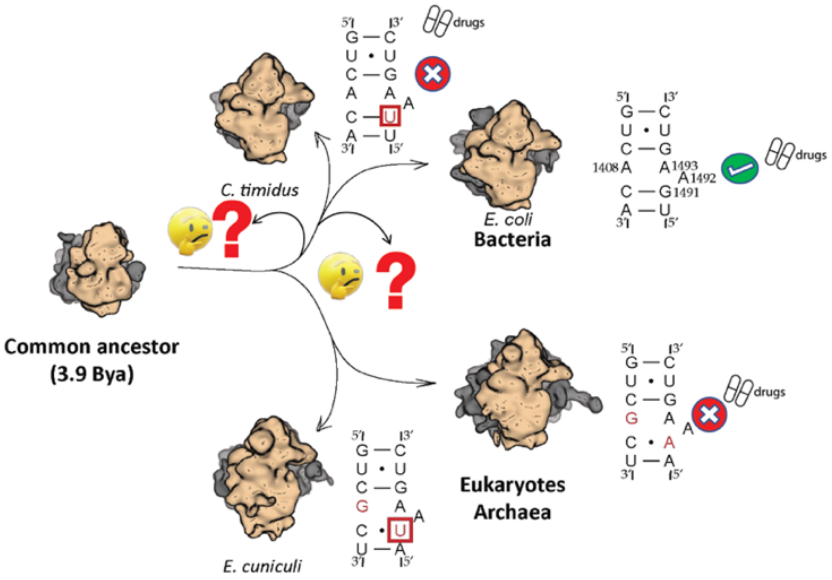

Figure 1.13 | The specific aims of this study.
Ribosome-targeting drugs are traditionally viewed as broad-spectrum inhibitors of bacterial protein synthesis. This is because ribosomes, as universally conserved molecules, are divided into two major lineages: bacterial and archaeo-eukaryotic. Over time, these ribosomes have accumulated mutations, including changes in drug-binding sites. Comparing this drug-binding site in bacterial ribosomes with those of eukaryotes, including humans, reveals two key mutations in human ribosomes (highlighted in red) that prevent drug association. As a result, these drugs are used to selectively inhibit bacterial protein synthesis, without affecting human cells. However, growing evidence suggests that bacterial ribosomes are not as highly conserved as once thought. For instance, the bacterium *Calidithermus timidus* has a mutation in its drug-binding site compared to *E. coli* ribosomes. This finding implies that some bacterial species may have structurally distinct ribosomal drug-binding sites, making them intrinsically resistant to certain ribosome-targeting antibiotics.

My research focuses on addressing these questions and has the following aims:

Aim 1 | How does the sequence of ribosomal drug-binding residues of model eukaryotes compare to those of other eukaryotes?

To date, most of our understanding of the targeting of eukaryotic ribosomes with small molecule drugs comes from studies of the human or yeast ribosomes (21,48). But studies of a few other eukaryotes — such as microsporidia (84) and *Leishmania* (85) — illustrate that the drug-binding residues of eukaryotic ribosomes are not strictly conserved. However, it remains elusive how many other eukaryotes have dissimilar sequence of ribosomal drug-binding sites compared to those of model organisms, including humans. My first aim was to determine this conservation across the eukaryotic domain of life.

Aim 2: How do the drug-binding sites of ribosomes in the model bacterium *E. coli* compared to those of other bacterial species?

Similarly to studies of eukaryotic ribosomes, previous studies of bacterial ribosomes have demonstrated that certain bacterial species exhibit structural dissimilarities in the drug binding sites compared to those of *E. coli* ribosomes (76). However, the extent and prevalence of these differences across bacterial species remain largely unknown. Here, I will answer this question by first retrieving rRNA sequences of all known studied bacteria species from trusted public database of high quality rRNA sequences.

Aim 3 | Determine whether the natural variation in the sequence of ribosomal drug-binding residues lead to intrinsic resistance or hypersensitivity of some species to anti-ribosome drugs.

Finally, my aim was to test whether the naturally occurring changes in the sequence of ribosomal drug-binding residues alter the ribosome affinity to drugs and thereby render certain organisms either intrinsically resistant or hypersensitive to some of the ribosome-targeting drugs.

Chapter 2. Materials and Methods

2.1 Method 1 – Analysis of drug-binding sites in eukaryotic ribosomes.

2.1.1 Locating the drug-binding residues in eukaryotic ribosomes.

To identify the ribosomal residues that are directly involved in drug recognition, we analysed 29 previously determined structures deposited in the Protein Data Bank (86) in which eukaryotic ribosomes were bound to a representative of each family of ribosome-targeting drugs (**Table 2.1**). Using ChimeraX (87), we selected non-hydrogen atoms of the ribosome located within 4.3 Å from a drug. These sets of atoms were then reduced to only include atoms that belonged to amino acid side chains of ribosomal proteins and aromatic bases of rRNA. This allowed us to determine the coordinates of each ribosomal residue that makes a sequence-dependent contact with ribosome-targeting drugs, as well as the numbering correspondence between conserved rRNA residues of *E. coli*, *S. cerevisiae* and *H. sapiens* ribosomes (**Table 2.2**).

2.1.2 Creating a high-fidelity dataset of rRNA sequences for evolutionary analyses.

To enable accurate analysis of rRNA sequences, we used the SILVA database and have devised a multi-step data reduction strategy in order to bypass the notorious issues of automated data annotation and sequencing, including the occurrence of chimeric sequences, misannotated phylogeny, non-genomic DNA and pseudogenes (**Table 2.3 and 2.4**). In brief, as our starting point we used the SILVA's dataset NR99 v138.1, which contains 510,508 16S/18S rRNA sequences corresponding to 40,239 unique "species" (including metagenomic variants, unknown species, species candidates and other ambiguously defined species) ("SSU dataset") and 95,286 sequences of 23S/5.8S rRNA from 14,849 unique "species" ("LSU dataset") from all domains of life (88). We first reduced these SILVA datasets by eliminating sequences from non-eukaryotic species as well as from unidentified eukaryotes for which we could not confirm the identity of an organism. This included sequences whose headers contained the words "unidentified", "uncultured", "metagenome", "cluster" and "sp.", as well as sequences whose names began with a lowercase letter. The obtained datasets were then further reduced by eliminating rRNA sequences that are encoded by plasmids and organelles. We then removed

all sequences of apparently poor sequencing quality, based on the presence of 'ambiguous' sites represented by symbols such as "R", "X", "N", and "S" instead of the standard set of RNA bases “A”, “G”, “C”, and “U”. The sequences from each of these datasets were initially aligned using MAFFT v7.490 with default settings (FFT-NS-2) (89) during the quality control analysis. The sequences that passed the quality control were then re-extracted from the original SILVA dataset of aligned rRNA sequences and are shown in (**Appendix 1, SI Data S3.1, S3.2**).

2.1.3 Assessing the conservation of the eukaryotic ribosomal drug-binding residues.

To simplify the assessment of conservation of drug-binding residues of the eukaryotic ribosome, we trimmed the aligned rRNA sequences to only the drug-binding residues. This file was then manually inspected for quality control, and the rRNA with apparent truncations in the drug-binding sites (based on the presence of gaps in the place of drug-binding residues) were removed from our further analysis. The remaining sequences were then reordered according to the location of species on the tree of life. The resulting dataset was further reduced to a single sequence per organism using the following rule: whenever the same organism contained several sequence variants, we used only one variant, which was identical (or the most similar) to the sequences of the adjacent members on the tree of life (e.g. other eukaryotic species from the same genus). This allowed us to identify mutations that were a common characteristic of a clade of species and eliminate sequencing and annotation artifacts, as well as mutations that were characteristic of an individual strain or an individual rRNA operon (**Appendix 1, SI Data S3.3, S3.4**).

2.1.4 Reconstructing the evolutionary history of mutations in eukaryotic ribosomal drug-binding sites

To trace the evolutionary history of sequence variations in the ribosomal drug-binding residues, we used 18S rRNA sequences listed in (**Appendix 1, SI Data S3.1**) to generate a phylogenetic tree. The tree was generated using default settings on Mega11 (90). The tree was then coloured by conservation of ribosome-drug-binding residues by highlighting species and lineages with the human-type and non-human-type sequences of ribosomal drug-binding residues (**Figures**

3.2 and 3.3). The relative age of each mutation was estimated using TimeTree (91) or the original studies cited where appropriate in the manuscript.

Table 2.1 | Structures of inhibitors the eukaryotic ribosome that were used to determine the ribosomal drug-binding residues.

PDB	Drug	Drug family	Drug origin	Organism	Binding site	Subunit
5MEI	Agelastatin A	Oroidins alkaloids	Sea sponge	*S. cerevisiae*	PTC/NCT	LSU
5I4L	Amicoumacin A	Dihydroisocoumarins	Bacteria	*S. cerevisiae*	mRNA tunnel	SSU
4U3M	Anisomycin	Pyrrolidines	Bacteria	*S. cerevisiae*	PTC/NCT	LSU
6XA1	PF846	Benzamides	Synthetic	*H. sapiens*	PTC/NCT	LSU
7NWH	Blasticidin S	Peptidyl nucleosides	Bacteria	*O. cuniculus*	tRNA (P-site)	LSU
8Q5I	Cephaeline	Alkaloids	Plant	*C. albicans*	mRNA tunnel	SSU
5TBW	Chlorolissoclimide	Lissoclimides	Shell mollusc	*S. cerevisiae*	tRNA (E-site)	LSU
6HHQ	Compound C45	Lissoclimides	Synthetic	*S. cerevisiae*	tRNA (E-site)	LSU
4U55	Cryptopleurine	Phenanthroquinolizidine	Plant	*S. cerevisiae*	mRNA tunnel	SSU
7N8B	Cycloheximide	Glutarimide	Bacteria	*S. cerevisiae*	tRNA (E-site)	LSU
4U53	Deoxynivalenol	Tricothecenes	Fungi	*S. cerevisiae*	PTC/NCT	LSU
4U4N	Edeine	Pentapeptide amides	Bacteria	*S. cerevisiae*	mRNA tunnel	SSU
6OKK	Emetine	Alkaloids	Plant	*P. falciparum*	PTC/NCT	LSU
5NDG	Geneticin	Aminoglycosides	Bacteria	*S. cerevisiae*	Decoding centre	SSU
5OBM	Gentamicin	Aminoglycosides	Bacteria	*S. cerevisiae*	Decoding centre	SSU
5ON6	Haemanthamine	β-crinane-type alkaloids	Plant	*S. cerevisiae*	PTC/NCT	LSU
7UCJ	Harringtonine	Cephalotaxus alkaloids	Plant	*O. cuniculus*	PTC/NCT	LSU
8A3D	Homoharringtonine	Cephalotaxus alkaloids	Plant	*Homo sapiens*	PTC/NCT	LSU
4U4R	Lactimidomycin	Glutarimide	Bacteria	*S. cerevisiae*	tRNA (E-site)	LSU
4U4U	Lycorine	Pyrrolophenanthridine	Plant	*S. cerevisiae*	PTC/NCT	LSU
4U52	Nagilactone C	Norditerpene lactones	Plant	*S. cerevisiae*	PTC/NCT	LSU
4U51	Narciclasine	Pyrrolode phenanthridine	Plant	*S. cerevisiae*	PTC/NCT	LSU
4U4Y	Pactamycin	Aminocyclopentitols	Bacteria	*S. cerevisiae*	mRNA tunnel	SSU
6AZ1 6AZ3	Paromomycin	Aminoglycosides	Bacteria	*L. donovani*	DC	SSU
7Q0F	Phyllanthoside	Glycosides	Plant	*C. albicans*	tRNA (E-site)	LSU
4U6F	T-2 Toxin	Trichothecenes	Fungi	*S. cerevisiae*	PTC/NCT	LSU
5NDW	TC007	Aminoglycosides	Semi-synthetic	*S. cerevisiae*	DC	SSU
6Y6X	Tetracenomycin X	Aromatic polyketide	Bacteria	*H. sapiens*	PTC/NCT	LSU
4U50	Verrucarin	Trichothecenes	Fungi	*S. cerevisiae*	PTC/NCT	LSU

Table 2.2 | Eukaryotic ribosomal drug-binding residues analysed in this study and their numbering in different species.

23S/25S/28S rRNA			16S/18S rRNA		
S. cerevisiae	**Human**	***E. coli***	***S. cerevisiae***	**Human**	***E. coli***
A876	A1593	**U744**	G904	G961	**G693**
C877	C1594	**G745**	A905	A962	**A694**
G878	G1595	**U746**	A998	A1055	**A787**
G880	G1597	**G748**	U999	U1056	**U788**
A884	A1601	**A752**	A1001	A1058	**A790**
U885	U1602	**A753**	G1002	G1059	**G791**
U2140	U3644	**U1782**	A1003	A1060	**A792**
G2400	G3904	**A2058**	A1005	A1062	**A794**
A2401	A3905	**A2059**	C1006	C1063	**C795**
G2403	G3907	**G2061**	C1007	C1064	**C796**
A2404	A3908	**A2062**	G1150	G1207	**G926**
G2619	G4196	**G2252**	C1641	C1705	**C1404**
U2763	U4340	**U2393**	G1642	G1706	**G1405**
C2764	C4341	**C2394**	U1643	U1707	**U1406**
C2765	C4342	**C2395**	C1644	C1708	**C1407**
G2793	G4370	**G2421**	G1645	G1709	**A1408**
G2794	G4371	**C2422**	C1646	C1710	**C1409**
A2808	A4385	**A2439**	U1752	U1821	**G1489**
G2816	G4393	**G2447**	A1753	A1822	**U1490**
A2820	A4397	**A2451**	A1754	A1823	**G1491**
C2821	C4398	**C2452**	A1755	A1824	**A1492**
U2822	U4399	**A2453**	A1756	A1825	**A1493**
U2869	U4446	**U2500**	G1757	G1826	**G1494**
A2872	A4449	**A2503**	U1758	U1827	**U1495**
U2873	U4450	**U2504**	C1759	C1828	**C1496**
G2874	G4451	**G2505**	G1768	G1837	**G1505**
U2875	U4452	**U2506**			
U2954	U4531	**U2585**			
U2955	U4532	**U2586**			
A2956	A4533	**A2587**			
A2971	A4548	**A2602**			
U2978	U4555	**U2609**			

Table 2.3 | Steps of quality control to prepare 18S rRNA sequences for the analysis.

Processing steps	Unique genera	Unique species	Number of total sequences
Initial eukaryotic SSU Sequences	14,005	23,378	58,549
Removal of unidentified species	13,424	22,386	34,498
Removal of non-genomic and duplicate organisms	13,409	22,354	33,429
Removal of low-quality sequences	11,367	18,415	27,891
Removal of all sequences without all drug binding residues	6,868	10,416	16,695
Removal of exotic sequences	5,187	8,632	13,003
Manual curation	5,148	8,563	8,563
Conserved	4,647	6,611	
Non conserved	501	1,952	

Table 2.4 | Steps of quality control to prepare 28S rRNA sequences for the analysis.

Processing steps	Unique genera	Unique species	Number of total sequences
Initial eukaryotic LSU Sequences	5,585	7,880	16,151
Removal of unidentified species	5,396	7,623	13,597
Removal of non-genomic and duplicate organisms	5,395	7,622	13,529
Removal of low-quality sequences	4,192	5,784	11,189
Removal of all sequences without all drug binding residues	2,787	1,976	6,265
Removal of exotic sequences	2,698	1,915	5,274
Manual curation	1,912	2,780	2,780
Conserved	1,911	2,776	
Non conserved	1	4	

2.2 Method 2 – Analysis of drug-binding sites in bacterial ribosomes.

2.2.1 Annotating bacterial ribosomal drug-binding residues.

To annotate the drug-binding residues of the ribosome, we used the Protein Data Bank (86) to retrieve previously determined ribosome structures in complex with 35 clinically relevant drugs (92–109,40,110–115), which corresponded to 21 chemical families of ribosome-targeting molecules (**Table 2.5**). We then used PyMOL (version 2.5.0) (116) to select ribosomal drug-binding residues located within hydrogen bond distance from the drug, with a distance cut-off of 3.3 Å for structures containing hydrogen atoms and 4.3 Å for structures lacking hydrogen atoms. To identify ribosomal residues that bind ribosome-targeting drugs in a sequence-dependent manner, we then excluded residues that bind drugs with either their sugar moiety or phosphate backbone of rRNA nucleotides. This allowed us to select only those rRNA residues that bind drugs using their nucleotide bases (**Table 2.6**).

2.2.2 Creating a high-fidelity dataset of rRNA sequences for evolutionary analyses.

To enable accurate analysis of rRNA sequences, we have used the public repository of rRNA sequences, SILVA, particularly the dataset NR99 v138.1 that contained 510,508 non-redundant 16S/18S rRNA sequences corresponding to 40,239 species (17,609 genera) ("SSU dataset") and 95,286 23S/25S rRNA sequences from 14,849 species (7,837 genera) ("LSU dataset") from all domains of life (88). To filter out false-positive sequence variations, we have devised a 10-step data reduction strategy to bypass the errors in sequence datasets that stem from automated annotation of sequencing data and sequencing mistakes, such as chimeric sequences (where a single sequence is assembled from fragments from different species), sequences with misannotated phylogeny, or sequences from non-genomic DNA and pseudogenes (**Table 2.7 and 2.8**). In this reduction strategy, the initial SILVA datasets were first reduced by eliminating sequences from non-bacterial species as well as from unidentified bacteria for which we could not confirm the identity of an organism. This included sequences whose headers contained the words "unidentified", "uncultured", "metagenome", "cluster" and “sp.”, as well as sequences whose names began with a lowercase letter. The obtained datasets were then further reduced by eliminating rRNA sequences that are encoded by plasmids and viruses. We then removed sequences of apparently poor sequencing quality, based on the presence of 'ambiguous'

nucleotides represented by symbols such as "R", "X", "N", and "S" instead of the standard set of RNA bases “A”, “G”, “C”, and “U”. This resulted in the 23S rRNA dataset containing 56,154 sequences from 5,726 bacterial species (from 1,678 genera) and the 16S rRNA dataset containing 94,486 sequences from 14,132 of bacterial species (from 2,967 genera) (**Appendix 2, SI Data S4.1 and S4.2**).

2.2.3 Assessing of drug-binding residues in bacterial rRNA.

To enable the analysis of rRNA conservation across bacterial species, the reduced sequence libraries of 16S and 23S rRNA were used for multiple sequence alignments. To reduce gaps and alignment errors, the datasets were first separated into sequences from individual bacterial phyla, and then the multiple sequence were produced using MAFFT v7.4908 (89) with default settings (FFT-NS-2) for each phylum. To assess the conservation of drug-binding residues, the aligned sequences of 16S and 23S rRNA were reduced to the sequences of drug-binding residues only (**Appendix 2, SI Data S4.3, and S4.4**). To remove potential “false-positive” sequence variations that originate from truncations, the errors of sequencing, alignment or genome assembly, we removed sequences that contained truncations in the ribosomal drug-binding sites. The resulting dataset was further reduced to a single sequence per organism using the following rule: whenever the same organism contained several sequence variants, we used only one variant, which was identical (or the most similar) to the sequences of the adjacent members on the tree of life. This allowed us to identify mutations that were a common characteristic of a clade of species and eliminate sequencing and annotation artifacts, as well as mutations that were characteristic of an individual strain (**Appendix 2, SI Data S4.3, and S4.4**). The full sequences of records remaining after applying all these stringent measures were re-extracted from the original Silva dataset, as shown in (**Appendix 2, SI Data S4.5 and S4.6**).

2.2.4 Mapping the conservation of bacterial ribosomal drug-binding residues on ribosome structure.

To highlight conservation of the drug-binding residues in the structure of the bacterial ribosome, we used ChimeraX v1.6 (87). First, we generated the profile sequence of the ribosomal drug-binding residues for each bacterial phylum in our dataset shown in (**Appendix 2, SI Data S4.7,**

and S4.8). We then aligned the profile sequences and calculated the percentage of conservation for each drug-binding residue in the aligned phyla-specific profile sequences. The resulting scores were then shown in (**Figure 4.4 and 4.5**).

2.2.5 Assessing the conservation of drug-binding residues in rRNA operons of the same bacterial species.

To assess potential variability of rRNA drug-binding residues between rRNA operons from the same species, we have repeated our analysis of rRNA-binding residues by using the manually curated dataset of rRNA operons rrnDB (version 5.8) (117) instead of the SILVA dataset. Our analysis showed that the drug-binding residues of rRNA encoded by different operons of the same species remain conserved, thereby excluding the possible variability of antimicrobial resistance between rRNA produced by different operons of the same bacterial species.

2.2.6 Tracing the evolutionary origin of variations in bacterial ribosomal drug-binding sites.

To trace the evolutionary history of variations in the ribosomal drug-binding residues, we used 16S rRNA sequences listed in (**Appendix 2, SI Data S4.5, and S4.6**), we used the dated bacterial tree generated using Mega11 with default settings (90), rooting the tree based on recent analyses (118,119). The relative age of each mutation was estimated based on a published bacterial time tree (119) or the original studies of *Mycoplasma* (120,121), *Helicobacter* (122,123) and *Rickettsiales* (124).

Table 2.5 | Ribosome-targeting antibiotics whose binding sites are assessed in this study.

Drug	Family	Subunit	Binding site	Organism	PDP	Application	Origin	Year
Linezolid	Oxazolidinone	50S	PTC	*E. coli*	7S1H	Clinical	Synthetic	2021
Erythromycin	Macrolide	50S	Tunnel	*E. coli*	4V7U	Clinical	Natural	2014
Clindamycin	Lincosamide	50S	PTC/ Tunnel	*E. coli*	4V7V	Clinical	Semi-synthetic	2014
Telithromycin	Ketolide	50S	Tunnel	*E. coli*	4V7S	Clinical	Semi-synthetic	2014
Chloramphenicol	Amphenicol	50S	PTC	*E. coli*	4V7T	Clinical	Synthetic	2014
Avilamycin	Orthosomycin	50S	A-site	*E. coli*	5KCR	Veterinary	Natural	2016
Evernimicin	Orthosomycin	50S	A-site	*E. coli*	5KCS	Clinical	Natural	2016
Quinupristin	Streptogramin B	50S	Tunnel	*E. coli*	4U1U	Clinical	Semi-synthetic	2014
Dalfopristin	Streptogramin A	50S	PTC	*E. coli*	4U24	Clinical	Semi-synthetic	2014
Tiamulin	Pleuromutilin	50S	PTC	*H. marismortui*	3G4S	Veterinary	Semi-synthetic	2009
Retapamulin	Pleuromutilin	50S	PTC	*D. radiodurans*	2OGO	Clinical	Semi-synthetic	2007
Virginiamycin	Streptogramin	50S	PTC	*E. coli*	4U25	Veterinary	Natural	2014
Puromycin	Aminonucleoside	50S	PTC	*H. marismortui*	1Q81	Research tool	Natural	2000
Sparsomycin	Sparsomycin	50S	PTC	*H. marismortui*	1VQ8	Antitumor, Antibacteria	Natural	2005
Carbomycin	Macrolide	50S	PTC/ Tunnel	*H. marismortui*	1K8A	Veterinary	Natural	2001
Azithromycin	Macrolide	50S	Tunnel	*H. marismortui*	1M1K	Clinical	Semi-synthetic	2002
Tetracenomycin X	Tetracenomycin	50S	Tunnel	*E. coli*	6Y69	Research tool	Natural	2020
Thiostrepton	Thiopeptides	50S	GTP-ase site	*D. radiodurans*	3CF5	Veterinary	Natural	2008
Blasticidin S	Peptidyl nucleoside	50S	P-site	*T. thermophilus*	4V9Q	Phytophar-maceutical	Natural	2014
Kasugamycin	Aminoglycoside	30S	E-site	*T. thermophilus*	2HHH	Research tool	Natural	2006
Spectinomycin	Aminocyclitol aminoglycoside	30S	Neck	*E. coli*	4V56	Clinical	Natural	2014
Neomycin	Aminoglycoside	30S	A-site	*E. coli*	4V52	Clinical	Natural	2014
Tigecycline	Glycylcycline	30S	A-site	*T. thermophilus*	4YHH	Clinical	Semi-synthetic	2015
Tetracycline	Tetracycline	30S	A-site	*E. coli*	5J5B	Clinical	Natural	2016
Streptomycin	Aminoglycoside	30S	A-site	*T. thermophilus*	4DR3	Clinical	Natural	2012
Edeine	Peptide	30S	E-site	*S. cerevisiae*	4U4N	Research tool	Natural	2014
Pactamycin	Aminoglycoside	30S	E-site	*T. thermophilus*	4W2G	Universal inhibitor	Natural	2014
Thermorubin	Anthraceno-pyranone	30/50S	A-site	*T. thermophilus*	4V8A	Research tool	Natural	2012
Negamycin	Pseudodipeptide	30S	A-site	*E. coli*	4WF1	Research tool	Natural	2002
Capreomycin	Tuberactinomycin	30S	A-site	*T. thermophilus*	4V7M	Clinical	Natural	2010
Viomycin	Tuberactinomycin	30S	A-site	*T. thermophilus*	6LKQ	Clinical	Natural	2020
Hygromycin B	Aminoglycoside	30S	A-site	*E. coli*	4V64	Clinical	Natural	2008

Paromomycin	Aminoglycoside	30S	A-site	*L. donovani*	6AZ1	Clinical	Natural	2017
Gentamicin	Aminoglycoside	30S	A-site	*E. coli*	4V53	Clinical	Natural	2007
Amikacin	Aminoglycoside	30S	A-site	*A. baumanii*	6YPU	Clinical	Semi-synthetic	2020

Table 2.6 | rRNA residues that directly contact ribosome-targeting antibiotics using their aromatic bases.

16S rRNA residue	Antibiotics	Position in the alignment (Appendix 2, SI Data S4.1)
G693	Edeine, and Pactamycin	1
A694	Pactamycin	2
A787	Pactamycin	3
A790	Edeine	4
G791	Edeine	5
A792	Edeine, Kasugamycin	6
A794	Edeine, Kasugamycin	7
C795	Edeine, Kasugamycin, Pactamycin	8
C796	Pactamycin	9
G926	Edeine, Kasugamycin	10
C1054	Negamycin, Tetracycline, Tigecycline	11
C1063	Spectinomycin	12
G1064	Spectinomycin	13
C1066	Spectinomycin	14
A1191	Spectinomycin	15
C1192	Spectinomycin	16
G1193	Spectinomycin	17
C1400	Tetracycline	18
C1403	Hygromycin B,	19
C1404	Amikacin, Gentamicin, Hygromycin B, Viomycin,	20
G1405	Amikacin, Gentamicin, Hygromycin B, Neomycin	21
U1406	Amikacin, Gentamicin, Hygromycin B	22
C1407	Amikacin, Gentamicin, Neomycin, Paromomycin, Viomycin	23
A1408	Amikacin, Capreomycin, Gentamicin, Neomycin, Paromomycin, Thermorubin, Viomycin	24
C1409	Amikacin, Capreomycin, Gentamicin, Paromomycin, Thermorubin	25
G1489	Paromomycin	26
U1490	Neomycin, Paromomycin	27
G1491	Amikacin, Capreomycin, Gentamicin, Neomycin, Paromomycin, Thermorubin, Viomycin	28
A1492	Amikacin, Capreomycin, Viomycin	29
A1493	Amikacin, Capreomycin, Hygromycin B, and Viomycin	30
G1494	Amikacin, Capreomycin, Gentamicin, Hygromycin B, Neomycin, Paromomycin, Viomycin	31
U1495	Amikacin, Gentamicin, Hygromycin B, Neomycin, Paromomycin, Viomycin	32
C1496	Amikacin, Gentamicin, Hygromycin B, Neomycin, Viomycin	33
G1497	Amikacin, Hygromycin B	34
U1498	Amikacin	35
G1505	Edeine, Kasugamycin	36

23S rRNA residues	Antibiotics	Position in the alignment (Appendix 2, SI Data S4.2)
U746	Azithromycin, Erythromycin, and Telithromycin	1
G748	Telithromycin	2
A752	Telithromycin	3
A1067	Thiostrepton	4
A1095	Thiostrepton	5
A1096	Thiostrepton	6
U1782	Tetracenomycin X, Quinupristin	7
A1913	Capreomycin, Viomycin, and Thermorubin	8
C1914	Capreomycin, Viomycin	9
U1915	Thermorubin	10
A1916	Thermorubin	11
G2057	Clindamycin	12
A2058	Azithromycin, Carbomycin, Clindamycin, Erythromycin, Quinupristin, and Telithromycin	13
A2059	Azithromycin, Carbomycin, Clindamycin, Erythromycin, Quinupristin, and Telithromycin,	14
G2061	Azithromycin, Carbomycin, Clindamycin, Dalfopristin, Linezolid, Puromycin, Retapamulin, Tiamulin, and Virginiamycin	15
A2062	Carbomycin, Chloramphenicol, Erythromycin, Tetracenomycin X, Dalfopristin, Linezolid, Quinupristin, Retapamulin, Sparsomycin, Telithromycin, Tiamulin, and Virginiamycin	16
C2063	Dalfopristin, Puromycin, Retapamulin, and Virginiamycin	17
G2251	Blasticidin S	18
G2252	Blasticidin S	19
A2439	Blasticidin S, and Virginiamycin	20
A2451	Carbomycin, Chloramphenicol, Clindamycin, Dalfopristin, Linezolid, Puromycin, Retapamulin, Sparsomycin, Tiamulin, and Virginiamycin	21
C2452	Carbomycin, Chloramphenicol, Clindamycin, Dalfopristin, Puromycin, Retapamulin, Sparsomycin, Tiamulin, and Virginiamycin	22
A2469	Avilamycin, and Evernimicin	23
G2470	Avilamycin, and Evernimicin	24
A2471	Avilamycin, and Evernimicin	25
A2478	Avilamycin, and Evernimicin	26
U2479	Evernimicin	27
C2480	Evernimicin	28
A2482	Evernimicin	29
A2503	Azithromycin, Carbomycin, Chloramphenicol, Clindamycin, Erythromycin, Dalfopristin, Linezolid, Retapamulin, Telithromycin, Tiamulin, and Virginiamycin	30
U2504	Chloramphenicol, Clindamycin, Dalfopristin, Linezolid, Retapamulin, and Virginiamycin	31
G2505	Azithromycin, Clindamycin, Erythromycin, Quinupristin, and Retapamulin	32
U2506	Chloramphenicol, Clindamycin, Dalfopristin, Puromycin, and Retapamulin	33
U2533	Evernimicin	34
A2534	Evernimicin	35
G2535	Avilamycin, and Evernimicin	36
G2553	Puromycin	37

G2583	Dalfopristin, and Puromycin	38
U2584	Dalfopristin, Puromycin, and Sparsomycin	39
U2585	Tetracenomycin X, Linezolid, Puromycin, Tiamulin, and Virginiamycin	40
U2586	Tetracenomycin X, and Quinupristin	41
A2587	Tetracenomycin X	42
A2602	Puromycin	43
U2609	Tetracenomycin X, Quinupristin, and Telithromycin	44
C2610	Erythromycin, and Quinupristin	45
C2611	Azithromycin, Carbomycin, Clindamycin, Erythromycin, Quinupristin, and Telithromycin	46

Table 2.7 | Steps of quality control to simplify the 16S rRNA SILVA dataset.

Quality control steps	Criteria	Search words	Filtered records	Sequences left	Unique species	Unique genus
Silva SSU raw data			0	510,508	40,578	17,731
Remove non genomic sequences	Plasmid or phage encoded sequence	Phage, phage, prophage, Plasmid, plasmid	184	510,324	40,577	17,731
Remove organellar encoded sequence	Sequence from mitochondrial or chloroplast origin	Mitochondria, chloroplast	6,237	504,087	39,761	17,401
Remove metagenomic sequence		Metagenome	8,792	495,295	39,761	17,401
Remove poorly characterized sequences	Sequences of unknown taxonomy, unknown species and unknown genus (small caps genus name)	aff., sp., archaeon, associated, bacterium, Candidatus, cf., clone, cluster, culture, environmental, Epixenosomes, eukaryotum, euryarchaeote, -group, Incertae Sedis, isolate, -like, phytoplasma, proteobacterium, snow, symbiont, Thermogales str, unclassified, unidentified, uncultured, unknown family	356,249	139,046	32,631	14,201
Remove low quality sequence	Nucleotides different from the canonical A, G, C and U	Nucleotides designated as: B, D, H, K, M, N, R, S, V, W, X, Y and Z	15,857	123,189	32,631	14,201
Remove records from archaeal and eukaryotic origin	Records annotated as archaea and eukaryotes	Archaea, Eukaryote	28,703	94,486	14,132	2,967
Remove unnatural mutants	Mutant record overlapping with non-mutant record	None	18,427	76,059	14,130	2,967
Remove truncated active sites	Sequence with deletion in any of their drug-binding residues	Ribosomal drug-binding residues designated as gap (-)	13,912	62,147	8,728	2,171
Remove duplicates	Species with more than one record	None	53,194	8,953	8,728	2,171
Remove misclassified records	Eukaryotic species classified as bacteria, bacterial species classified as a bacterial lineage other than their taxonomically characterized lineage and other poorly characterized sequence	None	282	8,671	8,671	2,126

Table 2.8 | Steps of quality control to simplify the 23S rRNA SILVA dataset.

Quality control steps	Criteria	Search words	Filtered records	Sequences left	Unique species	Unique genus
Silva LSU raw dataset			0	95,286	14,912	7,871
Remove non genomic sequences	Plasmid or phage encoded sequence	Phage, phage, prophage, Plasmid, plasmid	182	95,104	14,912	7,871
Remove organellar encoded sequence	Sequence from mitochondrial or chloroplast origin	Mitochondria, chloroplast	2,543	92,561	14,062	7,405
Remove metagenomic sequence		Metagenome	1,516	91,045	14,062	7,405
Remove poorly characterized sequences	Sequences of unknown taxonomy, unknown species and unknown genus (small caps genus name)	aff., sp., archaeon, associated, bacterium, Candidatus, cf., clone, cluster, culture, environmental, Epixenosomes, eukaryotum, euryarchaeote, -group, Incertae Sedis, isolate, -like, phytoplasma, proteobacterium, snow, symbiont, Thermogales str, unclassified, unidentified, uncultured, unknown family	19,929	71,116	13,661	7,134
Remove low quality sequence	Nucleotides different from the canonical A, G, C and U	Nucleotides designated as: B, D, H, K, M, N, R, S, V, W, X, Y and Z	3,440	67,676	11,674	5,898
Remove records from archaeal and eukaryotic origin	Records annotated as archaea and eukaryotes	Archaea, Eukaryotes	11,522	56,154	5,726	1,678
Remove unnatural mutants	Non conserved record overlapping with conserved record	None	158	55,996	5,726	1,678
Remove truncated active sites	Sequence with deletion in any of their drug-binding residues	Ribosomal drug-binding residues designated as gap (-)	9,272	46,724	4,422	1,252
Remove duplicates	Bacterial species with more than one record in our dataset	None	42,260	4,464	4,422	1,252
Remove misclassified records	Eukaryotic species classified as bacteria, bacterial species classified as a bacterial lineage other than their taxonomically characterized lineage and other poorly characterized sequence	None	42	4,422	4,422	1,252
Alphaproteobacterial cleaning						
Extract Alpha proteobacter	Remove all records not corresponding	Alphaproteobacteria	90,814	4,472	1,232	588

ia record from the original Silva dataset	to Alphaproteobacteria					
Remove truncated active sites	Sequence with deletion in any of their drug-binding residues	Ribosomal drug-binding residues designated as gap (-)	166	4,306	1,999	575
Remove poorly characterized sequences	Sequences of unknown taxonomy, unknown species and unknown genus (small caps genus name)	sp., proteobacterium, metagenome, bacterium, uncultured, Incertae, Candidatus, endosymbionts	1,799	2,507	692	250
Remove duplicates	Bacterial species with more than one record in our dataset	None	1,809	692	692	250

2.3 Method 3 – Cryo-EM analysis of ribosomes from the antibiotic-producing bacteria, *Streptomyces.*

2.3.1 Media and buffer

- *Streptomyces* glucose yeast malt agar was prepared using the following items purchased from various suppliers: D-glucose (Formedium), Yeast extract (Gibco), Malt extract broth (Millipore), agar powder (Better equipped), Calcium carbonate (Sigma Aldrich) and Potassium hydroxide (Sigma Aldrich).
- *Streptomyces glucose yeast malt broth* was prepared using the following items purchased from various suppliers: D-glucose (Formedium), Yeast extract (Gibco), Malt extract broth (Millipore) and Potassium hydroxide (Sigma Aldrich).
- Buffer A: Tris(hydroxymethyl)aminomethane (Merck), Hydrochloric acid (Merck), Magnesium acetate tetrahydrate (Sigma Aldrich), and Potassium chloride (Better equipped).
- Polyethylene glycol 20,000 was purchased from Sigma Aldrich

2.3.2 Bacterial species

Two antibiotic-producing species of *Streptomyces* were used in this study. They include *S. griseus* DSM 40759 and *S. fradiae* DSM 40063 purchased from German Collection of Microorganisms and Cell Cultures (DSMZ).

2.3.3 Culture activation of S. griseus DSM 40759 and S. fradiae DSM 40063 freeze dried cell pellets.

As model bacterial species with diverged ribosomal drug-binding sites, we used the antibiotic-producing strains of *S. griseus* (streptomycin producer) and *S. fradiae* (neomycin producer). First, freeze-dried cell pellets of *S. griseus* (DSM 40759) and *S. fradiae* (DSM 40063) obtained from DSMZ German Collection of Microorganisms and Cell Cultures, were rehydrated in 1 mL of distilled water in their respective vials. An aliquot (0.5 mL) of the sample for each organism was inoculated onto freshly prepared *Streptomyces* GYM agar (DSMZ medium 65:

glucose [4g], yeast extract [4g], malt extract [10g], $CaCO_3$ [2g], pH 7.2, agar [20g]) and incubated at 28ºC for 5 days (**Figure 5.1**).

2.3.4 Comparing the growth curve of E. coli, S. griseus and S. fradiae.

Growth curves *of E. coli*, *S. griseus* and *S. fradiae* were determined by first diluting a 22-hour broth culture of each organism in 10 mL GYM broth to a final OD_{600} of approximately 0.1 (*E. coli* = 0.105, *S. griseus* = 0.101, *S. fradiae* = 0.1). An aliquot of 100 µL of the individual organism was inoculated into 900 µL of GYM broth in 24 well plates and incubated in a plate reader at 28ºC for 48 hours with continuous shaking. OD_{630} readings measured every 10 minutes of the cycle (**Figure 5.2a, b**).

2.3.5 Biomass production of S. griseus DSM 40759 and S. fradiae DSM 40063.

For ribosome isolation from *S. griseus*, the agar-grown culture was transferred to 10 mL GYM broth (glucose [3 g], yeast extract [3 g], malt extract [7.5 g], pH 7.2) and incubated in a shaker (SciQuip Incu-Shake Mini) at 150 rpm and 28ºC. Subsequently, 3 mL of this overnight culture was inoculated into 750 mL of GYM broth and incubated at 28ºC, for 49 hours with shaking at 250 rpm until optical density at 600 nm (OD_{600}) value of 0.385 was reached. The liquid culture was then incubated on regular ice for 1 hour at room temperature, and *Streptomyces* mycelia were recovered by centrifuging at 5,000g for 20 minutes at 4ºC yielding a pellet of approximately 4.2 g.

For ribosome isolation from *S. fradiae*, the agar-grown culture was similarly inoculated into 10 mL GYM broth and incubated overnight at 28°C with shaking at 150 rpm. An aliquot (3 mL) of this culture was then transferred into 750 mL GYM broth and incubated under identical conditions for 26 hours until an OD_{600} of approximately 2.216 was reached. After incubation, the culture was placed on ice for 1 hour, and mycelia were recovered by centrifuging at 5,000 g at 4°C for 20 minutes, yielding a pellet mass of 7.4 g.

2.3.6 Ribosome isolation and purification

To lyse *Streptomyces* mycelia, first the pellets were resuspended in buffer A (50 mM Tris-HCl pH 7.5, 20 mM magnesium acetate, and 50 mM KCl) in a 1:1 ratio (w/v) and transferred to 2

mL microcentrifuge tubes containing 0.1 mL of 0.5 mm of zirconium beads (Sigma-Aldrich BeadBug). The cell suspension was lysed using a bead beater (Thermo FastPrep FP120 Cell Disrupter) at 6.5 ms^{-1} for 30 s. To remove cell debris, the lysate was centrifuged at 16,000g for 5 minutes at 4°C and the supernatant collected. To precipitate crude ribosomes from the supernatant, PEG 20,000 (25% w/v) was added to a final concentration of 12.5% w/v. Ribosome pellets were recovered by centrifuging under the same conditions mentioned earlier and stored at -20°C until needed for cryo-EM analysis.

To further purify pigmented *S. fradiae* ribosome, the pellets were first resuspended in buffer A (50 mM Tris-HCl pH 7.5, 20 mM magnesium acetate, and 50 mM KCl) and then the resulting solution was passed through PD Spin Trap G-25 microspin columns (GE healthcare) to remove molecules less than 5 kDa. The corresponding filtrate had an OD_{260} reading of 17.81 and $OD_{260/280}$ of 1.71 corresponding to ribosome concentration of 427 nM. This was split into 40 µL aliquots and stored in -20°C until needed for electron microscopic studies. To estimate the approximate concentration of *S. fradiae* ribosome in the sample, 100 µL of the isolated *S. fradiae* ribosome, was first thawed on ice and loaded on 10-30% sucrose gradient in buffer A. After 3 hours of centrifugation at 35,000 rpm and 4°C in a SW40 rotor (Beckam Coulter). Fractions characteristic of ribosomes was pooled together, and concentration determine through OD_{260} reading.

2.3.7 Negative stain.

To confirm the presence of ribosomes for *S. fradiae* sample, 10 µL aliquot of the ribosome samples was applied on a 300-mesh grid. Excess sample was removed by touching the edge of the grids with Whatman's 50 filter paper. 10 µL aliquot of 2% uranyl acetate was applied to the grid and removed after a few seconds with filter paper. The sample on the grid was left to dry before viewing in the transmission electron microscope (**Figure 5.3a**).

2.3.8 Cryo-EM sample preparation and data collection.

To prepare the samples for cryo-EM analysis, ribosome pellets of *S. griseus* transported on regular ice for approximately 1 hour to the structural biology facility at York University, UK. The pellets were resuspended in modified buffer A (50 mM Tris-HCl pH 7.5, 20 mM $MgCl_2$

and 50 mM KCl) to a final concentration of ~564 nM with an OD_{260} average absorbance unit of 24.51 (**Figure 5.4**). For good particle distribution on Quantifoil grids (R2/2, 200 mesh, copper), the sample was further diluted in buffer A to a 300 nM concentration. Next, an aliquot of 3.5 µL was loaded onto glow discharged grids (20 mA, 0.26 mBar, 60s, negative polarity, Pelco easiGlow), blotted for 2.5 s using blotting force of -10 at 100% humidity and 4ºC, and vitrified by plunging in liquid nitrogen cooled ethane on Vitrobot Mark IV (Thermo Scientific).

To prepare *S. fradiae* ribosome samples for cryo-EM data analyses, crude ribosomes samples of about 40 µL were first thawed on ice. An aliquot of 3.5 µL of the sample was loaded onto glow-discharged (20 mA, 0.26 mBar, 60 s, negative polarity, Pelco easiGlow) Quantifoil holey carbon grids (200 mesh, R1.2/1.3, copper). Then, the grids were blotted for 2.5 s using blotting force of -5 at 100% humidity and 4 ºC and vitrified in liquid nitrogen cooled ethane on Vitrobot Mark IV (Thermo Scientific).

The grids were screened using the Thermo Scientific EPU application on a Glacios electron microscope equipped with a Falcon detector (200 kV), located at the York Structural Biology Laboratory, University of York, UK. Data collection was done using the parameters listed in **Table 2.9**.

Table 2.9 | Cryo-EM data collection parameter for *S. griseus* ribosomes.

Parameters	**Dataset *S. griseus* ribosome**
Voltage (kV)	200
Total dose (e-/A2)	50
Exp. Time (s)	7.94
Number of EER frames	1911
Fluence over vacuum (e/px/s)	8.99
Fluence over vacuum (e/A2/s)	6.29
Magnification	120K
Defocus range (microns)	-2.0 to -0.6
Probe mode	NanoProbe
Spot size	5
Intensity	0.442
C2 Aperture (microns)	50
Calibrated pixel size	1.2
Spherical aberration Cs (mm)	2.7
Acquisition Mode (AFIS/normal)	AFIS

2.3.9 Cryo-EM data processing for S. griseus and S. fradiae ribosomes.

The dataset corresponding to *S. griseus* ribosome (**Figure 5.10**) was processed using Relion 5.0 beta-1(125–127), as summarised in **Appendix 3, SI Figure S5. 1,** using parameters shown in **Table 2.10**. To generate the electron density map of *S. griseus* ribosomes, a total of 495,610 particles were picked from 2,803 micrographs using Laplacian of Gaussian picker (200-330 Å particle diameter, 0.5 s.d threshold). Particle images were initially downscaled 3x and extracted in a 150-pixel box. Two rounds of 2D classification were done to select good particles and 85,421 particles were selected for 3D refinement. These particles were rescaled to full size and re-extracted in a 512-pixel box. Initial 3D refinement resulted in a 3.92 Å resolution map. Further adjustments to the contrast transfer function (CTF) were made to correct for beam tilt, optical distortions, and uneven magnification. The CTF was calculated for each particle, while astigmatism was measured for each image. After improving particle quality and performing 3D refinement, a map with a resolution of 3.1 Å was obtained, allowing for more precise angle measurements for the next stage of focused classification

The dataset corresponding to *S. fradiae* ribosome was processed using cryoSPARC 4.6 (128), as summarized in **Appendix 3, SI Figure S5.3**. To generate the electron density map of *S. fradiae* ribosome, initial analysis of 702,209 particles was picked from 3,983 micrographs using blobpicker was done to generate template for the actual particle picking. Using this template, 966,178 particles were picked from the same micrographs. Following inspection to ensure the accuracy of the particle picking, 466,627 particles were extracted from 3,977 micrographs. Two rounds of two-dimensional (2D) classification were done to select apparent ribosome particles and 250,126 particles picked for 3D refinement. The initial low resolution 3D reconstruction generated from these particles was further refined through homogeneous refinement to 3.05 Å.

Table 2.10 | Cryo-EM data processing parameters for *S. griseus* ribosomes.

Data processing	**Dataset 2 *S. griseus* ribosomes**
Symmetry imposed	C1
Initial particle images	371,502
Final particle images	85,421
Map resolution (Å)	3.1
FSC threshold	0.143
Map local resolution range	2.5 – 13

2.3.10 Model building, refinement and deposition.

The atomic model of *S. griseus* ribosome was built using AlphaFold predicted models (129,130) and Coot v0.8.9.2(131) and. As a starting model, we used atomic models of the 5S, 16S, and 23S rRNAs of *S. griseus* (accession number: NZ_JBFBHO010000061) generated by AlphaFold 3 and AlphaFold models of the *S. griseus* NCTC 7807 ribosomal proteins generated by AlphaFold DB version 2022-11-01. These models were fitted into the cryo-EM electron density maps using ChimeraX v1.9 and refined in Coot by checking the density validity analysis and refining using real-space refinement and rigid-body refinement tools.

The tRNAs were modelled by docking the E-site tRNA from PDB 8V9J and the P-site tRNA from PDB 7K00 into the electron density corresponding to both tRNAs.

2.3.11 Homology search of ribosomal proteins bL37 and bS22.

Bacterial homologs of ribosomal proteins bL37 and bS22 were identified by running a BLAST search for each protein on UniProt using these identities A0QTP4 (bL37) and A0QR10 (bS22) from *M. smegmatis* (strain ATCC 700084/mc^2 155) located within gene loci Msmeg_1916 and Msmeg_0945, respectively. The BLAST run resulted in 195 apparent homologs of bL37 and 250 for homologs of bS22. However, none of these apparent hits included for any of the two *Streptomyces* species (*S. griseus* and *S. fradiae*) that I was interested in.

As an extra measure to further improve the quality of my search, I used a more rigorous, sensitive and advanced database, HMMER v3.4 (132) to search for homologs of bL37 and bS22 ribosomal proteins. HMMER uses profile hidden Markov models to identify homologs of biological sequences. Using these parameters (Cmd: phmmer -E 1 --domE 1 --incE 0.01 --incdomE 0.03 --mx BLOSUM62 --pextend 0.4 --popen 0.02 --seqdb UniProt), we found 225 apparent homologs for bL37 and 3,336 homologs for bS22. The bL37 homologs are present in only a few bacterial species in the Actinomycetota phylum, while bS22 homologs were widespread across 13 bacterial and 1 eukaryotic taxonomic group.

To remove unclassified and poorly annotated records, I first removed records with no taxonomic assignment (i.e., records without information about their phylum). Next, I removed

records unclassified records characterized by the presence of any of these words: ‘Candidatus’, ‘bacterium’ or ‘sp.’ in their taxonomic assignment. This reduced the taxonomic assignment of bacterial phyla to only 3 phyla and 1,710 unique species for bS22 and 122 unique Actinomycetota species for bL37 (**Appendix 3, SI Tables S5.1 and S5.2, Figure 5.14**).

Chapter 3. Evolution of drug-binding residues in eukaryotic ribosomes.

3.1 Summary

Drugs that target eukaryotic ribosomes are becoming increasingly important as research tools and potential therapies against cancer and pathogenic eukaryotes. However, in the absence of comparative studies, we currently do not know how many eukaryotes possess ribosomal drug-binding sites identical to those in humans, and how many significantly differ from humans. To address this, we traced the evolutionary history of individual ribosomal drug-binding residues from the emergence of eukaryotes to the present day. We found that ribosomal drug-binding sites are divergent across eukaryotic clades, with some of the clades exhibiting more substitutions in their ribosomal drug-binding sites compared to humans than humans do compared to bacteria. Overall, our work provides a resource for understanding the evolutionary divergence of drug-binding sites in eukaryotic ribosomes, which may inform the use of ribosome inhibitors as research tools and lineage-specific drugs against eukaryotic parasites.

3.2 Introduction

Small molecule inhibitors of eukaryotic ribosomes are widely used as research tools and experimental medicine (133–138). With over twenty chemical families available for ribosome targeting, we can arrest ribosomes at every step of their work cycle (133). This enables the use inhibitors like puromycin, cycloheximide and others in ribosome profiling (138), and drugs like homoharringtonine and ataluren treat cancer and genetic disorders (139–141). Furthermore, ribosome inhibitors can be photocaged to halt protein synthesis with a light signal, facilitating studies of protein synthesis in neurons during memory formation (142–144).

This widespread use of ribosome inhibitors relies on the assumption that ribosomes are highly conserved, allowing commonly studied organisms, including humans, to serve as generalized model eukaryotes (133,145). However, emerging evidence indicates that ribosomes from some eukaryotes have divergent drug-binding sites and varying affinities to ribosomal inhibitors. For example, the aminoglycoside-binding site of the ribosome is divergent in the parasitic fungi Microsporidia (due to the 18S rRNA substitution A1491U) and pathogens *Leishmania* and

Trypanosoma (bearing the substitution C1409U) (146,147,95). Both these substitutions increase aminoglycoside resistance (148,149). However, in the absence of comparative analyses, it is unknown whether eukaryotes with divergent drug-binding sites are exceptions or a common evolutionary trend. Consequently, we do not know how many eukaryotes have identical or different ribosomal drug-binding sites to humans.

The lack of such comparative studies originates in part from the problem of spurious mutations in biological sequences. Previous studies have shown that datasets of biological sequences may contain errors resulting from incorrect base calls during sequencing, assembly mistakes, or erroneous annotations of sequencing data (150,151). Because many biological sequences are assembled from multiple shorter reads, public repositories were estimated to contain up to 20% chimeric sequences, where different segments of a single sequence originate from distinct species rather than a single source. Other prevalent artifacts include sequencing errors, contamination from DNA of organelles, plasmids, and viruses, and the presence of pseudogenes (150,151).

This problem of a high prevalence of pseudogenes is especially acute for eukaryotes. For example, a typical bacterium like *E. coli* bears only 10-20 pseudogenes, equating to roughly one pseudogene per 300 genes (152). By contrast, the human genome bears at least 19,724 pseudogenes or roughly one pseudogene for each protein-coding gene (153). The pseudogene count is even higher in other eukaryotes, especially plants, with barley, for example, bearing 89,440 pseudogenes per 35,000 genes of its genome (154). As a result, evolutionary analyses of ribosomal genes are typically focused on larger structural changes, such as insertions or deletions, especially in bacterial species (155–160), leaving a knowledge gap about the variability of the ribosomal drug-binding residues across eukaryotes.

Here, we address this problem by implementing a novel comparative approach that resolves common problems in public sequencing data repositories—such as chimeric sequences, species misannotations and pseudogenes—thereby ameliorating the impact of database errors on our analyses and conclusions (150,151). This allowed us to compare rRNA sequences of ribosomal drug-binding residues in 8,563 eukaryotes from all major branches of eukaryotes, identify their

most common variants and trace their evolutionary history throughout 2 billion years of eukaryotic history.

3.3 Results

3.3.1 Mapping substitutions in ribosomal drug-binding sites during eukaryotic evolution.

To help resolve the problem of pseudogenes and better distinguish signal from noise in eukaryotic rRNA datasets, we devised an approach based on similarity of rRNA sequences in closely related species on the tree of life (**Figure 3.1**). In this approach, we filtered out sequence variants that are present only in a single sequence, single rRNA operon, single strain, or a single species (**Figure 3.1a**), but not in neighbouring species on the tree of life (**Figure 3.1b**). This allowed us to identify changes at drug-binding sites that are present in at least two closely related eukaryotic species, thereby helping distinguish false positives and very recently acquired mutations from ancient, genuine evolutionary changes that represent common features of eukaryotic clades (**Figure 3.1**).

Using this approach, we assessed the conservation of 58 ribosomal drug-binding residues in rRNA sequences from the SILVA database, which is the most complete database of non-redundant rRNA sequences (**Methods**, **Table 2.1**) (88). We then traced the evolutionary history and conservation of individual drug-binding residues across 8,563 (**Appendix 1, SI Data S3.5**) representative eukaryotes from 5,148 distinct genera. Thus, we were able to reconstruct the evolution of drug-binding residues in eukaryotic ribosomes at the levels of single residue, single species and single ribosome-targeting drug (**Figure 3.2, 3.3**).

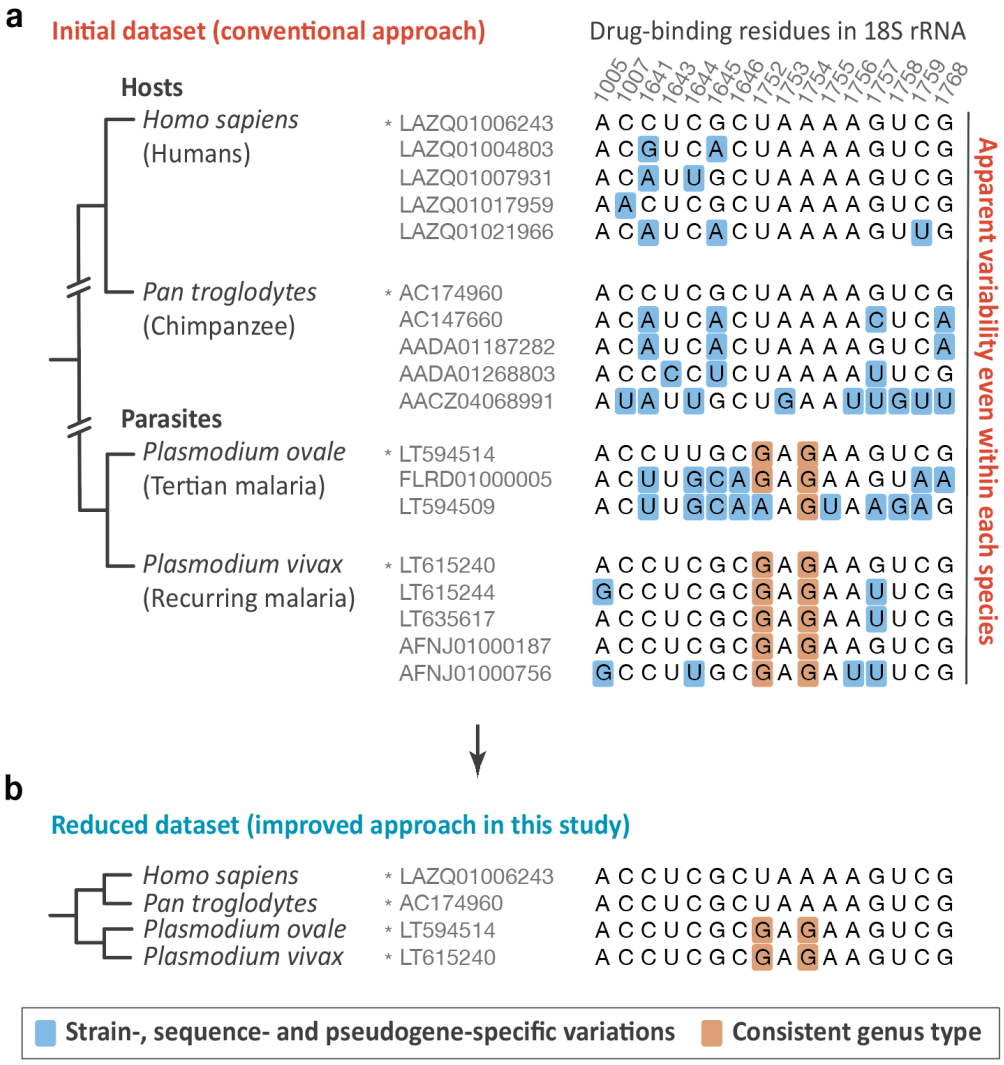

Figure 3.1| Evolutionary proximity reveals common variants at drug-binding sites in eukaryotic ribosomes.

(a) Multiple sequence alignments compare the ribosomal drug-binding residues of the 18S rRNA from a few representative eukaryotes, including humans and chimpanzees, as well as *Plasmodium* parasites. The rRNA sequences are shown as deposited in the SILVA database, which is the most commonly used database for studying rRNA sequences across species. The panel illustrates that the ribosomal drug-binding residues appear to be highly variable even within a single species, but this seeming variability may be attributed to pseudogenes. **(b)** Multiple sequence alignment shows the reduced dataset of 18S rRNA sequences, which includes only those sequences from panel **(a)** that are conserved between immediate neighbours on the tree of life. This approach illustrates the key idea of our study: we reasoned that if a certain rRNA substitution is ancient, it will be present not only in a given species but also in its neighbour on the tree of life (e.g., other eukaryotes from the same genus). By contrast, mutations that are either most recently acquired or false positives (due to misannotations, sequencing errors, or pseudogenes) should be present only in a single sequence, single rRNA operon, single strain, or a single species, but not in neighbouring species on the tree of life. This approach helps eliminate pseudogenes and reveal the most common variants of the ribosomal drug-binding sites of eukaryotic ribosomes.

3.3.2 Drug-binding sites of the small subunit are highly variable across eukaryotes.

Our analysis showed that the large and small ribosomal subunits have strikingly dissimilar conservation of their drug-binding rRNA nucleotides (**Figure 3.2, Appendix 1, SI Data S3.3 and S3.4**). The large subunit exhibits an exceptionally high degree of sequence conservation: U2393 and G2422 were the only variable drug-binding residues, having been replaced with As in the pathogenic yeast *Malassezia*, a causative agent of seborrheic dermatitis and tinea versicolor (161). Thus, the large subunit of eukaryotic ribosomes appears to have the uniform structure of the drug-binding sites.

In stark contrast, in the small subunit residues, the majority of drug-binding residues were variable, including 15 of the 26 residues in 18S rRNA. Some variations—such as A787C, C796U, and C1404U—were rare, occurring in only 20 to 40 eukaryotes within our dataset. Other variations, including U1489G/C and A1491G/C/U, were highly prevalent, each observed in nearly 2,000 species. Notably, we observed variations not only in rRNA residues that differ between bacteria and humans but in residues currently viewed as universally conserved (**Figure 3.2**). Thus, we found that 23% of eukaryotes harbour between one and four fixed changes in their rRNA drug-binding residues compared to humans.

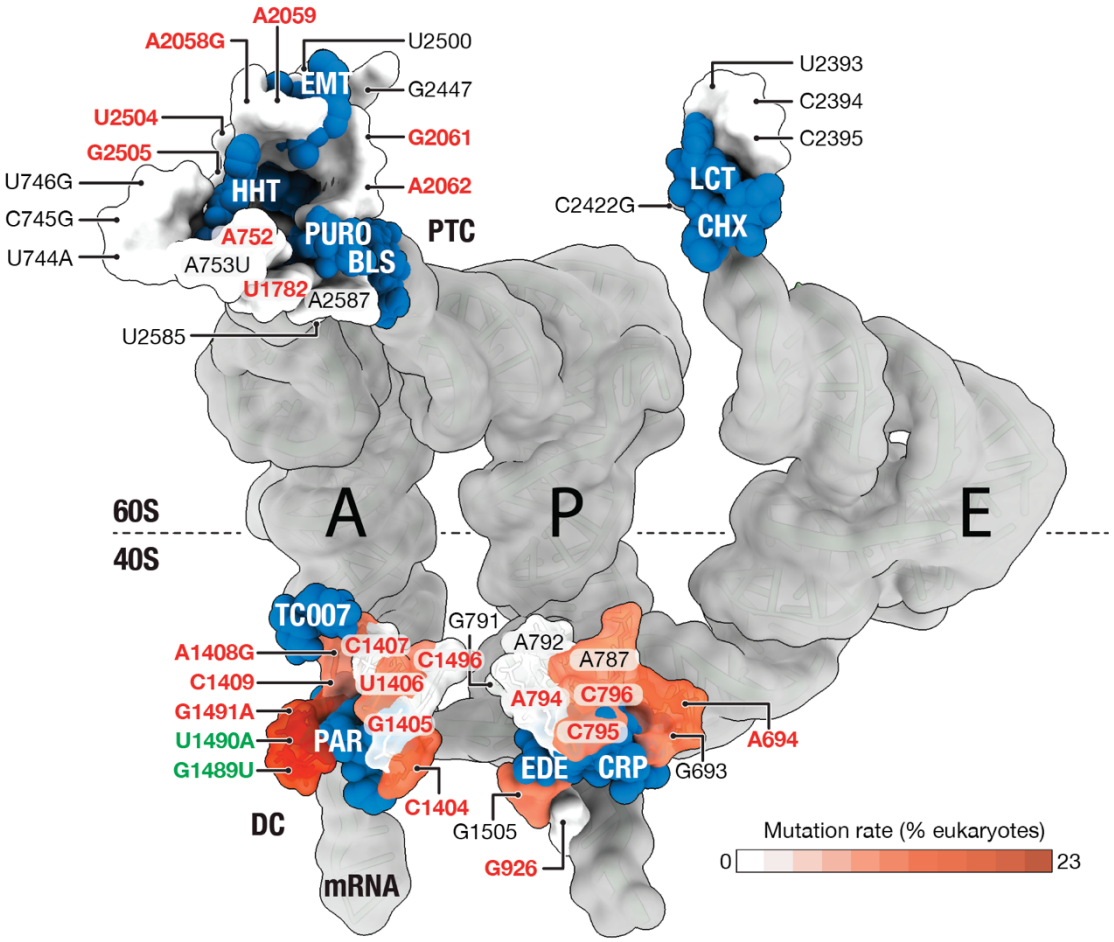

Figure 3.2 | Most variable drug-binding residues of eukaryotic ribosomes.
Superposed structures highlight the binding sites for ribosome-targeting drugs (in blue) in the ribosome, with each drug-binding residue of eukaryotic ribosomes colored by its conservation across the 8,563 representative eukaryotic sequences analyzed in this study. The figure represents the superposition of multiple PDB structures that capture eukaryotic ribosomes in complex with drugs, as listed in (**Table 2.1**). The drugs are labeled as follows: EMT – emetine, HHT – homoharringtonine, PURO – puromycin, BLS – blasticidin S, LCT – lactimidomycin, CHX – cycloheximide, PAR – paromomycin, EDE – edeine, CRP - cryptopleurine. The figure shows that, in the large ribosomal subunit, drug-binding residues are highly conserved across eukaryotes, suggesting that all eukaryotes may share a uniform recognition of drugs that target the large ribosomal subunit. However, the drug-binding residues of the small ribosomal subunit are highly variable, both in the decoding centre and in the mRNA channel of the ribosome, which illustrates the frequent occurrence of species-specific features of the drug-binding pockets in the small subunit of the eukaryotic ribosome.

3.3.3 The evolution of drug-binding residues of the eukaryotic ribosome.

We next traced the evolutionary history of variations for individual drug-binding residues of eukaryotic ribosomes (**Figure 3.3**). This allowed us to estimate the evolutionary age of these variations and their occurrence across eukaryotes. Previously, the last common ancestor of modern eukaryotes, LECA, was estimated to have emerged around 1.8-2.3 billion years ago (162,163), with the divergence of stem eukaryotes from archaea occurring somewhat earlier (2.7-2.2 Ga, (163)). Our analysis indicates that some of the key differences between bacterial and eukaryotic ribosomes in terms of drug sensitivity were already established before the divergence of eukaryotes from Archaea. For example, our analysis indicates that G1408 and A1491 in 18S rRNA (compared to A1408 and G1491 in bacterial 16S rRNA) were already established prior to the archaea-eukaryote divergence Importantly, each of these mutations has been characterized as a critical determinant for the species-specific recognition of aminoglycoside antibiotics: they prevent the binding of paromomycin in the ribosomal decoding centre due to the steric clash between the rRNA base and the antibiotic (133), leading to approximately 1,000-fold lower ribosome affinity for aminoglycosides (148). Our analysis showed that the major lineages of eukaryotes accumulated additional drug-binding variants during their early diversification.

Specifically, after Discoba separated from the other eukaryotes approximately 1.4 to 1.8 billion years ago (163), it acquired the substitution U1489C. Subsequently, most Discoba, including the branches of Jakobida and Discicristata, also acquired the substitution C1409U. As a result, these species have gained a structurally distinct drug-binding site that bears the C1409U and U1489C substitutions compared to humans. Notably, these substitutions have been previously characterized in the ribosomal structures of *Trypanosoma* and *Leishmania* species (146,147,95,149). Our analysis shows that these mutations are evolutionarily ancient and represent a common characteristic not only of *Trypanosoma* and *Leishmania* but of the entire eukaryotic clade of Discoba, which includes human pathogens *Naegleria fowleri* and *Balamuthia mandrillaris*.

The TSAR lineage also acquired conserved drug-binding site changes after diverging from other eukaryotes, including U1489G as well as G1491A, which reverted the sequence to make

it identical to the bacterial variant, A1491. Both these substitutions have been fixed and shared by all species of this branch, including modern plants, algae, and single-celled eukaryotes from SAR species, including *Plasmodium* species and other human pathogens.

The Amorphea branch further split into the ancestor of modern fungi and animals (Obazoa), most of which have retained the ancestral ribosomal state, and the branch of amoeba-bearing Amoebozoa, which have acquired the mutation of the A1498 base shared by all members of this clade, including human pathogens *Entamoeba*, *Acanthamoeba* and others.

These early mutational events were later followed by the acquisition of numerous additional mutations, resulting in more than 60 unique combinations of the sequence of drug-binding residues among modern eukaryotes (**Figure 3.3, Appendix 1, SI Data S3.3, and S3.4**).

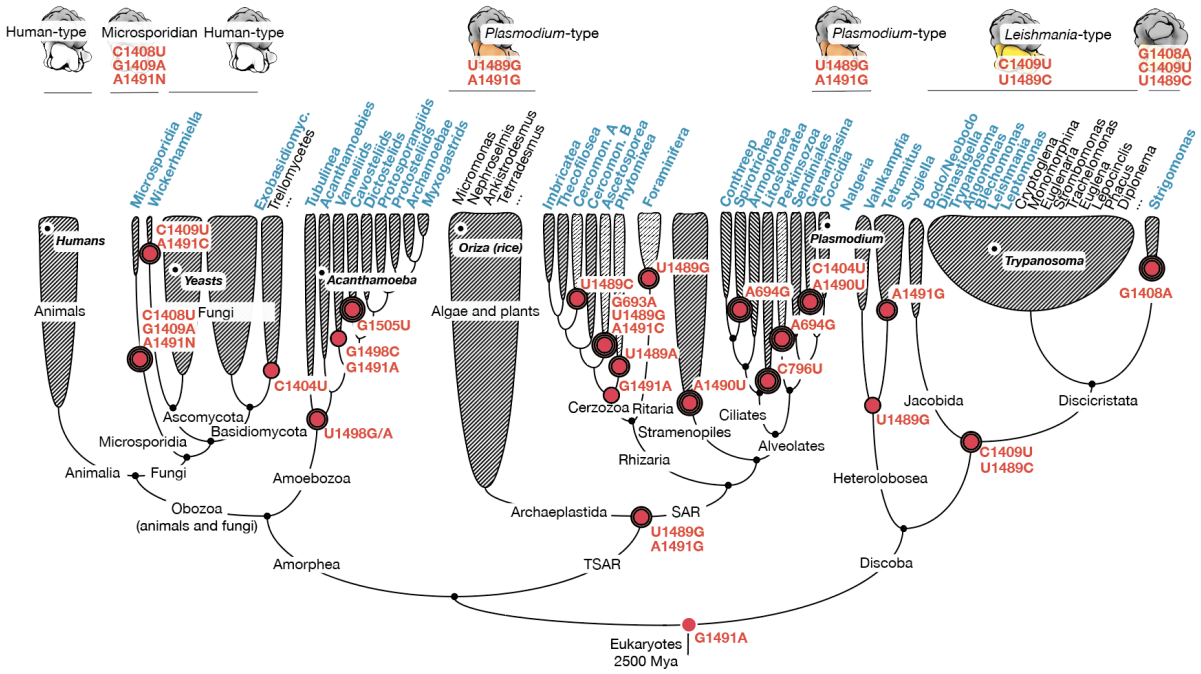

Figure 3.3 | Most common variants of the drug-binding residues of eukaryotic ribosomes. The eukaryotic tree of life shows the evolutionary history of the naturally occurring variations in the drug-binding residues of the eukaryotic ribosome. Genera highlighted in blue correspond to branches including parasitic species. Red circles indicate evolutionary events related to the acquisition of substitutions in ribosomal drug-binding sites and provide an estimated age of these mutations based on the existing phylogenetic evidence listed in (**Appendix 1, SI Data S3.3 and S3.4**). Overall, the figure shows that yeasts and humans, traditionally viewed as representative model eukaryotes, in fact bear relatively unusual ribosomal binding site of aminoglycoside antibiotics—due to the residue A1491 compared to G1491 in the majority of eukaryotes from non-animal and non-fungal branches. Therefore, almost all other eukaryotes have structurally distinct binding sites for aminoglycoside antibiotics, where G1491 is present instead of A1491, with some branches (e.g., Discicristata) bearing additional mutations in this and other drug-binding sites of the ribosome (e.g., C1404U, G1408A and C1409U) compared to humans.

3.3.4 Certain clades of fungi bear altered ribosomal drug-binding sites compared to humans.

Our further analysis of the eukaryotic tree of life showed that, although most animals and fungi share conserved drug-binding residues, certain fungal lineages have gradually acquired multiple changes at these sites compared to humans (**Figure 3.4**). This was observed, for example, in the deep-branching fungal lineage Microsporidia, all members of which are fungal parasites of animals, including humans (164). In Microsporidia, the initial mutation likely occurred shortly after the split into *Nematocida* species, which retained human-type (that is, ancestral) drug-binding sites, and the remaining microsporidia, which acquired a mutation in the decoding centre at residue A1491, which has been identified as a key determinant of species specificity for aminoglycoside antibiotics (148,133). Subsequent evolution of microsporidia has led to additional mutations in the decoding centre, including C1489U in the *Vavraia* branch and G1048A in species of *Enterocytozoon*. Hence, most microsporidia exhibit a more dissimilar decoding centre compared to humans than humans compared to *E. coli*.

The remaining fungal lineages were further split into several clades, including Ascomycota and Basidiomycota, with specific branches within these clades acquiring mutations in both the aminoglycoside-binding site and the mRNA channel. These branches include the fungi *Trellomycetes* and *Exobasidomycetes* (C1409U), which encompass pathogenic organisms, such as *Tilletia horrida* (C1404U), a common rice pathogen, and *Gjaerumia minor* (C1404U, C1407U, A1494C), implicated in keratitis of humans. Overall, among the 1,201 fungal species analyzed in our study, we found approximately 7% to exhibit dissimilar ribosomal drug-binding sites compared to humans, due to variations in the 18S rRNA bases A787, C1408, C1409 and A1491 (*E. coli* numbering is used throughout the manuscript. Please refer to Table S2 for the correspondence between species) within the decoding centre and the mRNA channel of eukaryotic ribosomes.

Thus, we found that most fungi have identical ribosomal drug-binding residues compared to those in humans, suggesting that ribosome-targeting drugs are unlikely to serve as broad-spectrum antifungal agents. However, species from certain fungal clades, particularly

microsporidia, possess multiple mutations in their drug-binding residues compared to humans, indicating the potential for their safe lineage-specific targeting.

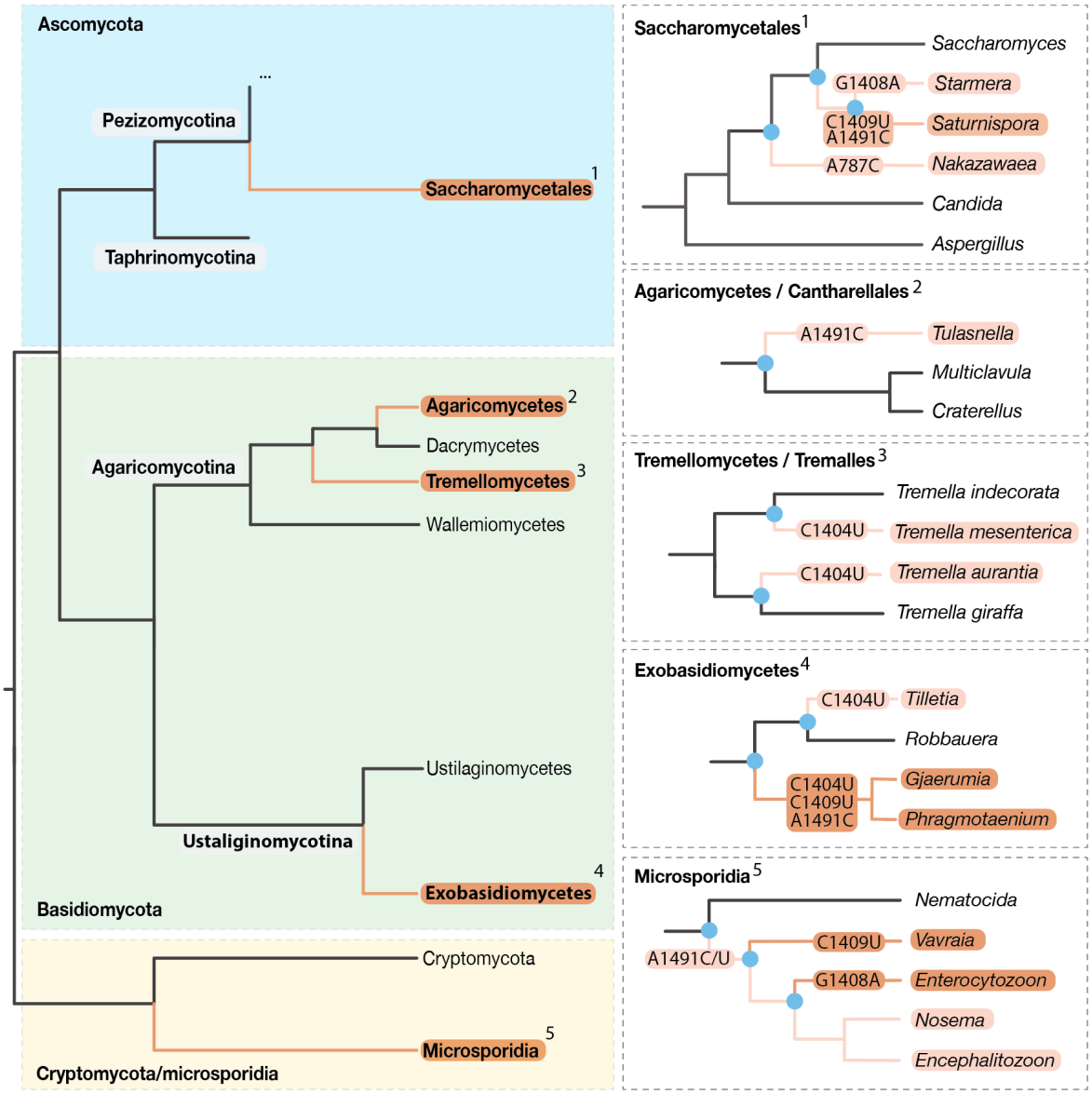

Figure 3.4 | Many fungi bear derived ribosomal drug-binding sites compared to humans. The schematic structure of the fungal tree of life shows that, after separating from animals, some lineages of fungi, such as Microsporidia and Saccharomycetales, continued to diversify their ribosomal drug-binding residues. In total, of the 1,253 genera of fungi analysed in this study, 101 (~7%) were found to carry one or more mutations in their ribosomal drug-binding residues compared to humans.

3.4 Discussion

3.4.1 Animals and fungi possess distinct ribosomal drug-binding sites compared to most other eukaryotes

In this study, we have assessed the evolutionary history and conservation of ribosomal drug-binding residues across the eukaryotic domain of life. We determined the natural variations for each of the 58 ribosomal drug-binding residues in 8,563 representative eukaryotes, enabling us to identify lineages with dissimilar residues compared to humans. One major finding of our work is that yeasts and humans, traditionally used as model organisms for studying ribosome-targeting drugs in eukaryotes, exhibit rather unusual variants of drug-binding residues compared to most other eukaryotes. Specifically, yeasts and humans, along with most Amorphea species, appear to have kept the ancestral sequence variant of the drug-binding sites, whereas the other branches of eukaryotes have acquired substitutions in the drug-binding residues G1408, C1409, A1491 of the 18S rRNA. Importantly, some of these substitutions have reverted the rRNA sequences of eukaryotic rRNA to its bacterial-type variants (e.g. in the 18S rRNA residue G1491 in Diaphoretickes).

One important implication of this finding is how we currently study eukaryotic ribosome targeting with small molecules. From the perspective of drug sensitivity, ribosomes from different organisms are often separated into two major groups: bacterial-type and eukaryotic-type (145). This separation is based on the overall protein content and the presence of rRNA expansion segments, allowing the use of organisms like *E. coli* or *T. thermophilus* as representative bacteria and organisms like yeasts or humans as representative eukaryotes (133). However, our work shows that this division, while helpful in many studies of eukaryote-specific ribosomal proteins and rRNA expansion segments, is incomplete when applied to the drug-binding residues of the eukaryotic ribosome. For instance, some groups of eukaryotes, such as SAR, share more similarities in their drug-binding residues with bacteria than with humans due to the convergent evolution of the 18S rRNA variation A1491G (165). Additionally, some others, like microsporidia, are highly dissimilar to both bacteria and humans. Instead, our work shows that the simplistic division of ribosomes into bacterial and eukaryotic is mostly accurate only when applied to the large ribosomal subunit. By contrast, a range of different residues, and

so potentially drug-binding sites and sensitivities, are found across eukaryotes in the small subunit of the ribosome, including (roughly) an animal/fungi-type, *Leishmania*-type, and *Plasmodium*-type, among many others.

3.4.2 Many of the naturally occurring variations in ribosomal drug-binding sites predate the origin of antibiotic-producing bacteria.

Since when have eukaryotic ribosomes started to diversify their drug-binding residues? And what were the evolutionary forces driving this diversification of ribosomal drug-binding residues? Our mapping of the rRNA sequence variants on the tree of life allows us to gain insights into both of these questions. According to this analysis, substitutions at the drug-binding sites of eukaryotic ribosomes began to accumulate from the origin of the first eukaryotic branches >1.3 Ga (163), with some mutations mapping to the stem lineages of major groups including Amorphea, Discoba and TSAR. This means that common 18S rRNA variants such as A1491G in SAR, and G1409A and C1489U in Discoba species, emerged significantly earlier than the antibiotic-producing genus *Streptomyces*, which is responsible for most natural ribosome-targeting drugs known to date and is estimated to be 382 million years old (166). This analysis suggests that the evolution of drug-binding residues in nature, at least during early eukaryotic evolution, differs from their evolution in clinical settings and has likely been driven by factors other than the existence of antibiotics in the environment.

3.4.3 Implications for species-specific targeting of eukaryotic ribosomes.

Previous studies showed that mutations in individual rRNA drug-binding residues can confer drug resistance by reducing drug-affinity as much as 1,000 fold (212). In this study, we showed that some of these variations, previously observed in clinical isolates of human pathogens or laboratory-engineered resistant strains, are widely present in nature.

Our analysis, along with the previously obtained experimental studies, suggests that some of the naturally occurring variations are likely neutral. Specifically, variations of residues G1489U and U1490A have been characterized as neutral for ribosome targeting by aminoglycoside drugs, as demonstrated through ribosome mutagenesis in *Mycobacterium smegmatis* and *E. coli* (168,69,94).

However, other variations, including 13 residues of the 18S rRNA, have been shown to alter the shape of the drug-binding pocket and define species-specific ribosome targeting with drugs (red labels in **Figure 3.2** and **Tables 4.1 and 4.2**). For example, the variations A1408G and G1491A in the ribosomal decoding site have been characterized as determinants of species-specific binding of aminoglycoside antibiotics, allowing for the safe targeting of bacterial ribosomes (A1408 and G1491) without affecting ribosomes in humans (G1408 and A1491) (164). Experiments in yeasts showed that when eukaryotic ribosomes are mutated to introduce the bacteria-specific variant G1491 in the 18S rRNA (instead of A1491), they develop aminoglycoside sensitivity similar to *E. coli*, evidenced by a 60-fold higher sensitivity to the antibiotic paromomycin. Similarly, mutating the G1408 site to the bacteria-type A1408 resulted in a ~200-fold increase in sensitivity of yeast ribosomes to the antibiotics neomycin and kanamycin A (148). Our analysis reveals that these variants are not limited to bacteria, but are also prevalent across eukaryotes, naturally occurring in up to 23% of eukaryotic species.

Overall, our findings present both concerns and opportunities for using drugs to target eukaryotic ribosomes. We show that the drug-binding sites of eukaryotic ribosomes often exhibit significant variability across different eukaryotic lineages, thus necessitating caution and additional analyses prior to applying ribosome-targeting drugs to non-model eukaryotes. On the opportunity front, our work suggests the possibility for lineage-specific ribosome-targeting drugs across a wide variety of eukaryotes. Notably, we demonstrate that structural variants identified in *Leishmania* and *Plasmodium*, previously considered idiosyncratic to rare eukaryotic lineages, are in fact common characteristics of entire eukaryotic supergroups. What's more, some lineages of eukaryotes have more dissimilar ribosomal drug-binding sites compared to humans than humans do compared to bacteria. Since eukaryotic pathogens pose significant and emerging global health challenges, our work suggests that novel therapeutics can be found among new generations of ribosome inhibitors that target lineage-specific substitutions in the rRNA.

Chapter 4. Evolution of drug-binding residues in bacterial ribosomes.

4.1 Summary

Ribosomes from certain bacteria possess divergent drug-binding sites compared to those of *Escherichia coli*, leading to natural evasion or hypersensitivity to antibiotics. However, in the absence of systematic studies, it is unknown whether this observed divergence is a rare exception or a common occurrence among bacterial species. Here, we address this question by reconstructing the evolutionary history of drug-binding residues of the ribosome from the origin of bacteria to the present day. This analysis reveals the extent of natural diversity of ribosomal drug-binding sites between bacterial species, which may inform the development of species-specific antimicrobials and a more accurate and personalized choice of ribosome-targeting drugs for a given pathogen.

4.2 Introduction

When *Escherichia coli* was introduced as a model for studying bacterial ribosomes, it rapidly became a foundational system for understanding how ribosomes interact with antibiotics (167–170). However, subsequent studies revealed that the sequence of the ribosomal drug-binding residues is not strictly conserved across bacteria, leading to variation in ribosome affinity for antibiotics (173–176,155,69,115,177,178). Specifically, species of the human pathogens *Propionibacteria* bear the naturally occurring 16S rRNA substitution G1491U (compared to *E. coli*), which confers intrinsic resistance to aminoglycosides (177). Some species of *Mycoplasma* carry the 23S rRNA substitution G2057A, which confers resistance to macrolides (178). And the bacterium *Thermus thermophilus* carries the substitutions U1782C/U2586C in the 23S rRNA, rendering this species resistant to tetracenomycin X (176). Without systematic studies, it is currently unknown whether this observed variation in the ribosomal drug-binding sites is rare or common among bacteria.

This lack of systematic studies was caused by two main issues. First, there is a data availability bias, as the majority of genomic sequences for bacterial species belong to only two phyla, Proteobacteria and Firmicutes (179). Consequently, Proteobacteria may be represented by over 10,000 genome sequences for a single species, while other phyla have only about 20 sequences combined for all species. This disparity skews average conservation scores, favouring rRNA conservation in Proteobacteria and Firmicutes over all bacteria.

The second, more challenging issue is the occurrence of false-positive changes in biological sequences. Previously, datasets of biological sequences were shown to bear spurious mutations resulting from errors of sequencing, assembly or annotation of sequencing data (150,180). Particularly, since many biological sequences are assembled from multiple shorter reads, public repositories were estimated to contain up to 20% chimeric sequences in which different parts of a given sequence originate from different species instead of a single species (150,180). Other common errors include sequencing errors, contamination with viral DNA and plasmids, and misannotation of species (150,180). Consequently, many bacterial species exhibit hundreds of alternative sequence variants of a single gene, complicating the distinction between conserved changes fixed in a lineage from rare mutations and sequence errors.

We addressed these challenges by developing an approach that simplifies the analysis of large biological sequence datasets based on the phylogenetic proximity of bacterial species. This allowed us to assess natural variation at the 82 individual ribosomal drug-binding residues across 8,671 representative species from all bacterial phyla, providing the first comprehensive atlas of the evolutionary diversity of these medically relevant residues in the active sites of bacterial ribosomes.

4.3 Results

4.3.1 Evolutionary-based filtering reveals common variations in drug-binding sites of bacterial ribosomes.

To assess the conservation of drug-binding residues in bacterial ribosomes, we used the public repository of rRNA sequences known as the SILVA dataset NR99 v138.1 because this is the most complete dataset of non-redundant rRNA sequences. This dataset comprises 510,508 sequences for 16S rRNA and 95,286 sequences for 23S rRNA (88). We first simplified the dataset by discarding all rRNA sequences of unclear evolutionary origin, and then excluded sequences that originate from phages, plasmids, and eukaryotic hosts of pathogenic bacteria, as well as those with truncations in ribosomal active centres (see **Methods**). However, even the simplified dataset contained up to 800 alternative rRNA sequences for individual species (**Appendix 2, SI Data 4.1 and 4.2**). This illustrated a common obstacle in analysing the evolutionary variations across large groups of species: for example, for *E. coli* alone, we observed 39 dissimilar variants of the ribosomal drug-binding residues, which was partly due to the presence of sequences from clinical strains (**Figure 4.1a**).

Therefore, we further simplified the dataset based on the evolutionary proximity of species in the tree of life. In this approach, we selected one representative rRNA sequence per species, choosing the sequences that are most similar to sequences from the closest relatives in the tree (**Figure 4.1b**). This approach discarded sequence variants that were specific to a single sequence or strain of a given species but minimized the risk of detecting false positives and thereby revealing the most conserved sequence variants in each bacterial genus (**Figure 4.1b**). Using this approach, we identified the most common variants of 82 drug-binding residues in rRNA residues in 8,671 bacterial species (**Appendix 2, SI Data S4.9**) and traced the evolutionary origin and age of these variants (see **Tables 2.6, Figure 4.2**). We have summarized our findings in (**Appendix 2, SI Data 4.3, and4.4**) to provide the most complete atlas of the conservation of ribosomal drug-binding sites across bacteria.

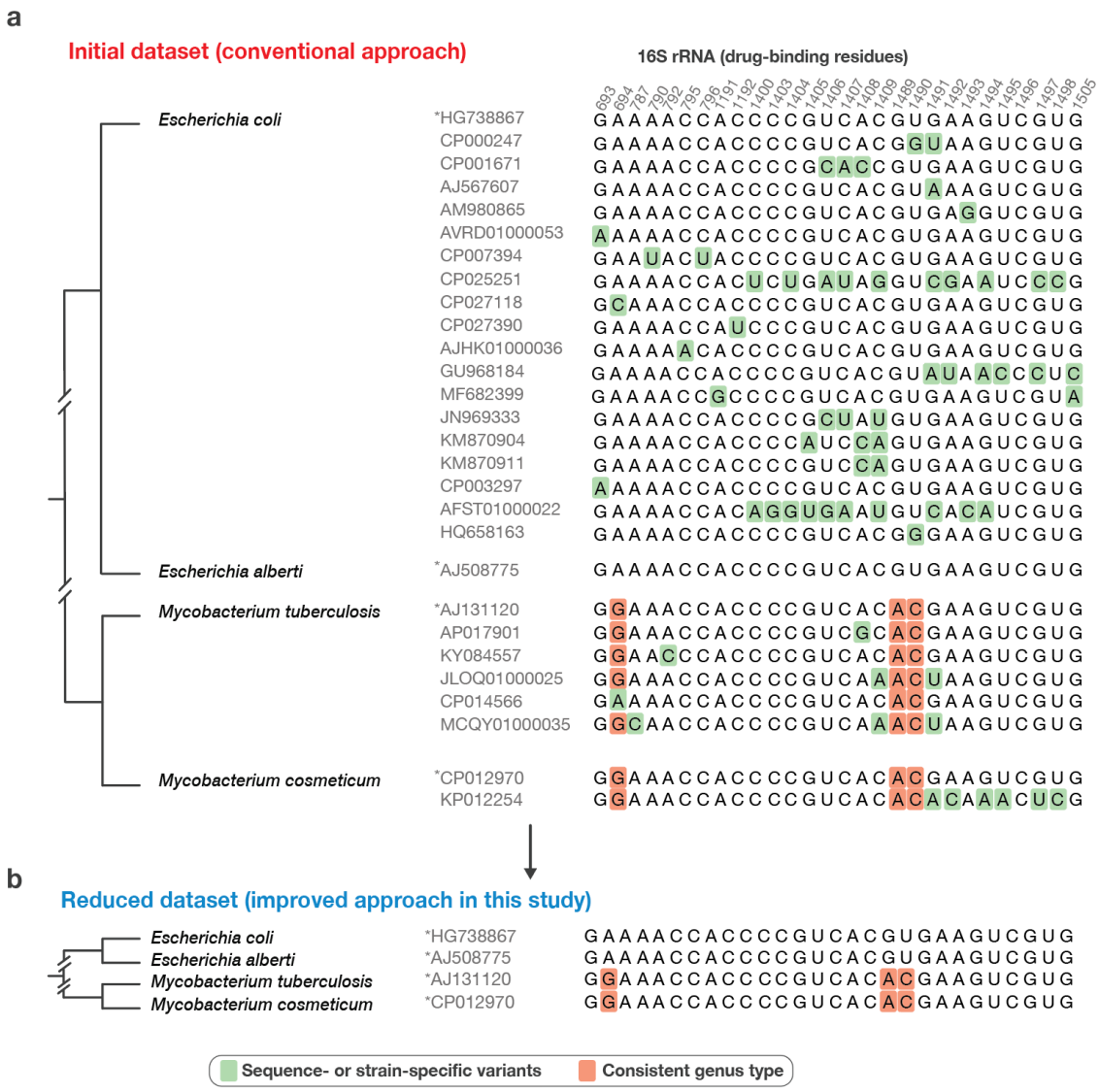

Figure 4.1 | Evolution-based filtering reveals common natural variants of the drug-binding residues of bacterial ribosomes.
(a) A fragment of aligned 16S rRNA sequences from the SILVA dataset (NR99 v138.1) illustrates the apparent variability of drug-binding residues in bacterial ribosomes among representative members of *Escherichia* and *Mycobacterium* species. Notably, the extensive number of sequences in current biological repositories suggests that *E. coli* alone contains at least 19 dissimilar variants of drug-binding residues. This high apparent degree of variability within a single organism complicates the identification of common variations in drug-binding residues and raises questions about the authenticity of these variants—specifically, how many of them are sequencing errors or strain-specific variants and how many are fixed in species or larger bacterial clades. **(b)** A reduced alignment of rRNA sequences demonstrates our methodology in which we represent each species by a single rRNA sequence, by filtering out the variants that are not shared (at least) between sister rRNA sequences on the tree of life. This approach markedly simplifies the analysis of large libraries of rRNA sequences. Although this method omits variations that are specific to individual sequences or individual bacterial strains, it effectively minimizes stochastic errors, making it possible to identify natural variations that are shared by bacterial genera or broader clades. We have applied this approach to assess conservation of drug-binding residues in 510,508 rRNA sequences from 8,671 bacterial species.

4.3.2 Phyla-specific variation in ribosomal drug-binding sites.

To assess the evolutionary origin and age of substitutions in ribosomal drug-binding sites, we

mapped these substitutions onto the bacterial tree of life (**Figure 4.2**). This mapping revealed that bacteria likely began to diversify their ribosomal drug-binding residues before their separation into the modern phyla. The earliest substitution likely occurred at least 3.8 billion years ago (Bya) when the branches of Dictyoglomi and Thermotogae separated from other bacteria, bearing the macrolide-binding residue G746 in the 23S rRNA, while the remaining bacteria (specifically of Terrabacteria) bore U746. Subsequently, bacterial ribosomes continued to diversify their drug-binding residues by accumulating lineage-specific substitutions in 23 rRNA bases that directly bind with ribosome-targeting drugs. As a result, we showed that each bacterial phylum has evolved an idiosyncratic set of variations in their ribosomal drug-binding residues (**Figure 4.2**).

Compared to *E. coli*, the most dissimilar drug-binding residues we observed among Firmicutes and Actinobacteria. Within these phyla, many species have acquired more substitutions compared to *E. coli* than *E. coli* is to humans. This can be seen, for example, in the order Propionibacteriales, which includes causative agents of skin infections (**Appendix 2, SI Data S4.3, and S4.4**). Compared to *E. coli*, these species exhibit up to 15 substitutions in their drug-binding residues in the binding sites for pactamycin, neomycin, and thermorubin.

Furthermore, some bacteria have substitutions in rRNA bases that are conserved between *E. coli* and humans and therefore viewed as targets of universal inhibitors of protein synthesis. For example, the 16S rRNA residue A694 binds the antibiotic pactamycin and conserved between *E. coli* and humans, which mediates comparable toxicity of pactamycin to both model bacteria and humans and limits pactamycin clinical applications (133,165). But the laboratory engineered substitution of this single residue from A to G confers pactamycin resistance (181). Our analysis showed that the A694G substitution is also widespread in nature, specifically among Firmicutes, Actinobacteria, Chloroflexi, Chlamydiota and all members of Spirochaetes (**Figure 4.2**). Aside from this substitution, we observed substitutions at 15 drug-binding residues with the same nucleotide state in *E. coli* and humans but different states in other bacteria (**Figure 4.2**). Overall, we found that bacteria have been diversifying their ribosomal drug-binding residues since the emergence of the first superphyla, leading to phyla-specific variants of drug-binding sites in bacterial ribosomes.

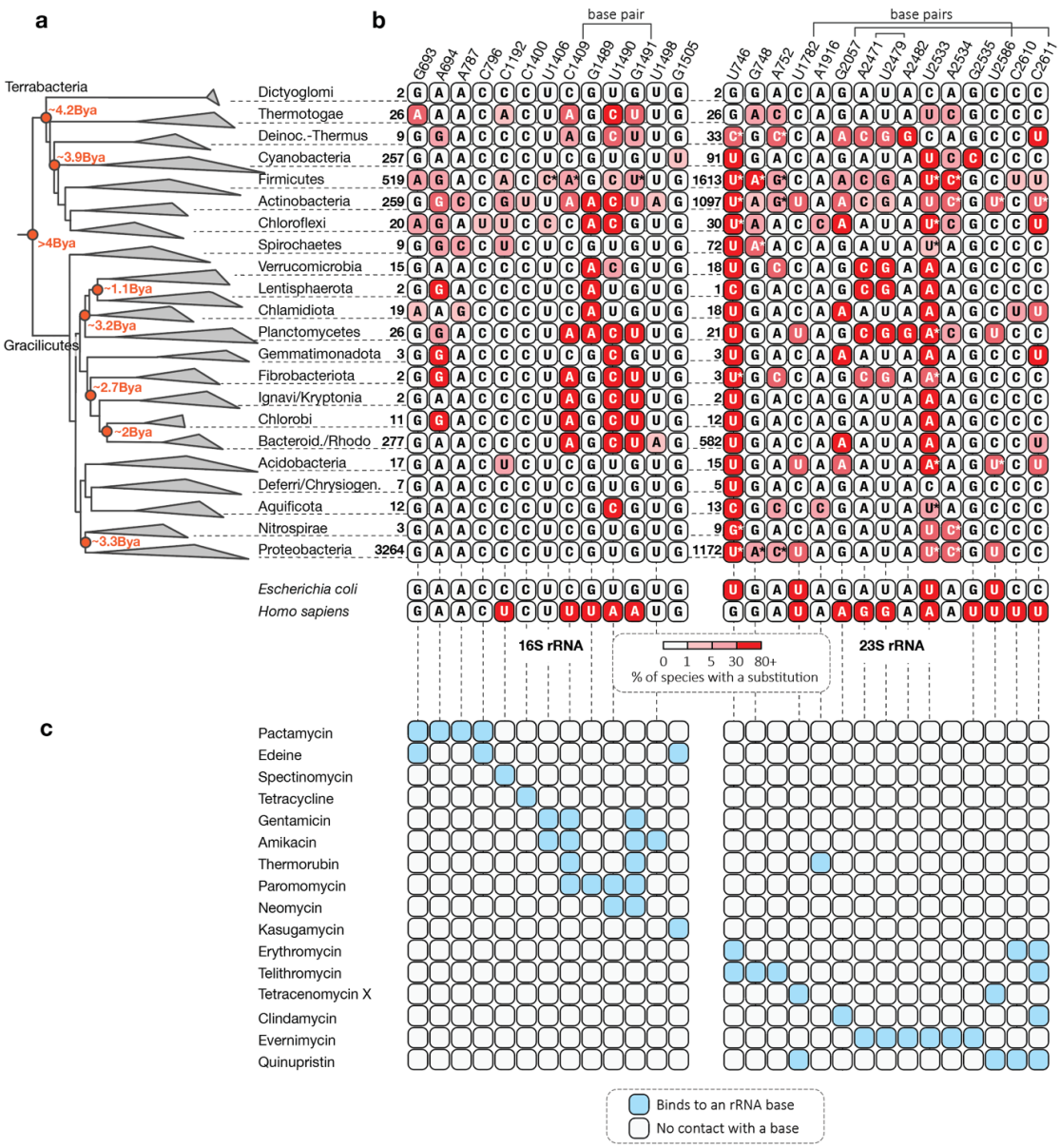

Figure 4.2 | Natural variation in ribosomal drug-binding sites across bacterial phyla.
(a) The bacterial tree of life calculated based on the conservation of the 16S rRNA illustrates the evolutionary diversification of ribosomal drug-binding residues **(b)** and shows which ribosome-targeting drugs bind to specific residues in rRNA **(c)**. Numbers in **(b)** correspond to the total count of representative rRNA sequences that were used to assess substitution profiles of drug-binding residues in rRNA. For simplicity, **(b, c)** display only those rRNA residues that form direct contacts between ribosome-targeting antibiotics and their variable bases (as opposed to the invariant backbone). This panel provides only a simplified summary of variations, while more comprehensive information regarding 8,671 bacterial species can be found in (**Appendix 2, SI Data S4.3, and S4.4**). Asterisks indicate sites that have multiple types of substitutions (e.g. G to U and A instead of G to U). Overall, the figure shows that most bacterial phyla exhibit multiple substitutions in their ribosomal drug-binding residues compared to *E. coli* and to one another. Some of these substitutions likely occurred at least 3 billion years ago (Bya), indicating their ancient origin and widespread distribution across bacteria.

4.3.3 Even closely related bacteria can have dissimilar ribosomal drug-binding sites.

We found that, after the separation into phyla, bacteria continued to diversify their ribosomal drug-binding residues, resulting in additional substitutions in smaller clades (**Figure 4.2, Appendix 2, SI Data S4.3, and S4.4**). As might be expected, the highest number of these additional substitutions were found in pathogenic bacteria with small genomes, particularly *Rickettsia*, *Helicobacter, Bartonella*, *Treponema* and *Mycoplasma* (**Figure 4.3, Appendix 2, SI Data S4.3, and S4.4**). Previously, these species were shown to accumulate genetic changes and evolve more rapidly than non-parasitic bacteria due to weaker natural selection associated with parasitic lifestyles (122,182,183). Here, we found that this rapid evolution likely extends to the ribosomal drug-binding residues, leading to significant differences even for species even within the same genus. For example, *Mycoplasma* species contain up to 10 substitutions of drug-binding residues compared to each other, leading to a greater divergence between some of these species than they are to *E. coli* (**Figure 4.3**).

Importantly, we found that *Mycoplasma* and other parasitic bacteria tend to bear substitutions which disrupt canonical pairing of the G2057-C2611 and other drug-binding base pairs. For example, in *Rickettsia and Neorickettsia* species, the aminoglycoside-binding base pair C1409-G1491 shows substitutions to A-G, G-U, or C-A pairs, suggesting substantial structural changes in this drug-binding site. Furthermore, rRNA substitutions also involve non-paired residues, such as the pactamycin-binding residues G693 and A694 in the 16S rRNA or the ketolide-binding residues U746 and G748 in the 23S rRNA, among others (**Figure 4.3**). These examples illustrate that species do not necessarily need to be distantly related to display highly divergent ribosomal drug-binding sites.

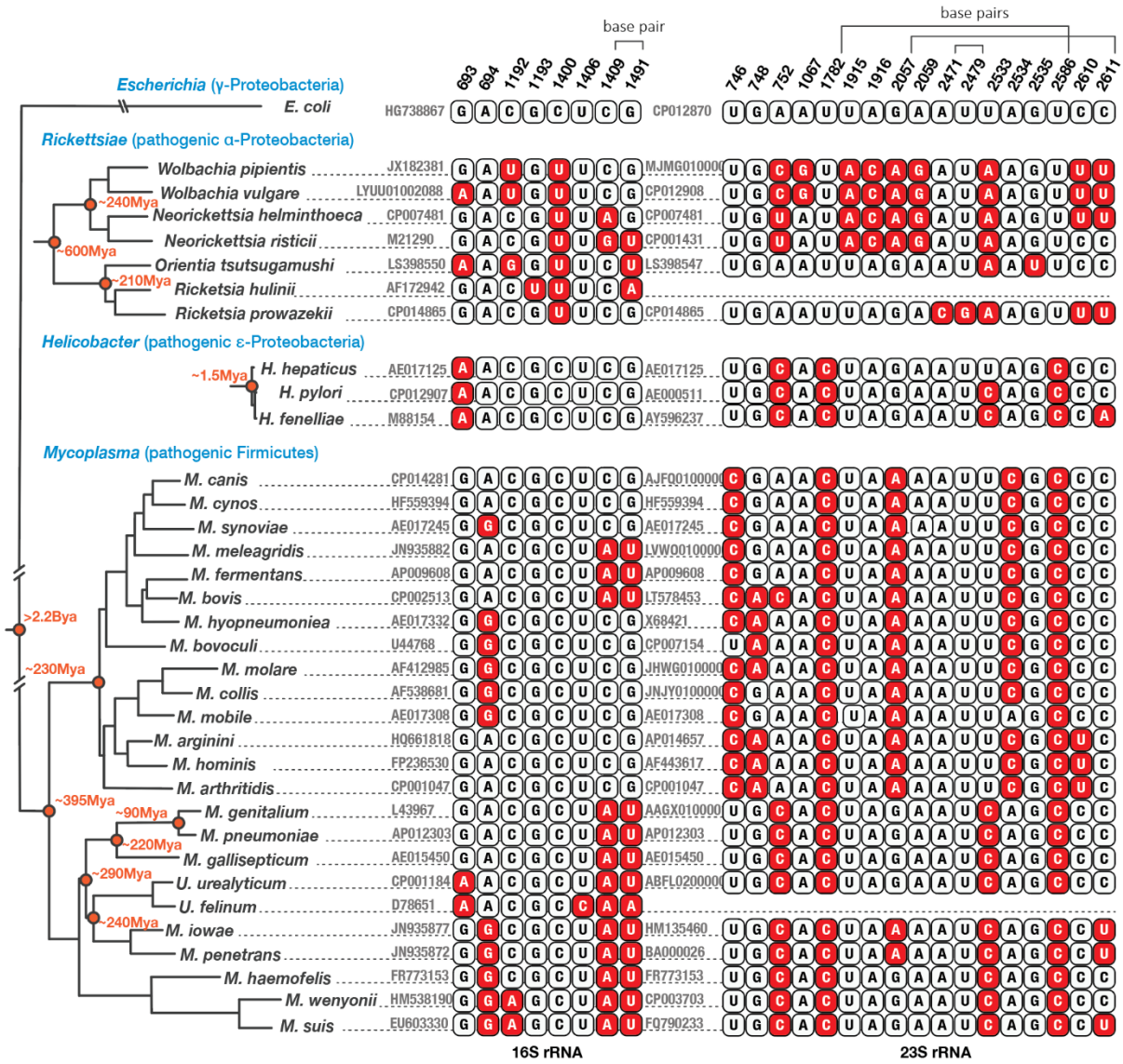

Figure 4.3 | Closely related bacteria can have highly divergent ribosomal drug-binding sites.
A phylogenetic tree and multiple sequence alignment illustrate the natural variations in ribosomal drug-binding residues of pathogenic bacteria *Mycoplasma*, *Helicobacter*, and *Rickettsiae*. The estimated ages of bacterial lineages in millions of years (Mya) are derived from genomic and fossil analyses of the corresponding branches (see **Methods**). Asterisks denote two *Mycoplasma* species (*M. hominis* and *M. pneumoniae*) where the natural divergence of rRNA residues G/A2057 was previously shown to confer intrinsic antibiotic resistance, as observed in an ~18,000x higher tolerance to 14- and 15-membered macrolides (178). Overall, this analysis reveals that drug-binding sites can diverge rapidly among even closely related bacteria.

4.3.4 Variants described as resistance-conferring in model bacteria are widespread in nature.

We next determined the most common variations in drug-binding residues in bacterial ribosomes. To lower the risk of bias toward overrepresented phyla (155,184,133,185), we first separated rRNA sequences into different phylogenetic groups and then determined representative profiles of individual drug-binding residues for each phylum (**Figure 4.2; Appendix 2, SI Data S4.4, and S4.3**). When rRNAs from different phyla were compared in this way that treats species and phyla more evenly, they revealed high overall variability of ribosomal drug-binding residues in bacteria (**Figures 4.4 and 4.5**).

We finally asked whether the naturally occurring variants identified in our analysis have been previously characterized as resistance-conferring in model bacteria. Our literature review revealed that most natural variants identified in our study were previously described as resistance-conferring in model bacteria, where they led to a 10- to 80,000-fold higher tolerance to the corresponding ribosome-targeting drug (**Tables 4.1 and 4.2**). For example, the 16S rRNA residue C1192, which base pairs with G1064, is recognized by the antibiotic spectinomycin (92). Previous studies showed that spectinomycin binding strictly requires the presence of G at position 1064 and C at position 1192 because mutating either of these residues results in up to a 1,000x higher spectinomycin resistance (186–188). These high levels of resistance were observed regardless of whether the substitutions maintained base pairing (e.g., C1064-G1192 or A1064-U1192) or not (e.g., U1064-U1192 or G1064-G1192) (186–188). Furthermore, the effect of these substitutions was observed in multiple model bacteria— including *E. coli*, *Pasteurella multocida*, *Salmonella enterica*, and *Borrelia burgdorferi*—where the substitutions C1192U or C1192G resulted in comparable levels of spectinomycin resistance (186–188).

However, our analysis revealed that the C1192U and C1192A variants are not restricted to the previously obtained laboratory strains but frequently occur in nature. Particularly, they are common for most members of the Firmicutes, Actinobacteria, and Chloroflexi phyla, suggesting intrinsic spectinomycin resistance in these species (**Figure 4.2, Appendix 2, SI Data S4.3, and S4.4**). Aside from these C1192 variations, we found that natural variations in 24 drug-binding residues have been characterized as resistance-conferring in model bacterial species (**Tables 4.1, 4.2**). Thus, we found that variants previously described as resistance-conferring in model bacteria are

widespread in nature.

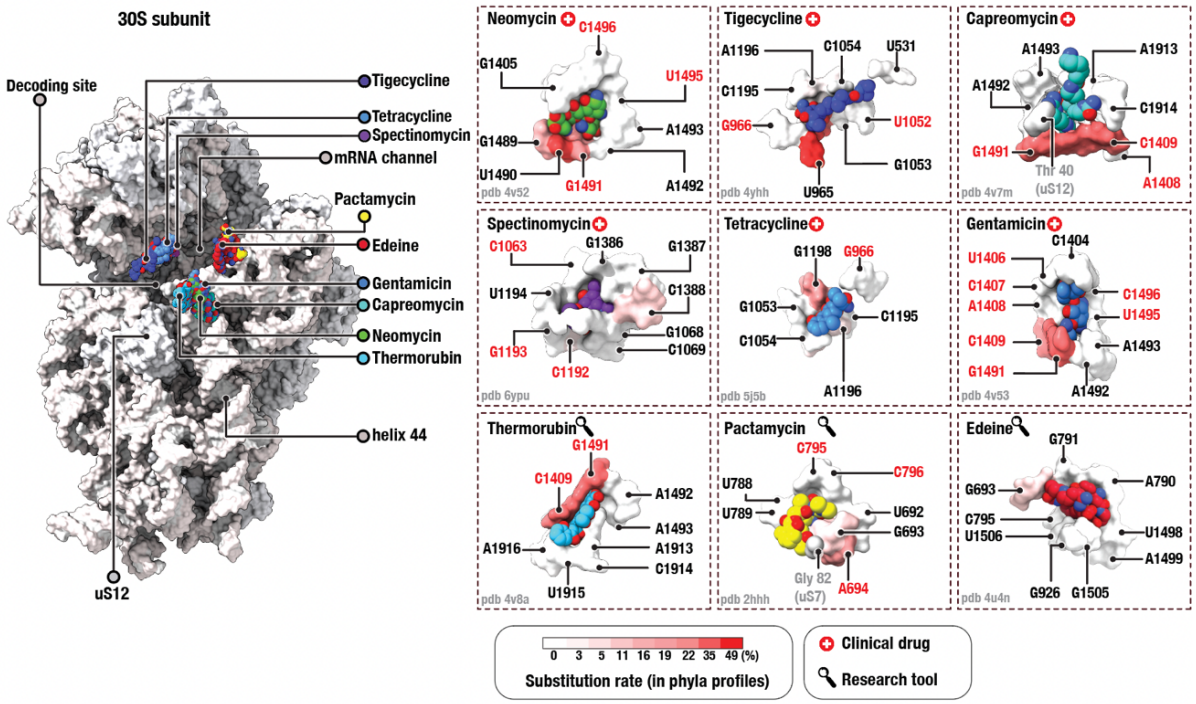

Figure 4.4 | Variable drug-binding sites of the small ribosomal subunit.
Structure of the small ribosomal subunit (on the left) and 9 representative drug-binding pockets (on the right) illustrate the conservation of individual drug-binding residues in the 16S rRNA across bacterial phyla. Ribosome-targeting drugs are shown as blobs coloured by atom type, and drug-binding residues—as surfaces coloured by conservation across phyla. Red labels (e.g., C1496 in the neomycin panel) indicate rRNA residues where mutations have been previously shown to confer antibiotic resistance in model bacteria (as summarized in **Table 4.1**).

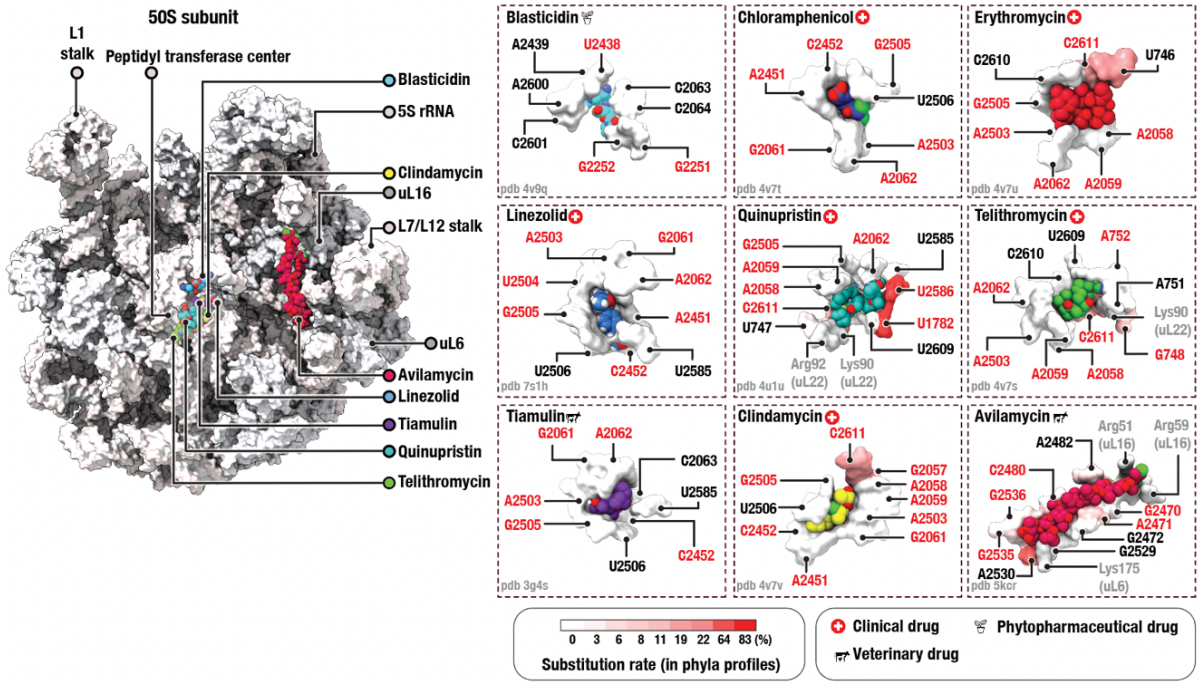

Figure 4.5 | Variable drug-binding sites of the large ribosomal subunit.
Structure of the large ribosomal subunit (on the left) and 9 representative drug-binding pockets (on the right) illustrate the conservation of individual drug-binding residues in the 23S rRNA across bacterial phyla. Ribosome-targeting drugs are shown as blobs coloured by atom type, and drug-binding residues—as surfaces coloured by conservation across phyla. Red labels (e.g., U2438 in the blasticidin panel) indicate rRNA residues where mutations have been previously shown to confer antibiotic resistance in model bacteria (as summarized in **Table 4.2**).

Table 4.1 | 16S rRNA mutations that are known to confer drug resistance.

Base	Organism	Organism type	Mutation	Effect	Ref
A694	*Halobacterium halobium*	Lab mutant	A to G	4-fold higher MIC of spectinomycin	(189)
C795	*Halobacterium halobium*	Lab mutant	C to U	4-fold higher MIC of spectinomycin	(189)
C796	*Halobacterium halobium*	Lab mutant	C to U	4-fold higher MIC of spectinomycin	(189)
C912	*Nicotiana plumbaginfolia*	Lab mutant	C to U	Streptomycin resistance	(190,191)
C912	*Euglena gracilis*	Lab mutant	C to U	Streptomycin resistance	(192)
C912	*Chlamydomonas reinhardtii*	Wild type	C to U	Streptomycin resistance	(193)
C912	*Nicotiana tabacum*		C to U	Streptomycin resistance	(194)
C912	*Nicotiana tabacum*		C to A	Streptomycin resistance	(195)
C912	*Escherichia coli*	Lab mutant	C to G	4-fold increase in resistance to streptomycin	(196)
A913	*Escherichia coli*		A to G	Streptomycin resistance	(197)
A914	*Thermus thermophilus*	Lab mutant	A to G	Streptomycin resistance	(198)
A914	*Escherichia coli*		A to C	Streptomycin resistance	(199)
A915	*Thermus thermophilus*	Lab mutant	A to G	Streptomycin resistance	(198)
U965	*Escherichia coli*		A to G	Streptomycin resistance	(197)
U965	*Helicobacter pylori*	Clinical isolate	A to G	Tetracycline resistance	(200)
G966	*Escherichia coli*	Lab mutant	G to U	4-fold higher MIC of tetracycline	(201)
G966	*Escherichia coli*	Lab mutant	G to U	2-fold higher MIC for negamycin	(201)
G966	*Escherichia coli*	Lab mutant	G to U	4-fold higher MIC for tetracycline and tigecycline	(202)
U1052	*Escherichia coli*	Lab mutant	U to G	8-fold higher MIC for negamycin	(201)
U1052	*Escherichia coli*	Lab mutant	U to G	4-fold higher MIC for tetracycline	(99)
U1052	*Escherichia coli*	Lab mutant	U to G	8-fold higher MIC for negamycin	(99)
G1058	*Escherichia coli*	Lab mutant	G to C	4-fold higher MIC for negamycin and tetracycline	(201)
U1060	*Escherichia coli*	Lab mutant	U to A	8-fold higher MIC for negamycin	(201)
C1063	*Escherichia coli*	Lab mutant	C to U	8-fold higher MIC for spectinomycin	(203)
G1064	*Escherichia coli*	Lab mutant	G to A, G	Spectinomycin resistance	(188)
G1064	*Neisseria meningitidis & Neisseria gonorrheae*	Clinical isolate	G to C	Spectinomycin resistance	(204)
C1066	*Escherichia coli*	Lab mutant	C to U	32- fold higher MIC for spectinomycin	(203)
C1066	*Escherichia coli*	Lab mutant	C to U	62-fold higher MIC for spectinomycin	(187)
A1191	*Chlamydomonas reinhardtii*		A to C, A to G	Streptomycin resistance	(193)
A1191	*Borrelia burgdorferi*	Lab mutant	A to G	>2,200-fold higher MIC for spectinomycin	(205)
A1191	*Chlamydomonas reinhardtii* (chloroplasts)	Lab mutant	A to G	500-fold higher MIC for spectinomycin	(206)
C1192	*Escherichia coli*	Lab mutant	C to G	32-fold higher MIC for spectinomycin	(203)
C1192	*Pasteurella multocida*	Veterinary	C to G	512-fold higher MIC for spectinomycin	(186)

C1192	*Salmonella typhimurium (wild type), E. coli (lab strain)*	Lab mutant	C to U	500-fold higher MIC for spectinomycin	(187)
C1192	*Borrelia burgdorferi*	Lab mutant	C to U	>2,250-fold higher MIC for spectinomycin	(205)
C1192	*Escherichia coli*	Lab mutant	C to U	Spectinomycin resistance	(207)
C1192	*Mycobacterium smegmatis*	Lab mutant	C to G	Spectinomycin resistance	(208)
G1193	*Escherichia coli*	Lab mutant	G to A	32-fold higher MIC for spectinomycin	(203)
G1193	*Chlamydia psittaci* rRNA expressed in *E. coli*	Lab mutant	G to C	Spectinomycin resistance	(209)
A1197	*Escherichia coli*	Lab mutant	A to U	16-fold higher MIC for negamycin	(201)
G1386	*Nicotiana tabacum*	Lab mutant	G to A	Spectinomycin resistance	(210)
U1406	*Mycobacterium smegmatis*	Lab mutant	U to C	64-fold higher MIC for hygromycin	(211)
U1406	*Thermus thermophilus*	Lab mutant	U to C	50-fold, 10-fold, 5-fold and 2-fold increase in resistance to kanamycin, gentamicin resistance, hygromycin and capreomycin respectively	(212)
U1406	*Thermus thermophilus*	Lab mutant	U to A	5-fold, 50-fold and 1,000-fold increase in resistance to hygromycin, kanamycin and gentamicin, respectively	(212)
U1406	*Thermus thermophilus*	Lab mutant	U to G	10-fold, 10-fold, 5-fold and 2-fold increase in resistance to kanamycin, gentamicin, hygromycin and capreomycin	(212)
U1406	*Escherichia coli*	Lab mutant	U to A	64-fold higher MIC for gentamicin C and tobramycin, 128-fold higher MIC for kanamycin A and G418	(213)
U1406	*Mycobacterium smegmatis*	Lab mutant	U to C	8-fold increase in resistance to neamine and ribostamycin, 16-fold increase in resistance to paromomycin, and 4-8-fold increase in resistance to lividomycin	(75)
C1407	*Escherichia coli*	Lab mutant	C to U	Impairs paromomycin binding to the ribosome	(214)
A1408	*Mycobacterium smegmatis*	Lab mutant	A to G	64-fold increase in resistance to paromomycin, more than 1,024-fold increase in resistance to neomycin, and more than 1,024 increase in resistance to gentamicin, tobramycin and kanamycin	(215)
A1408	*Borrelia burgdorferi*	Clinical isolate	A to G	90-fold increase in resistance to kanamycin and more than 240-fold increase in resistance to gentamicin	(205)
A1408	*Thermus thermophilus*	Lab mutant	A to G	25-fold higher MIC for streptomycin, 250-fold higher MIC for apramycin, 20-fold MIC for	(212)

				paromomycin, 500-fold MIC for neomycin, 1,000-fold MIC for gentamicin, 1,500-fold increase in resistance to kanamycin, and 20-fold increase in resistance to capreomycin	
A1408	*Mycobacterium smegmatis*	Lab mutant	A to G	16-fold higher MIC for neamine, more than 128 higher MIC for ribostamycin, 512-1,024-fold higher MIC for neomycin, 64-fold higher MIC for paromomycin resistance, and 32-fold higher MIC for lividomycin	(75)
C1409	*Mycobacterium smegmatis*	Lab mutant	C to G	32-fold higher MIC for paromomycin, 4-fold for neomycin, >1024-fold higher MIC for geneticin, 4-fold higher MIC for gentamicin and 16-fold higher MIC for tobramycin	(216)
C1409	*Mycobacterium smegmatis*	Lab mutant	C to U	8-fold higher MIC for paromomycin and tobramycin, 128-fold higher MIC for geneticin, 16-fold higher MIC for gentamicin	(216)
C1409	*Mycobacterium smegmatis*	Lab mutant	C to U	4-8-fold higher MIC for paromomycin, 8-fold higher MIC for gentamicin, 8-16-fold higher MIC for tobramycin and kanamycin.	(215)
C1409	*Thermus thermophilus*	Lab mutant	C to G	5-fold higher MIC for neomycin, 25-fold higher MIC for streptomycin, 50-fold higher MIC for paromomycin, 100-fold higher MIC for apramycin, 200-fold higher MIC for gentamicin and kanamycin and 20-fold higher MIC for capreomycin	(212)
C1409	*Mycobacterium smegmatis*	Lab mutant	C to U	4-fold higher MIC for neamine, 8-fold higher MIC for ribostamycin, 8-fold higher MIC for lividomycin and paromomycin	(75)
C1409	*Mycobacterium smegmatis*	Lab mutant	C to G	2-fold higher MIC for neamine, 16-32-fold higher MIC for paromomycin, 64-fold higher MIC for lividomycin and ribostamycin	(75)
G1491	*Mycobacterium smegmatis*	Lab mutant	G to A	64-fold higher MIC for paromomycin	(215)
G1491	*Thermus thermophilus*	Lab mutant	G to A	2-fold higher MIC for kanamycin, 5-fold higher MIC for paromomycin, 20-fold higher MIC for capreomycin and 50-fold higher MIC for apramycin	(212)
G1491	*Mycobacterium smegmatis*	Lab mutant	G to U/C	512-fold higher MIC for paromomycin	(216)

G1491	*Mycobacterium smegmatis*	Lab mutant	G to A	2-fold higher MIC for neamine, 4-fold higher MIC for neomycin, 16-fold higher MIC for ribostamycin, 64-fold higher MIC for paromomycin and 256-fold increase higher MIC for lividomycin	(75)
G1491	*Mycobacterium smegmatis*	Lab mutant	G to C	16-fold higher MIC for neamine, ~32-fold higher MIC for neomycin 128-fold higher MIC for ribostamycin, 512-fold higher MIC for paromomycin	(75)
G1491	*Mycobacterium smegmatis*	Lab mutant	G to U	16-fold higher MIC for neomycin, 16-fold higher MIC for neamine, 128-fold higher MIC for ribostamycin, 512-fold higher MIC for paromomycin and lividomycin	(75)
U1495	*Thermus thermophilus*	Lab mutant	U to C	2-fold higher MIC for kanamycin and 5-fold higher MIC for hygromycin	(212)
U1495	*Mycobacterium smegmatis*	Lab mutant	U to A	8-fold higher MIC for neomycin, 16-fold higher MIC for neamine 128-fold higher MIC for ribostamycin, 512-fold higher MIC for paromomycin and lividomycin	(75)
U1495	*Mycobacterium smegmatis*	Lab mutant	U to C	8-fold higher MIC for neamine, 16-fold higher MIC for ribostamycin, 8-fold higher MIC for neomycin, 128-fold higher MIC for paromomycin and 64-fold higher MIC for lividomycin	(75)
C1496	*Mycobacterium smegmatis*	Lab mutant	C to U	32-fold higher MIC for hygromycin	(211)
C1496	*Mycobacterium avium*	Clinical isolates	C to U	8-fold higher MIC for amikacin	(217,218)
U1498	*Mycobacterium smegmatis*	Lab mutant	U to C	16-fold higher MIC for hygromycin	(211)
U1498	*Mycobacterium abscessus*	Clinical isolates	U to A	16-fold higher MIC for amikacin	(217,218)

Table 4.2 | 23S rRNA mutations that are known to confer drug resistance.

Base	Organism	Organism type	Mutation	Effect	Ref
G748	*Mycoplasma bovis*	Lab mutant	G to A	4-fold higher MIC for lincomycin, 16-fold higher MIC for tilmicosin, and 64-fold higher MIC for tylosin	(219)
G748	*Mycoplasma bovis*	Veterinary isolate	G to A	1,024-fold higher MIC for tylosin, tilomicin, gamithromycin, and tildipirosin	(220)
A1067	*Escherichia coli*	Lab mutant	A to C, A to U	Reduced ribosome affinity to thiostrepton to about 35% of the wild-type strain	(221)
A1095	*Escherichia coli*	Lab mutant	A to C, A to U	Significantly decreased thiostrepton affinity in ribosomes bearing this mutation	(222)
U1782	*Escherichia coli*	Lab mutant	U to C	16-fold higher MIC for tetracenomycin X	(176)
G2057	*Propionibacterium acnes*	Clinical isolate	G to A	Erythromycin resistance	(223)
G2057	*Mycoplasma fermentans,*	Type strain	G to A	>18,000-fold higher MIC for erythromycin, >2,000-fold higher MIC for clarithromycin, >130-fold higher MIC for azithromycin, 64-fold higher MIC for quinupristin, 35-fold higher MIC to telithromycin, 8-fold higher MIC for josamycin, tylosin, and 4-fold higher MIC for midecamycin, pristinamycin and spiramycin,	(178)
G2057	*Mycoplasma pulmonis*	Type strain	G to A	>18,000-fold higher MIC for erythromycin, >2,000-fold higher MIC for clarithromycin, >530-fold higher MIC for azithromycin, >133-fold higher MIC for midecamycin >66-fold higher MIC for josamycin, 35-fold higher MIC for telithromycin, 32-fold higher MIC for spiramycin, 4-fold higher MIC for pristinamycin	(178)
G2057	*Escherichia coli*	Lab mutant	G to A	Chloramphenicol and erythromycin resistance	(224)
A2058	*Propionibacterium acnes*	Clinical isolate	A to G	Erythromycin, tylosin, spiramycin, josamycin, and clindamycin resistance	(223)
A2058	*Streptococcus pneumoniae*	Clinical isolate	A to G	512-fold higher MIC for clarithromcyin, 256-fold higher MIC for azithromycin, 64-fold higher MIC for clindamycin, 32-fold higher MIC for midekamycin	(225)
A2058	*Escherichia coli*	Lab mutant	A to G	>6-fold higher MIC for erythromycin, 7.5-fold higher MIC for clarithromycin	(226)

A2058	*Treponema denticola*	Lab mutant	A to G	Erythromycin resistance	(182)
A2058	*Mycobacterium smegmatis*	Lab mutant	A to G	512-fold higher MIC for telithromycin, 32-fold higher MIC for carbomycin, 8-fold higher MIC for spiramycin, josamycin and desmycosin, 2-fold higher MIC for tylosin	(228)
A2058	*Mycobacterium smegmatis*	Lab mutant	A to C	4,096-fold higher MIC for telithromycin, 256-fold higher MIC for carbomycin, and josamycin, 32-fold higher MIC for spiramycin, 16-fold higher MIC for desmycosin, 4-fold higher MIC for tylosin	(228)
A2058	*Mycoplasma pneumoniae*	Clinical isolate	A to G	32,000-fold higher MIC for azithromycin, 17,000-fold higher MIC for clarithromycin and erythromycin, 260-fold higher MIC for midecamycin, 130-fold higher MIC for josamycin, 64-fold higher MIC for clindamycin, 32-fold higher MIC for lincomycin	(229)
A2058	*Mycoplasma pneumoniae*	Clinical isolate	A to C	17,000-fold higher MIC for erythromycin and clarithromycin, 8,000-fold higher MIC for azithromycin, 1,000-fold higher MIC for midecamycin, 500-fold higher MIC for josamycin, 66-fold higher MIC for rokitamycin, 8-fold higher MIC for lincomycin and clindamycin	(229)
A2058	*Streptococcus pneumoniae (originally clinical isolate)*	Lab mutant	A to G	2,000-fold higher MIC for azithromycin, erythromycin and clarithromycin, 125-fold higher MIC for lincomycin, 100-fold higher MIC for telithromycin, 31-fold higher MIC for clindamycin, 16-fold higher MIC for spiramycin, 4-fold higher MIC for streptogramin B	(230)
A2058	*Mycoplasma bovis*	Lab mutant	A to U	64-fold higher MIC for tylosin, 16-fold higher MIC for tilmicosin, 4-fold higher MIC for lincomycin	(219)
A2058	*Mycobacterium smegmatis*	Lab mutant	A to G	64-fold higher MIC for clindamycin, 2-fold higher MIC for valnemulin	(231)
A2058	*Mycobacterium smegmatis*	Lab mutant	A to G	128-fold higher MIC for clindamycin, 64-fold higher MIC for erythromycin and azithromycin, 8-fold higher MIC for spiramycin, and josamycin, 2-fold higher MIC for tylosin	(232)

A2058	*Escherichia coli*	Lab mutant	A to U	Oleandomycin, niddamycin, tylosin, spiramycin, lincomycin, clindamycin and osteogrycin B resistance	(207)
A2509	*Mycobacterium smegmatis*	Lab mutant	A to G	4,096-fold higher MIC for telithromycin, 256-fold higher MIC for carbomycin and josamycin, 64-fold higher MIC for tylosin and desmycosin, 32-fold higher MIC for spiramycin	(228)
A2059	*Streptococcus pneumoniae (originally clinical isolate)*	Lab mutant	A to G	20,000-fold higher MIC for azithromycin, 1,000-fold higher MIC for spiramycin, 625-fold higher MIC for erythromycin, 312-fold higher MIC for clairthromycin, 10-fold higher MIC for clindamycin, 7.8-fold higher MIC for lincomycin, 3-fold higher MIC for telithromycin,	(230)
A2059	*Mycoplasma pneumoniae*	Clinical isolate	A to G	32,000-fold higher MIC for azithromycin, 17,000-fold higher MIC for erythromycin, 2,000-fold higher MIC for josamycin, 4,266-fold higher MIC for midecamycin, 533-fold higher MIC for rikotamycin, 8-fold higher MIC for lincomycin, and clindamycin	(229)
A2059	*Propionibacterium acnes*	Clinical isolate	A to G	Erythromycin, tylosin, spiramycin, josamycin, clindamycin, azithromycin, and pristinamycin resistance	(223)
G2061	*Escherichia coli*	Lab mutant	G to C	This mutation is deleterious to *E. coli*	(233)
G2061	*Thermus thermophilus*	Lab mutant	G to A	Tiamulin and chloramphenicol resistance	(234)
G2061	*Thermus thermophilus*	Lab mutant	G to U	Tiamulin resistance	(234)
A2062	*Mycoplasma bovis*	Lab mutant	A to U, A to C	64-fold higher MIC for tylosin, 16-fold higher MIC for tilmicosin	(219)
A2062	*Mycobacterium hominis*	Type culture	A to G, A to U	2,133-fold higher MIC for josamycin, and miocamycin	(235)
A2062	*Deinococcus radiodurans*	Lab mutant	A to C	Linezolid and pleuromutilin resistance	(236)
A2062	*Halobacterium halobium*	Lab mutant	A to C	1,024-fold higher MIC for spiramycin, 64-fold higher MIC for josamycin, and tylosin, 32-fold higher MIC for pristinamycin I, 2-fold higher MIC for pristinamycin II	(237)
A2062	*Halobacterium halobium*	Lab mutant	A to C	26-fold higher MIC for lincomycin	(238)
G2252	*Thermus aquaticus*	Lab mutant	G to A	Caused drastic reduction in peptidyl transferase activity	(239)
U2438	*Halobacterium halobium*	Lab mutant	U to C	Amicetin resistance	(240)

A2451	*Thermus thermophilus*	Lab mutant	A to U	Tiamulin and chloramphenicol cross-resistance	(234)
C2452	*Halobacterium halobium*	Lab mutant	C to U	53-fold higher MIC for lincomycin	(238)
C2452	*Thermus thermophilus*	Lab mutant	C to U	Tiamulin resistance	(234)
C2452	*Deinococcus radiodurans*	Lab mutant	C to U	Linezolid, chloramphenicol and anisomycin cross-resistance	(236)
C2452	*Haloarcula marismortui*	Lab mutant	C to U	50-fold higher MIC for anisomycin	(241)
C2452	*Sulfolobus acidocaldarius*	Lab mutant	C to U	Celesticetin, chloramphenicol and carbomycin resistance	(242)
A2453	*Halobacterium halobium*	Lab mutant	A to C	5-fold higher MIC for lincomycin	(238)
A2453	*Halobacterium halobium*	Lab mutant	A to G	43-fold higher MIC for lincomycin	(238)
A2469	*Streptococcus pneumoniae*	Lab mutant	A to C	16-fold higher MIC for avilamycin	(243)
G2470	*Halobacterium halobium*	Lab mutant	G to U	220-fold higher MIC for avilamycin	(244)
A2471	*Halobacterium halobium*	Lab mutant	A to G	2,000-fold higher MIC for Evernimicin	(245)
A2471	*Halobacterium halobium*	Lab mutant	A to C	5,400-fold higher MIC for Evernimicin	(245)
A2471	*Halobacterium halobium*	Lab mutant	A to G, A to C	220-fold higher MIC for avilamycin	(244)
A2478	*Halobacterium halobium*	Lab mutant	A to C	220-fold higher MIC for avilamycin	(244)
A2478	*Halobacterium halobium*	Lab mutant	A to C	5,400-fold higher MIC for Evernimicin	(245)
U2479	*Halobacterium halobium*	Lab mutant	U to C	220-fold higher MIC for avilamycin	(244)
U2479	*Halobacterium halobium*	Lab mutant	U to C	5,400-fold higher MIC for Evernimicin	(245)
C2480	*Halobacterium halobium*	Lab mutant	C to U	220-fold higher MIC for avilamycin	(244)
C2480	*Halobacterium halobium*	Lab mutant	C to A	5,400-fold higher MIC for Evernimicin	(245)
C2480	*Halobacterium halobium*	Lab mutant	C to U	5,400-fold higher MIC for Evernimicin	(245)
C2480	*Streptococcus pneumoniae*	Lab mutant	C to U	16-fold higher MIC for Evernimicin	(243)
C2499	*Halobacterium halobium*	Lab mutant	C to U	10-fold higher MIC for lincomycin	(238)
U2500	*Halobacterium halobium*	Lab mutant	U to C	66-fold higher MIC for lincomycin	(238)
U2500	*Thermus thermophilus*	Lab mutant	U to A	Tiamulin resistance	(234)
A2503	*Mycoplasma gallisepticum*	Lab mutant	A to U	128-fold higher MIC for erythromycin, 64-fold higher MIC for chloramphenicol, 62.5-fold higher MIC for valnemulin, 32-fold higher MIC for florfenicol, 8-fold higher MIC for lincomycin	(232)
A2503	*Mycobacterium smegmatis*	Lab mutant	Ato G	4-fold higher MIC for linezolid, 4-fold higher MIC for chloramphenicol	(231)
A2503	*Mycobacterium smegmatis*	Lab mutant	A to U	16-fold higher MIC for josamycin and clindamycin, 8-fold higher MIC for spiramycin and linezolid, 4-	(232)

				fold higher MIC for valnemulin and chloramphenicol	
U2504	*Brachyspira hyodysenteriae, Brachyspira pilosicol*	Lab mutant	U to C	Tiamulin and chloramphenicol resistance	(246)
U2504	*Halobacterium halobium*	Lab mutant	U to G	60-fold higher MIC for lincomycin	(238)
U2504	*Mycobacterium smegmatis*	Lab mutant	U to G	16-fold higher MIC for chloramphenicol, 4-fold higher MIC for linezolid, 2-fold higher MIC for valnelium and clindamycin	(231)
U2504	*Mycobacterium smegmatis*	Lab mutant	U to G	16-fold higher MIC for chloramphenicol and florfenicol, 4-fold higher MIC for spiramycin, linezolid, valnemulin, and josamycin, 2-fold higher MIC for clindamycin	(232)
U2504	*Deinococcus radiodurans*	Lab mutant	U to C	Linezolid resistance	(236)
U2504	*Staphylococcus aureus, Enterococcus faecium and coagulase negative Staphylococci*	Clinical isolate	U to A	Linezolid resistance	(247)
U2504	*Escherichia coli*	Lab mutant	U to Ψ	16-fold higher MIC for clindamycin, 8-fold higher MIC for linezolid, 4-fold higher MIC for tiamulin	(248)
G2505	*Mycobacterium smegmatis*	Lab mutant	G to A	8-fold higher MIC for linezolid, 4-fold higher MIC for chloramphenicol	(231)
G2505	*Deinococcus radiodurans*	Lab mutant	G to A	Linezolid resistance	(236)
G2505	*Enterococcus faecium*	Clinical isolate	G to A	16-fold higher MIC for linezolid	(249)
A2534	*Staphylococcus epidermidis*	Clinical	C to U	3-fold higher MIC for linezolid	(250)
G2535	*Streptococcus pneumoniae*	Lab mutant	G to A	8-fold higher MIC for Evernimicin	(243)
G2535	*Halobacterium halobium*	Lab mutant	G to A	170-fold higher MIC for Evernimicin	(245)
G2535	*Halobacterium halobium*	Lab mutant	G to A	22-fold higher IC_{50} for avilamycin	(244)
G2535	*Enterococcus feacalis*	Veterinary isolate	G to A, G to U	Evernimicin resistance	(251)
G2536	*Streptococcus pneumoniae*	Lab mutant	G to C	8-fold higher MIC for Evernimicin	(243)
G2553	*Escherichia coli*	Lab mutant	G to C	Caused severe growth defects in cells grown on erythromycin containing media	(252)
U2586	*Escherichia coli*	Lab mutant	U to G, U to A	16-fold higher MIC for tetracenomycin X	(178)
U2586	*Escherichia coli*	Lab mutant	U to C	8-fold higher MIC for tetracenomycin X	(176)
U2609	*Escherichia coli*	Lab mutant	U to A	4-fold higher MIC for tetracenomycin X	(176)
U2609	*Escherichia coli*	Lab mutant	U to G	8-fold higher MIC for tetracenomycin X	(176)
C2611	*Escherichia coli*	Lab mutant	C to U	5-fold higher MIC for erythromycin and clarithromycin	(226)

C2611	*Mycoplasma pneumoniae*	Clinical isolate	C to G	500-fold higher MIC for erythromycin, 60-fold higher MIC for clarithromycin, 15-fold higher MIC for azithromycin, 4-fold higher MIC for midecamycin	(229)
C2611	*Streptococcus pneumoniae*	Lab mutant (originally clinical isolate)	C to A	39-fold higher MIC for clarithromycin, 32-fold higher MIC for streptogramin B, 16-fold higher MIC for azithromycin and erythromycin, 4-fold higher MIC for spiramycin	(230)
C2611	*Streptococcus pneumoniae*	Lab mutant (originally clinical isolate)	C to G	5,000-fold higher MIC for clarithromycin, 2,000-fold higher MIC for erythromycin, 128-fold higher MIC for streptogramin B, 125-fold higher MIC for azithromycin, 8-fold higher MIC for spiramycin, 4-fold higher MIC for lincomycin	(230)
C2611	*Escherichia coli*	Lab mutant	C to U	Erythromycin resistance	(253)

4.4 Discussion

4.4.1 Bacterial phyla have diverged ribosomal drug-binding sites.

Prior to our study, the conservation of rRNA residues was estimated using one of the following two approaches. In the first, conservation estimates were derived from sequence alignments, where rRNA sequences were used to calculate the overall conservation of rRNA nucleotides without separation of sequences into phyla and adjustments for sample size of individual clades (175,155,115,184,185,172,254). These analyses were crucial for identifying immutable rRNA bases, but they were biased toward common species and phyla, particularly Proteobacteria, which caused an overestimation of ribosomal drug-binding site conservation. Alternatively, a more accurate and targeted approach involved determining the variations of rRNA drug-binding residues by comparing ribosome structures (174,175,133,167,165). These analyses provided detailed information about the diversity of ribosomal drug-binding residues, but for only a handful of model organisms.

Here, we described the evolutionary variants of individual rRNA drug-binding residues across more than 8,000 representative bacteria. We traced the evolutionary history of individual drug-binding residues from the last bacterial common ancestor to the present day, enabling us to estimate variations not only in currently known species but also in those yet to be discovered, based on their position on the tree of life. This analysis revealed that bacterial phyla exhibit a greater diversity of ribosomal drug-binding residues than previously appreciated, illustrating that the occasional findings of divergent variants in species like *Propionibacterium*, *Thermus*, or *Mycoplasma* are common occurrences in bacterial species.

One implication of our work is that individual bacterial organisms may not serve as reliable generalized models for bacterial ribosomes in the absence of evolutionary analyses. For example, we show that the popular model organism *E. coli* exhibits relatively atypical drug-binding sites for the antibiotics quinupristin, tetracenomycin X, and Evernimicin due to the 23S rRNA variations (U1782, U2533, and U2586) because these variants are found in Proteobacteria, but not in most other bacteria. This finding shows that our commonly used division of ribosomes into bacterial and eukaryotic types in the structural studies of ribosomes (133,145,174) is incomplete and oversimplified, given the substantial diversity of ribosomal drug-binding residues within the bacterial domain of life.

4.4.2 Implications for clinical practice.

Previously, the discovery of intrinsic antibiotic resistance in *Propionibacteria* and *Mycoplasma* has changed the clinical targeting of these human pathogens (69,177,178,255). For example, *M. pneumoniae*, a respiratory mycoplasma, which has the *E. coli*-type macrolide-binding base G2057 in the 23S rRNA, can be effectively treated with macrolides, lincosamides, streptogramins, and ketolides. However, *M. hominis*, a genital mycoplasma, which bears the A2057G substitution, cannot be treated with 14- and 15-membered macrolides and ketolides due to its natural resistance. For example, this species is 5,000 more tolerant to the macrolide erythromycin. Therefore, this species of *Mycoplasma* is treated with other antibiotics that bind less divergent sites (178,255). Thus, the knowledge on structural diversity of ribosomal drug-binding sites resulted in a more accurate selection of ribosome-targeting antibiotics for a given pathogen.

We anticipate a similar revision for a much broader range of bacterial species because our work showed that approximately one in ten representative bacteria carry rRNA substitutions that have been observed in clinical isolates of drug-resistant human pathogens (**Appendix 2**, **SI Data S4.3, and S4.4**). This finding suggests that the intrinsic resistance previously observed in *Mycoplasma*, *Propionibacterium* and *Thermus* species is likely prevalent among non-model bacteria due to the presence of comparably or even more divergent drug-binding sites. However, our evolutionary analyses have one caveat worth considering: the phenotypic impact of the observed changes at drug-binding sites might, in some cases, be compensated by changes at other sites close in the ribosome structure; thus, the precise effects on drug resistance of the lineage-specific variants we identified will require further study for individual bacteria. Nonetheless, our work presents the first comprehensive overview of the structural variability of ribosomal drug-binding sites in bacteria which may inform a more accurate and personalized choice of ribosome-targeting drugs for a given pathogen.

Chapter 5. Atomic structure of the ribosome with a diverged drug-binding site.

5.1 Introduction

Previous advances in X-ray crystallography and cryo-electron microscopy (cryo-EM) have enabled high-resolution structural analysis of ribosome-drug interactions, shedding light on the molecular mechanisms by which these drugs inhibit protein synthesis (256). In this study, cryo-EM was used to assess the structural impact of naturally occurring rRNA sequence substitutions at one of the drug-binding sites within ribosomes from the antibiotic-producing *S. griseus* and *S. fradiae.* Species within the *Streptomyces* genus are prolific producers of natural ribosome-targeting antibiotics (32, 256–273), and as a result certain *Streptomyces* species have evolved more than one self-protection mechanism against the antibiotics they produce.

The computational analysis done in Chapter 4, revealed that these antibiotic producers bear previously uncharacterized rRNA substitutions in two known drug-binding sites of the ribosome. These include the aminoglycoside-binding site, which bears G1489A and U1490C substitutions in the 16S rRNA, and the orthosomycin-binding site which bears the A2534C substitution in 23S rRNA (compared to that of *E. coli*). These observations gave rise to two key questions:

- Do these rRNA substitutions impact how ribosomes interact with antibiotics?
- Could these rRNA substitutions serve as an overlooked mechanism of antibiotic self-protection in *Streptomyces*?

To address these questions, atomic structures of ribosomes from *S. griseus* and *S. fradiae* were determined. These structures were analysed to assess the potential effects of the identified natural rRNA substitutions on ribosome-drug interaction.

5.2 Results

5.2.1 The antibiotic-producing species S. griseus and S. fradiae can be successfully maintained in the laboratory while monitoring stages of bacterial growth.

To understand the impact of rRNA substitutions on the structure of ribosomal drug-binding sites, a reliable method for culturing *Streptomyces* species under laboratory conditions was first

established. This ensured the use of viable cells for ribosome isolation, thereby minimizing potential artifacts from rRNA degradation caused by cellular death.

To resuscitate freeze-dried *Streptomyces* cells obtained from the German Collection of Microorganisms and Cell Cultures, the samples were plated onto solid agar media. *S. fradiae* formed pinkish colonies (**Figure 5.1a**), while *S. griseus* initially exhibited filamentous growth but later formed distinct white colonies after several culture passages (**Figure 5.1b, c**).

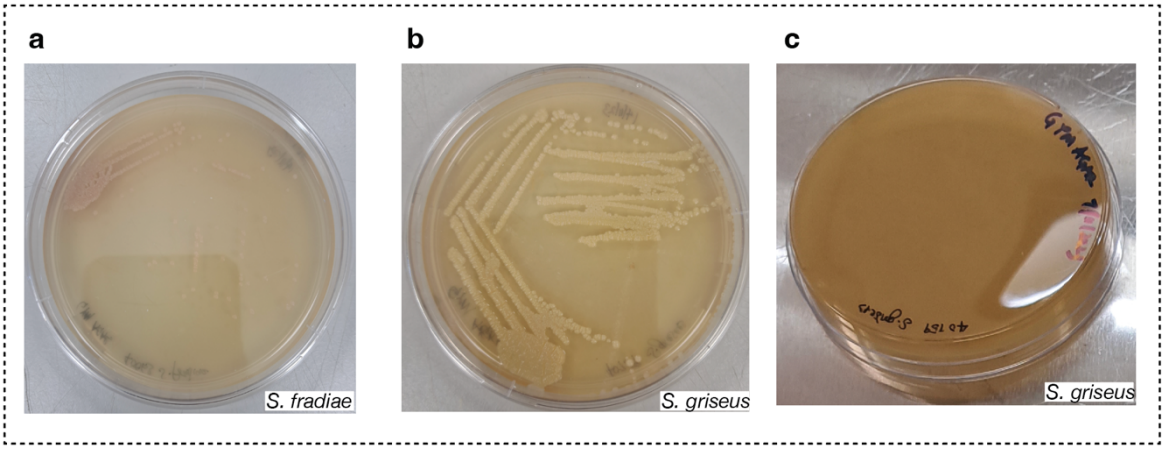

S.griseus and *S. fradiae* growth on solid medium

Figure 5.1 | *S. griseus* and *S. fradiae* growth can be resuscitated by placing freeze-dried cells on solid media (GYM agar).
(a) Pigmented (pinkish) colonies of *S. fradiae* on solid media. **(b)** Later distinct whitish colonies of *S. griseus* on solid media obtained after several passages. **(c)** Earlier filamentous growth of *S. griseus* on solid media.

To enable ribosome isolation, biomass production was initiated after successfully cultivating viable *Streptomyces* colonies. The aim was to obtain a homogeneous population of actively growing cells, thereby minimizing the accumulation of dead or sporulated cells that could compromise sample quality. To achieve this, *S. griseus* and *S. fradiae* were grown in a rich liquid medium (GYM), and the results showed their ability to grow by forming characteristic clumps (**Figure 5.2**), a typical feature of certain *Streptomyces* species in the liquid medium (275).

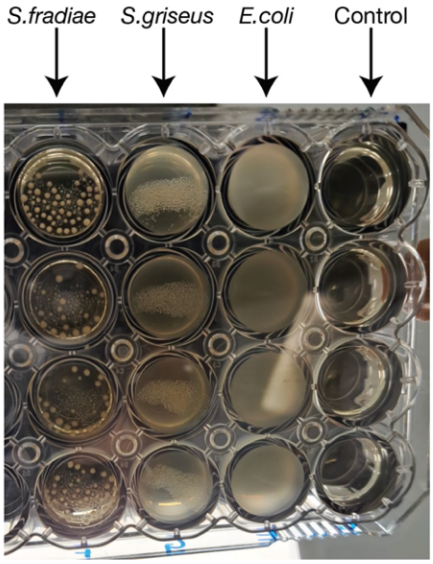

Figure 5.2 | *S. griseus* and *S. fradiae* can be maintained in liquid media (GYM broth).
Cells of *S. fradiae* and *S. griseus* tended to form clumps in liquid media, unlike *E. coli*. However, the clumps formed by *S. fradiae* were bigger than those of *S. griseus*.

Despite *Streptomyces* cells' tendency to form clumps in liquid media, growth dynamics of *S. griseus* and *S. fradiae* were successfully monitored using optical density (OD_{630}) measurements at 630 nm (**Figure 5.3**). Over 48 hours, both cultures transitioned from active growth to the stationary phase, with no visible signs of cell death (**Figure 5.3**).

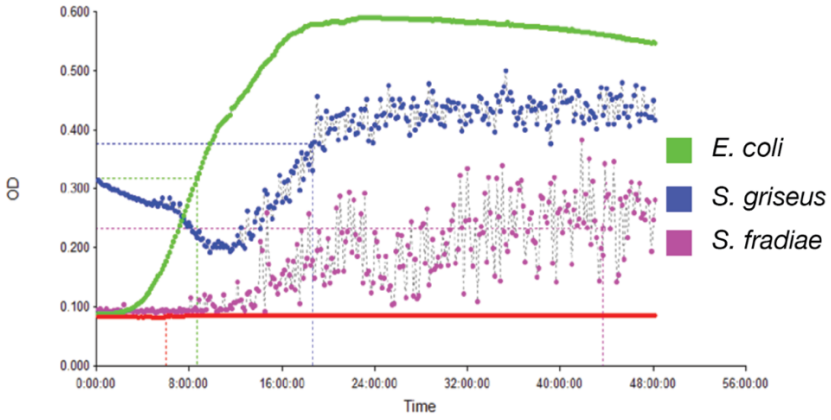

Figure 5.3 | Despite cell clumping, the growth of both *S. griseus,* and *S. fradiae* can be monitored using visible light absorbance.
Growth curve of 3 bacterial species—*E. coli* (green), *S. griseus* (blue) and *S. fradiae* (magenta)— grown at 28°C with continuous shaking at 250 rpm for over 48 hours reveal their growth pattern. The "noisy" pattern of growth for *S. griseus* and *S. fradiae* species is due to the formation of clumps of cells. However, despite this noise, both species have comparable overall shapes of their growth curves to that of *E. coli*, which makes it possible to monitor the growth of these *Streptomyces* cultures in liquid media.

Overall, this experiment showed that *S. griseus* and *S. fradiae* cultures can be effectively maintained in liquid media under laboratory conditions.

5.2.2 Streptomyces biomass can be produced in sufficient quantities for ribosome isolation.

To estimate the amount of biomass required for ribosome isolation from *Streptomyces* species, previously reported data on ribosome abundance and isolation protocols were considered. For example, an *E. coli* cell is estimated to contain a minimum of 10,000 ribosomes at any of growth stage (276). Standard ribosome isolation methods, such as those based on ultracentrifugation or chemical precipitation of ribosomes from lysates, typically require ~100 mg of cell pellets to yield sufficient ribosomes for cryo-EM analyses (277). Based on this knowledge, *S. fradiae* and *S. griseus* biomass was produced in 750 mL of GYM broth per species under slightly different conditions. Upon harvest, 7.4 g of cell mass was obtained for *S. fradiae,* and 4.2 g for and *S. griseus,* yielding sufficient cell material for downstream ribosome isolation.

5.2.3 Ribosomes can be efficiently isolated from Streptomyces using chemical precipitation with polyethylene glycol with subsequent sucrose gradient fractionation.

To isolate ribosomes from the obtained biomass, a protocol developed by Helena-Bueno et al., was used (278). This method involved two main steps: (i) initial chemical precipitation of crude ribosomes using polyethylene glycol 20,000 (PEG 20K), and (ii) purification of ribosomes using sucrose gradient (10-30%) fractionation.

First, to release the soluble contents of the cellular cytosol containing ribosomes, cells were disrupted by mechanical shaking with glass beads, followed by removal of cell debris. Ribosomes were then precipitated from the cell lysate using PEG 20K, a water soluble polymer that reduces the solubility of macromolecules, including ribosomes, thereby causing their reversible precipitation (279). This approach was chosen for its efficiency and ability to minimize ribosome degradation by endogenous nucleases and proteases. Unlike traditional ultracentrifugation-based method, which typically requires several hours, PEG-based precipitation enabled ribosome recovery in under 10 minutes (280).

The success of the ribosome isolation procedure was confirmed by negative staining transmission electron microscopy. This technique revealed the presence of apparent ribosome-like particles, visible as negatively stained white objects of ~20 nm in diameter (**Figure 5.4**).

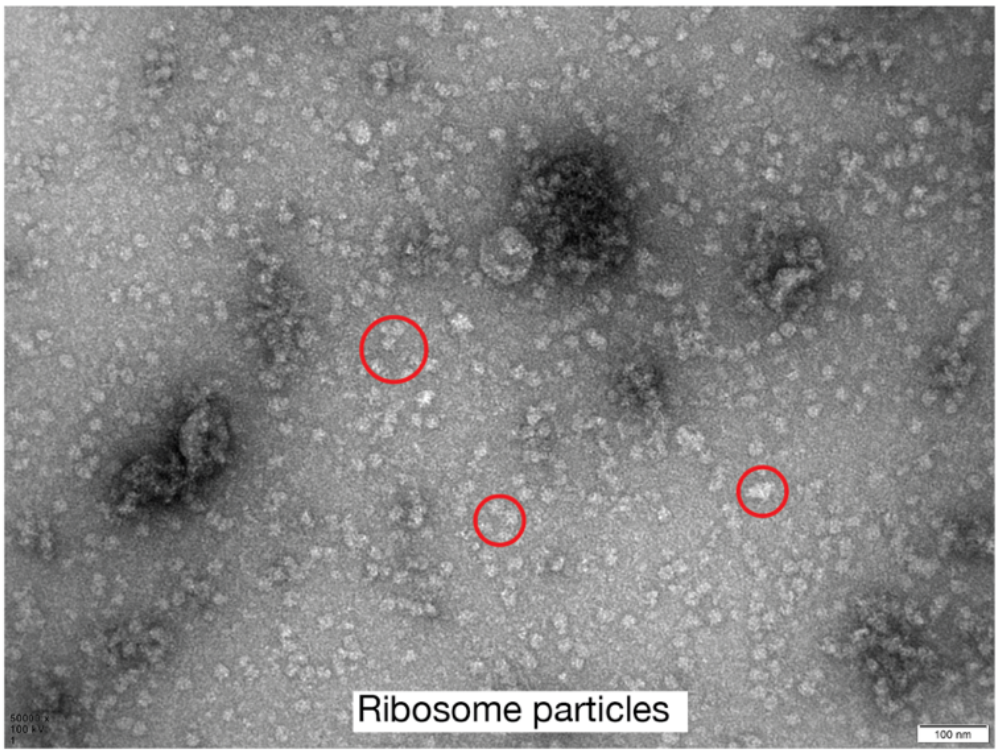

Figure 5.4 | Negative stain image of PEG 20K precipitated ribosome particles of *S. griseus*. The micrograph shows a negative stain image of *S. griseus* ribosome particles (observed as ~20 nm-size white objects on a dark background). Red circles highlight some of the apparent ribosome particles. A scale bar of 100 nm is shown at the bottom right corner of the image.

To enable accurate determination of ribosome concentration and ensure optimal sample quality for cryo-EM, the crude ribosome samples were further purified using sucrose gradient fractionation This method allows molecules to be separated based on their sedimentation rate, which depends on their molecular weight. The sucrose gradient profile revealed a characteristic peak corresponding to 70S ribosomes (**Figure 5.5**).

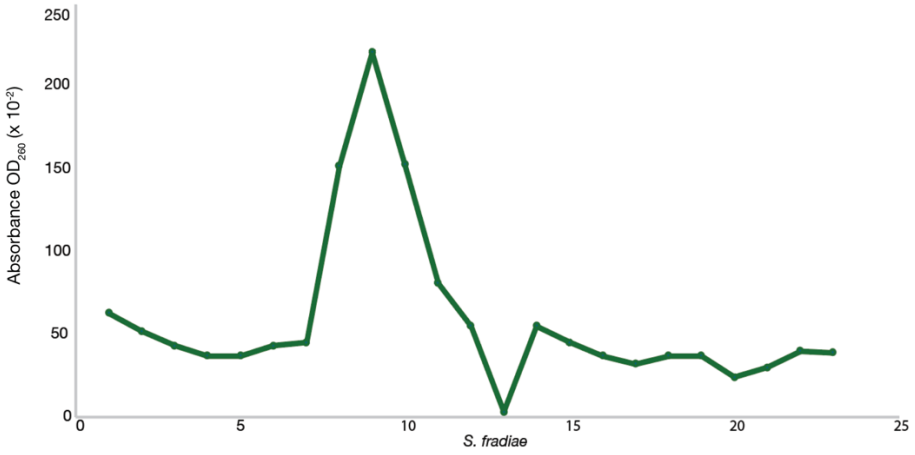

Figure 5.5 | Sucrose gradient analysis of *Streptomyces* ribosome samples.
A plot of OD_{260} absorbance unit against individual sucrose gradient analysis fractions reveals the portions of the crude ribosome sample that contains ribosomes.

5.2.4 Optical density measurements allow to prepare ribosome concentration for structural analyses.

To ensure that the concentration of purified ribosome samples was sufficient for cryo-EM analysis, the absorbance unit of the ribosome-containing fractions was measured at 260 nm (OD_{260}). This step was important because an optimal sample concentration ensures a densely populated yet non-overlapping distribution of ribosome particles on the cryo-EM grid surface (281). Previous studies showed that 3-5 µL samples with concentrations between 10 and 5,000 nM, are suitable for cryo-EM analysis,—with 300-400 nM being optimal for grids without carbon support (282,283). Based on this, the concentration of the purified ribosome sample was estimated to be ~564 nM (A_{260} = 24.52) in a final volume of 1 mL, which is near the optimal range requiring minimal dilution for subsequent data collection. Thus, sufficient quantities of pure, and optimally concentrated ribosome samples were obtained for cryo-EM analysis.

5.2.5 Ribosomes can be successfully applied to cryo-EM grids for data collection.

To understand the theoretical principles of optimal particle distribution in cryo-EM grid holes, calculations were performed to estimate grid hold size and ribosome sample concentration (in particles per 1 μm^3) at an OD_{260} value of 1. These calculations confirmed that a 300 nM ribosome solution would achieve a densely populated, non-overlapping distribution of particles in grid hole (**Appendix 3, SI Calculations S5.1**).

An aliquot of the 300 nM diluted ribosome sample was loaded onto a Quantifoil copper grid and plunge frozen in liquid ethane for data collection. Inspection of particle distribution in a few random grid holes revealed optimal distribution of particles in broad orientation (**Figure 5.6**). Consequently, over 3,900 micrograph movie frames were collected (**Figure 5.6, Appendix 3 SI Figure S5.1**), for *S. griseus* and *S. fradiae* (**Appendix 3 SI Figure S5.3)** datasets using the parameters listed in **Tables 2.9 and 2.10**. For clarity, data from *S. griseus* is presented in the subsequent sections of this chapter, while data corresponding for *S. fradiae* are provided in the **Appendix 3 SI Figure S5.3-5.5**.

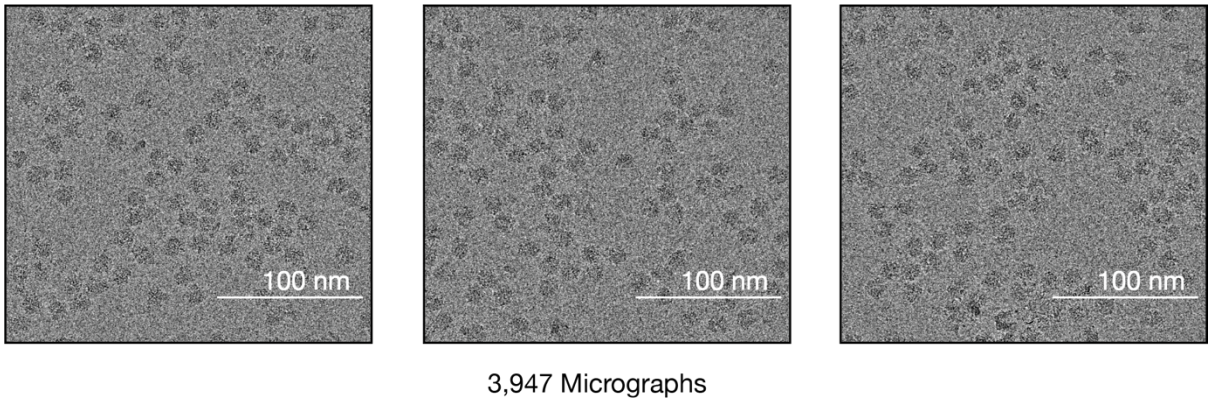

Figure 5.6 | A representative cryo-EM micrographs showing *S. griseus* ribosome particles on a cryo-EM grid.
Micrographs captured at 100 nm scale reveal ribosome particles, visible as dark, densely packed objects—~20 nm in diameter, contrasted against a lighter background within the grid holes.

5.2.6 Data collection produces 2D classes that confirm the presence of ribosomes.

To generate a cryo-EM map for structural model building, the data was processed by correcting electron beam-induced particle movement, aligning movie frames into micrographs and extracting apparent ribosome particles from the micrographs (**Appendix 3, SI Figure S5.1**). To separate ribosome particles from non-ribosome particles, standard 2D classification was performed, merging similar 2D projection images of ribosome particles to enhance the signal-to-noise ratio. This allowed ribosome images to be distinguished from non-ribosome images through visual inspection of each 2D classes (**Appendix 3, SI Figure S5.1**).

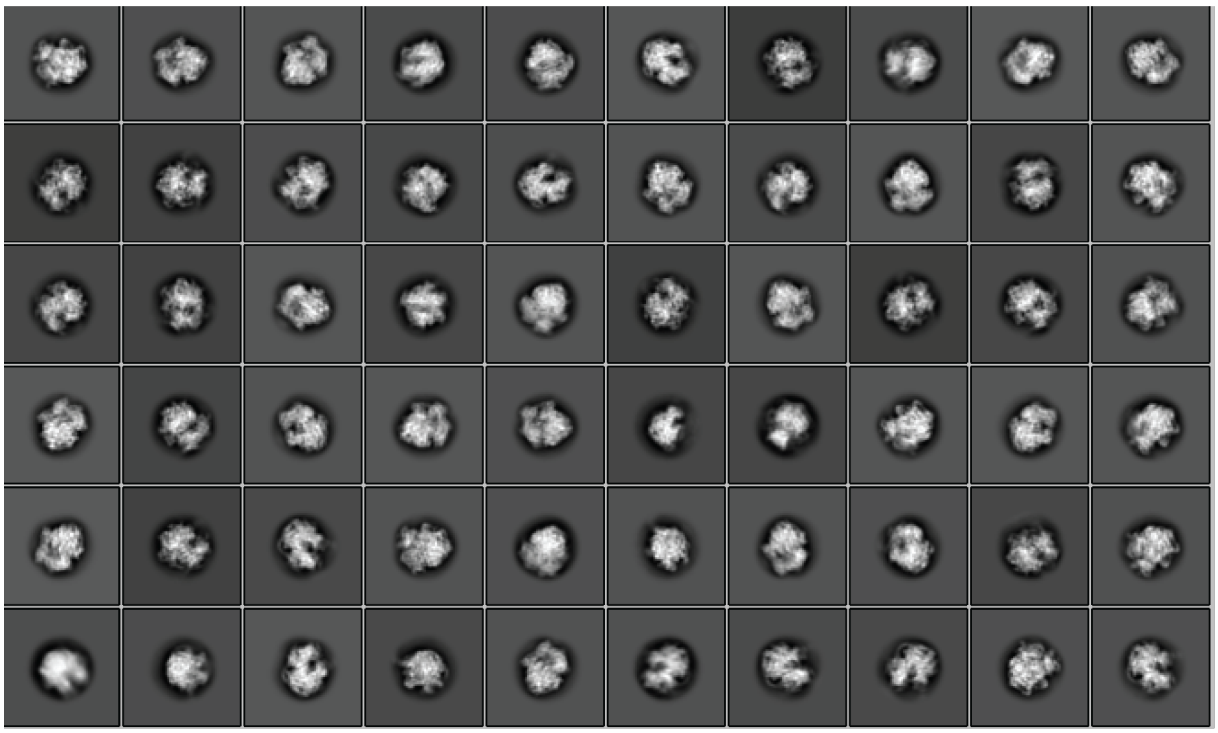

2D Class average of *S. griseus* ribosomes particles

Figure 5.7 | | 2D class average of *S. griseus* ribosome particles.
2D projections of apparent good ribosome particles showing the projections corresponding to the structural subunits of the ribosomes. The distribution of particles into distinct class averages allows for a glimpse at the heterogeneity of the particles.

From the dataset, 60 2D class averages, corresponding to 371, 502 particles, were selected. These classes confirmed that most particles were ribosomes and enabled their selection for further processing to generate the cryo-EM map (**Figure 5.7**).

5.2.7 3D reconstructions of the selected 2D classes result in a high-resolution map of the S. griseus 70S ribosome.

Previous studies revealed that tens of thousands of ribosome particles are typically sufficient to generate cryo-EM maps with resolutions of 3.5 Å or higher—enabling visualisation of atomic details such as protein side chains and the overall shapes of nucleotide bases (284,285). To generate a high-resolution 3D cryo-EM map, an initial low resolution cryo-EM showing the shape of an average ribosome was generated using the 371,502 selected ribosome particles (**Figure 5.8a, b**). Subsequent separation based on ribosome substates and sub-conformations identified the most common state, corresponding to 85,421 particles. Using these, a refined cryo-EM map of 3.1 Å resolution was produced, revealing detailed rRNA and protein features

(**Figure 5.8c, d, e**). This map enabled molecular modelling of the *S. griseus* ribosome architecture and its drug-binding sites.

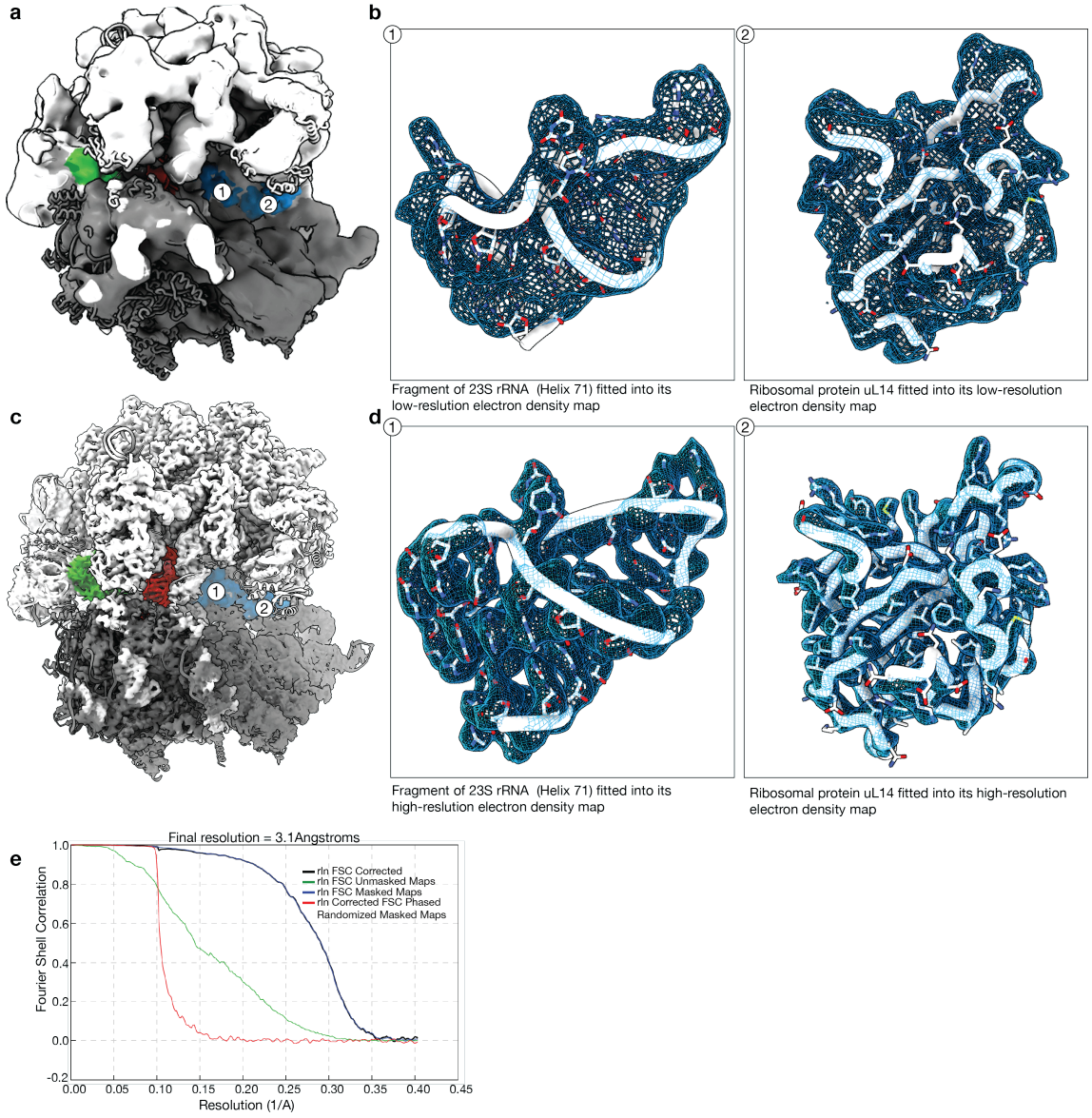

Figure 5.8 | Overview of 3D cryo-EM map of *S. griseus* ribosome.
(a) Initial low-resolution 3D reconstruction of *S. griseus* ribosome cryo-EM map. **(b)** Zoomed-in view of the map shown in **(a),** highlighting: (1) a segment of 23S rRNA—specifically Helix 71 (H71)—and (2) ribosomal protein uL14 both fitted into their corresponding electron density. **(c)** Refined high-resolution 3D map of *S. griseus* ribosomes with a final resolution of 3.1 Å. **(d)** Zoomed-in view of the high-resolution map in **(c),** showing atomic details of: (1) the rRNA bases in H71 and (2) amino acid side chains of ribosomal protein uL14. **(e)** Fourier shell correlation (FSC) plots confirming a final resolution of 3.1 Å for the refined map shown in **(c)**.

5.2.8 The model building of S. griseus ribosomes could be accelerated using AI-predicted molecular structures of ribosomal RNA and proteins.

To build the molecular model of *S. griseus* 70S ribosome, a time-efficient approach was adopted to accelerate the model building process. Traditional methods of building structural models into electron density maps typically involve either building models from scratch or modifying existing models based on sequence data and electron density maps. These methods, while important for modelling structures of proteins and other biomolecules in the past few decades, are usually labour-intensive and time-consuming.

The advent of AlphaFold, an advanced AI-based structure prediction tool, has revolutionised this process by enabling high-accuracy prediction of protein and other biomolecular structures from sequence data (129,130). Using this powerful tool, structural models of individual components of *S. griseus* 70S ribosome, including the three rRNAs (5S, 16S, and 23S rRNAs) (**Figure 5.9**) and 53 ribosomal proteins were generated from their sequence data (**Appendix 3, SI Figure S5.2**).

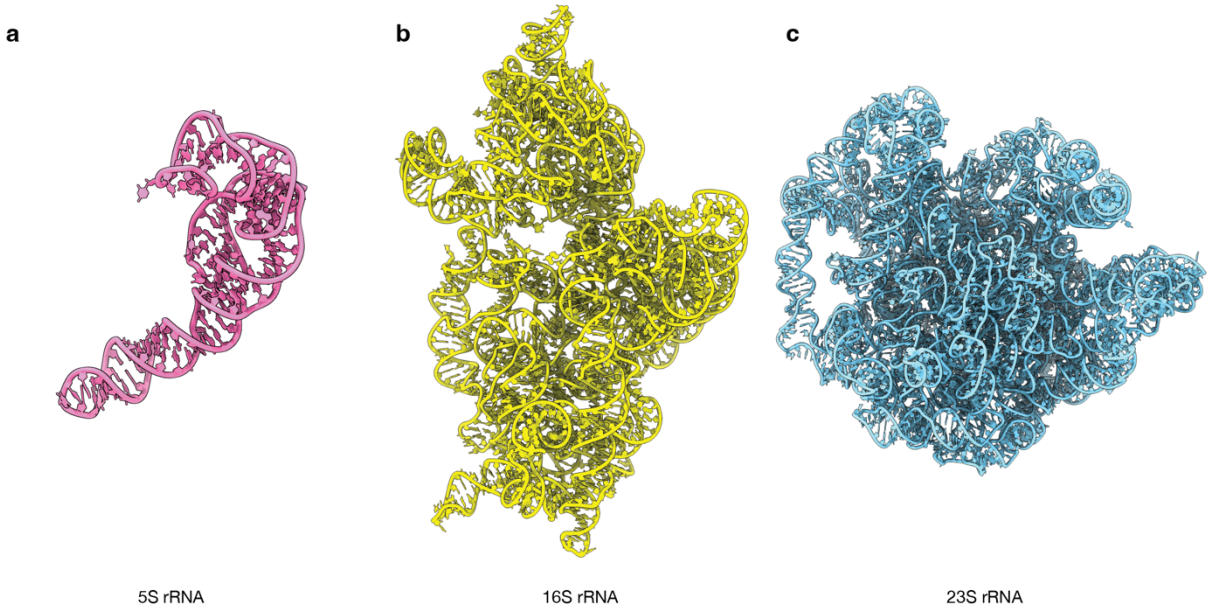

Figure 5.9 | AlphaFold predicts 3D models of *S. griseus* rRNAs.
(a-c) AlphaFold predicted model of *S. griseus* 5S rRNA (hot pink), 16S rRNA (yellow), and 23S rRNA (blue).

After generating AlphaFold models of *S. griseus* 70S ribosome components, these models were fitted into their corresponding electron density in the cryo-EM map. The *M. smegmatis* 70S ribosome model (285) was initially docked into the cryo-EM as a reference. Each AlphaFold-predicted *S. griseus* 70S ribosome components were then aligned to its homologous counterpart in the *M. smegmatis* model, ensuring accurate placement in the cryo-EM map. These models were manually refined, assembled and validated into the *S. griseus* 70S ribosome complex (**Figure 5.10, 5.11a**). This approach highlights the effective integration of artificial intelligence into cryo-EM workflows for modelling complex macromolecular assemblies.

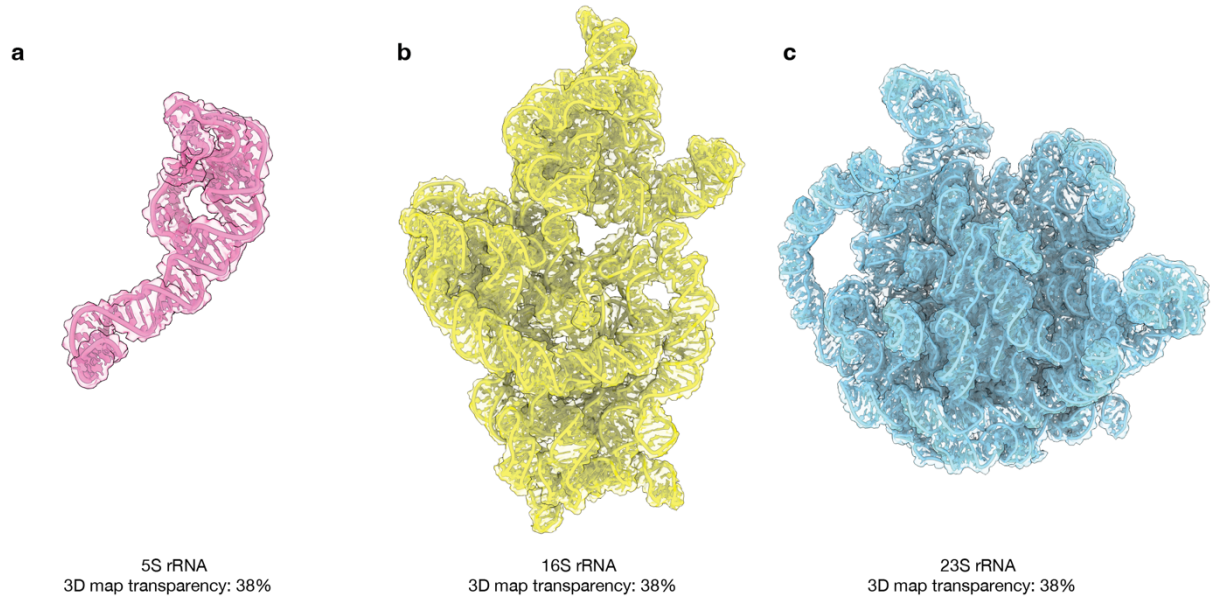

Figure 5.10 | 70S ribosome model of *S. griseus* built by fitting AlphaFold models in cryo-EM map. **(a-c)** Real space refined and rigid body fitted models of 5S rRNA (hot pink), 16S rRNA (yellow) and 23S rRNA (blue) in their corresponding electron density map (shown as surface) of *S. griseus* ribosome.

5.2.9 Structural features of ribosomes from the antibiotic-producing bacteria S. griseus.

To assess the impact of the observed evolutionary variations on *S. griseus* ribosome structure, initial analysis of the cryo-EM map showed that ribosome particles in the *S. griseus* dataset were bound to canonical protein synthesis ligands, including P-site, E-site and mRNA, indicating that translating ribosomes are the most predominant functional state of particles in this dataset (**Figure 5.11**). Distinctive architectural features of *Streptomyces* ribosomes were identified, including rRNA expansions in helices H54, H15 and H16. Notably, the expanded end of H54 interacts with ribosomal protein S1 of the 30S subunit, a unique yet functionally

uncharacterized, feature of *Streptomyces* ribosomes. Additionally, ribosomal protein, bS22 which differentiates *S. griseus* ribosomes from those of other bacteria like *E. coli* or *T. thermophilus* (**Figure 5.11**) was observed. This finding is consistent with observations in other Actinobacteria, including *M. smegmatis* and *M. tuberculosis*.

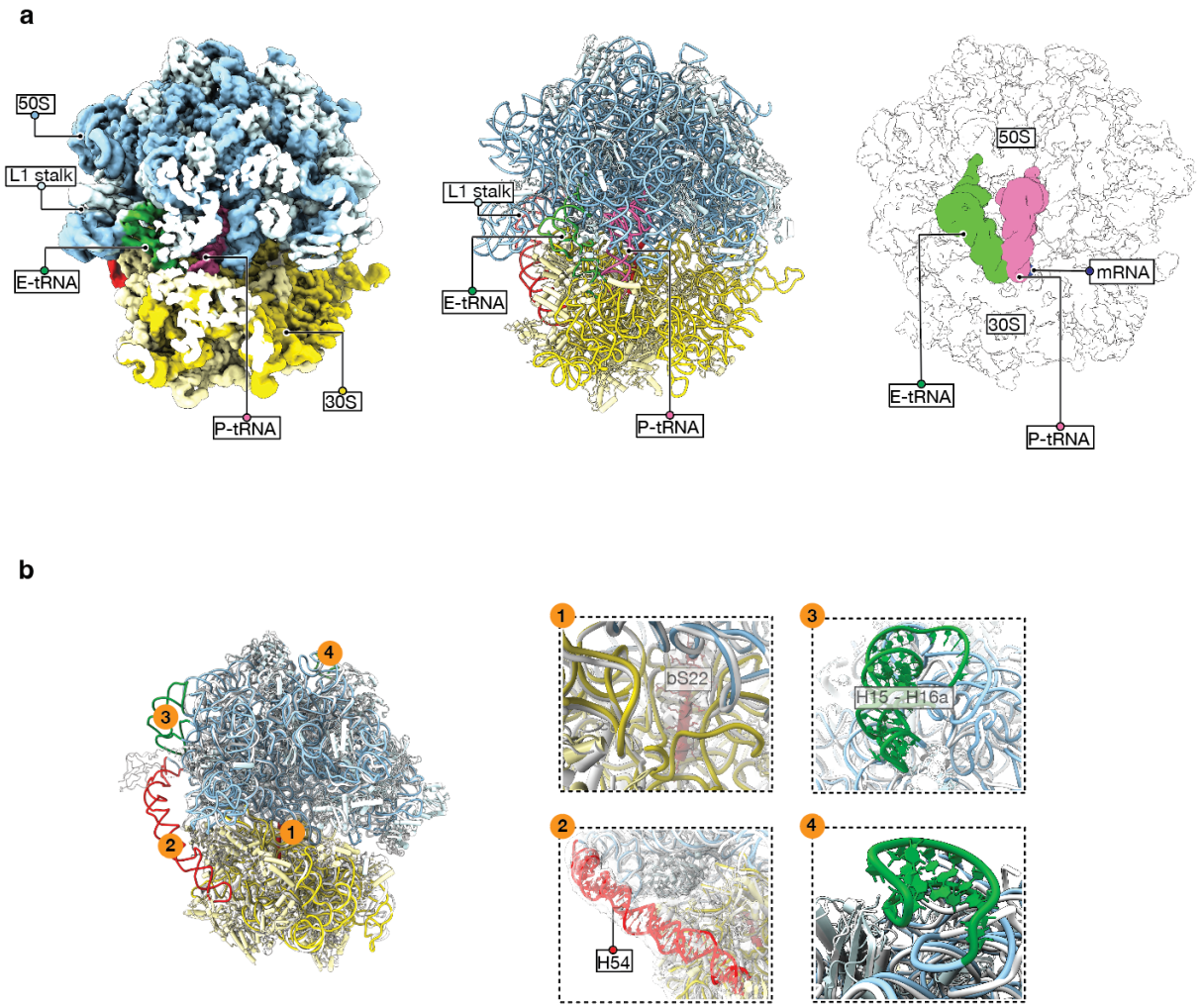

Figure 5.11 | Structural features of ribosomes from *S. griseus*.
(a) Cryo-EM map (coloured by protein and rRNA chains) reveals structural features of the 70S ribosome from the streptomycin-producing bacterium *S. griseus*. **(b)** Comparison of major features and proteins in ribosomes from *S. griseus* and *E. coli* (white) illustrates such characteristic features as the presence of the 23S rRNA helices H15, H16, and H54 along with the additional protein bS22, which distinguish ribosomes of Actinobacteria from those of *E. coli* and other bacterial phyla.

5.2.10 Sequence variation in S. griseus ribosomal drug-binding sites alters structure of the drug-binding pocket for peptide inhibitors of the large ribosomal subunit.

To understand the structural impact of the three rRNA mutations found in the drug-binding sites of *Streptomyces* ribosomes—two located in the decoding centre of the 30S subunit and one in the 50S subunit near the A site (**Appendix 2, SI Data S4.3 and S4.4**)—this study focused specifically on the mutation in helix 91 (H91) of the 23S rRNA, found at the orthosomycin drug-binding site (**Figure 5.12**). The mutations in the decoding centre were excluded because they have previously characterized in the distantly related, *M. smegmatis* (69).

Orthosomycin drugs, such as avilamycin and evernimicin, are natural antibiotics that inhibit bacterial translation by binding to the A site of the 50S ribosomal subunit. This binding specifically disrupts the late stage of aminoacyl-tRNA accommodation, thereby preventing proper tRNA positioning during protein synthesis (286,287).

Compared to *E. coli,* the *S. griseus* ribosome bears two-point mutations in this drug-binding site: A2530G and A2534C (**Figure 5.12a, b**). In both *E. coli* and *S. griseus*, residue A2530 interacts with evernimicin through its phosphate backbone, forming a non-sequence dependent interaction (**Figure 5.12c**). This suggests that the A2530G mutation is unlikely to alter ribosome-drug recognition. In contrast, the 23S rRNA residue, A2534 forms a sequence-dependent interaction with evernimicin through its nitrogenous base. The A2534C mutation, replaces the larger adenine (A) base with the smaller cytosine (C), creating a gap between the nucleotide and the terminal benzyl ring I of evernimicin. This structural change could weaken the interaction between the ribosome and evernimicin at this site.

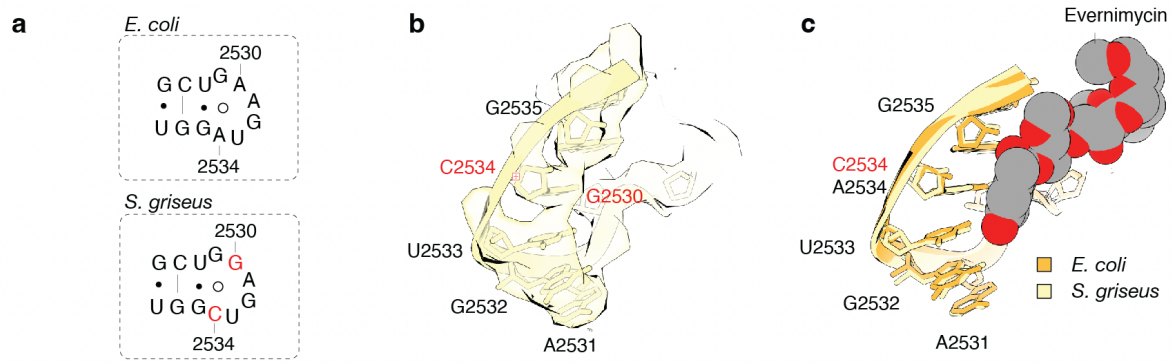

Figure 5.12 | Substitutions of rRNA drug-binding residue in *S. griseus* ribosomes alter the shape of the drug-binding pocket.
(a) Comparison of the secondary structures of *E. coli* and *S. griseus* rRNA reveals two sequence variations (highlighted in red) within one of the ribosomal drug-binding sites located in the 50S subunit. **(b)** Structure of *S. griseus* ribosomal drug-binding pocket showing the two mutated residues; G2530 and C2534 (highlighted in red). **(c)** Superposition of drug-binding pocket models from *E. coli* (PDB 4V53) and *S. griseus* shows the likely impact of A2534C mutation on the recognition of the natural antibiotic evernimicin. Evernimicin (shown in grey; PDB 5KCS) is docked into both *E. coli* and *S. griseus* ribosome models.

5.2.11 The aminoglycoside drug-binding site in S. griseus ribosomes possess an additional protein, bS22.

Previously, certain Actinobacteria species were shown to contain additional ribosomal proteins within the drug-binding sites of their ribosomes (77,78,81). Specifically, cryo-EM structures of *M. smegmatis* 70S ribosome revealed two additional ribosomal proteins, bS22 and bL37, with bS22 located near the aminoglycoside drug-binding site in the decoding centre (288). Further genetic studies showed that deletion of bS22 increases *Mycobacterium* sensitivity to aminoglycoside antibiotics, such as kanamycin and gentamicin (288,289). These studies provided an illustration that ribosomes from certain bacteria possess additional proteins in their drug-binding sites and, as a result, can have a significantly lower sensitivity to drugs without substitutions in their rRNA.

Here, the structure of the *S. griseus* 70S ribosomes determined in the study reveals the presence of the additional ribosomal protein, bS22 (**Figure 5.13a, b**). Similar to observations in *M. smegmatis* ribosomes, the conserved lysine residue (K16) of bS22 interacts with the phosphate backbone of the 16S rRNA residue U1406 (**Figure 5.13b**), thereby reducing the accessibility of the aminoglycoside-binding pocket for drug-targeting. This structural feature suggests that

S. griseus ribosomes may possess inherently higher tolerance to aminoglycoside antibiotics, similarly to the aforementioned study in *M. smegmatis* (288).

Additionally, extended evolutionary analysis revealed that the ribosomal protein bL37, previously considered a common feature of Actinobacteria ribosomes, is in fact missing in *S. griseus* ribosome. This absence is supported by the lack of corresponding electron density for bL37 in the cryo-EM map of *S. griseus* ribosomes from this study. Furthermore, bL37 was found in only ~7% of species with detectable bS22 homologs. The reason for bL37's presence in some Actinobacteria ribosomes and its sporadic occurrence in a small subset of species across different clades in Actinobacteria remains unknown (**Figure 5.13c, d**).

Overall, this analysis illustrates that—even when ribosomes from different bacterial species share conserved rRNA sequences in their drug-binding pockets—the atomic structures of these pockets can be dissimilar in these species due to variations in the protein content of ribosomes (for example, when bS22 is present in one species but absent in another).

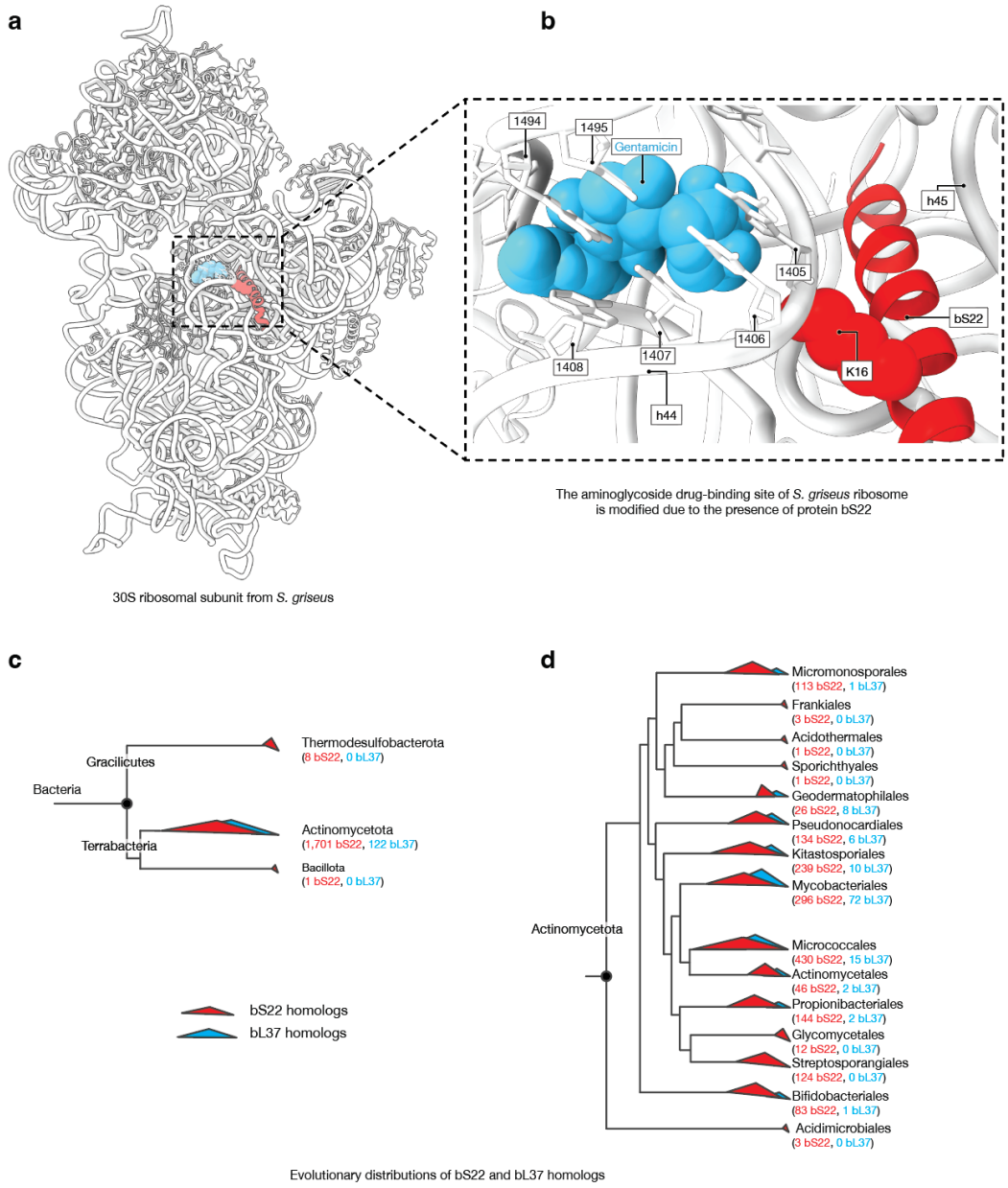

Figure 5.13 | *Streptomyces* possess an additional protein in one of their drug-binding sites. **(a)** The atomic model of the 30S ribosomal subunit from *S. griseus* (determined in this study) reveals the presence of an additional ribosomal protein bS22 (red) near the decoding centre of the ribosome. bS22 is located in the vicinity of the binding sites for drugs from the gentamicin family (the model of gentamicin is docked here for illustration purposes and shown in blue, PDB 4V53). **(b)** Zoomed-in view showing that the side chain of K16 residue of bS22 binds to the phosphate group of G1405 in the helix h44 in the 16S rRNA. **(c)** Taxonomic distribution of homologs of bS22 (red) and bL37 (blue) reveals that bS22 homologs are present in 3 bacterial phyla including Actinomycetota, Bacillota and Thermodesulfobacteriota, while bL37 homologs are found only in Actinomycetota phylum. **(d)** Phylogenetic of Actinomycetota showing the distribution of bS22 and bL37 homologs are in members of this branch.

5.3 Discussion and perspectives

In this study, structural analysis of the *S. griseus* ribosome revealed that naturally occurring rRNA sequence variations alter the architecture of the drug-binding pocket for orthosomycin-class antibiotics. By solving the 3D structure of this modified drug-binding pocket, the groundwork for potential rational design of lineage-specific ribosome-targeting antibiotic is laid. In addition to rRNA substitutions, the presence of an additional ribosomal protein, bS22, in *S. griseus* and likely other *Streptomyces* species, may influence the accessibility or affinity of the aminoglycoside-binding site for antibiotic interaction.

However, this work had limitations and raises important unresolved questions. Specifically, one limitation of this work stems from the lack of quantitative biochemical data on the impact of rRNA substitutions on ribosome-drug affinity. The finding from this study suggests that *Streptomyces* ribosomes can be less sensitive to evernimicin as the 23S rRNA substitution A2534C appears to eliminate the hydrophobic contacts between terminal benzyl ring I of the evernimicin and C2534— found in *S. griseus*, suggesting reduced binding potential. This line of reasoning is supported by previous findings where the 23S rRNA substitution C2534U—at the very same site, caused a 3 times increase in minimum inhibitory concentration in a clinical and linezolid -resistant strain of *Staphylococcus epidermidis* (250).

However, while this structural change could suggest potential impact, there is currently no biochemical data quantifying how the A2534C substitution affects the affinity of *S. griseus* ribosomes (and other ribosomes bearing this variation) for evernimicin. Therefore, future studies using quantitative biochemical or other functional methods will be required to address the following critical questions:

- How many of the naturally occurring substitutions in rRNA identified in this study are functionally neutral and how many render ribosomes more resistant or sensitive to ribosome-targeting antibiotics?
- And, for those substitutions that do impact the ribosome affinity to drugs, are these differences sufficient for the development of lineage-specific inhibitors of protein synthesis that would target only a subset of bacterial or eukaryotic ribosomes in naturally occurring species?

References

1. Palade GE. A small particulate component of the cytoplasm. J Biophys Biochem Cytol. 1955;1(1):59.

2. Berman HM, Westbrook J, Feng Z, Gilliland G, Bhat TN, Weissig H, et al. The protein data bank. Nucleic Acids Res. 2000;28(1):235–42.

3. Goodsell DS, Dutta S, Zardecki C, Voigt M, Berman HM, Burley SK. The RCSB PDB "molecule of the month": inspiring a molecular view of biology. PLoS Biol. 2015;13(5):e1002140.

4. Claude A. The constitution of protoplasm. Science. 1943;97(2525):451–6.

5. Roberts RB. Microsomal particles and protein synthesis; papers presented at the First Symposium of the Biophysical Society, at the Massachusetts Institute of Technology, Cambridge, February 5, 6, and 8, 1958.

6. Vanzi F, Vladimirov S, Knudsen CR, Goldman YE, Cooperman BS. Protein synthesis by single ribosomes. Rna. 2003;9(10):1174–9.

7. Fox GE. Origin and evolution of the ribosome. Cold Spring Harb Perspect Biol. 2010;2(9):a003483.

8. Mahendrarajah TA, Moody ER, Schrempf D, Szánthó LL, Dombrowski N, Davín AA, et al. ATP synthase evolution on a cross-braced dated tree of life. Nat Commun. 2023;14(1):7456.

9. Bowman JC, Petrov AS, Frenkel-Pinter M, Penev PI, Williams LD. Root of the tree: The significance, evolution, and origins of the ribosome. Chem Rev. 2020 June 10;120(11):4848–78.

10. Caetano-Anollés G. Tracing the evolution of RNA structure in ribosomes. Nucleic Acids Res. 2002;30(11):2575–87.

11. Caetano-Anollés G, Caetano-Anollés D. Computing the origin and evolution of the ribosome from its structure—Uncovering processes of macromolecular accretion benefiting synthetic biology. Comput Struct Biotechnol J. 2015;13:427–47.

12. Farías-Rico JA, Mourra-Díaz CM. A short tale of the origin of proteins and ribosome evolution. Microorganisms. 2022;10(11):2115.

13. Harish A, Caetano-Anolles G. Ribosomal history reveals origins of modern protein synthesis. PLoS One. 2012;7(3):e32776.

14. Petrov AS, Gulen B, Norris AM, Kovacs NA, Bernier CR, Lanier KA, et al. History of the ribosome and the origin of translation. Proc Natl Acad Sci. 2015 Dec 15;112(50):15396–401.

15. Petrov AS, Bernier CR, Hsiao C, Norris AM, Kovacs NA, Waterbury CC, et al. Evolution of the ribosome at atomic resolution. Proc Natl Acad Sci. 2014;111(28):10251–6.

16. Melnikov S, Ben-Shem A, Garreau de Loubresse N, Jenner L, Yusupova G, Yusupov M. One core, two shells: bacterial and eukaryotic ribosomes. Nat Struct Mol Biol. 2012;19(6):560–7.

17. Tenson T, Mankin A. Antibiotics and the ribosome. Mol Microbiol. 2006;59(6):1664–77.

18. Wilson DN. The A-Z of bacterial translation inhibitors. Crit Rev Biochem Mol Biol. 2009;44(6):393–433.

19. World Health Organization. The selection and use of essential medicines: report of the WHO expert committee on selection and use of essential medicines, 2021 (including the 22nd WHO model list of essential medicines and the 8th WHO model list of essential medicines for children). 2021;

20. Wilson DN. Ribosome-targeting antibiotics and mechanisms of bacterial resistance. Nat Rev Microbiol. 2014 Jan;12(1):35–48.

21. Garreau De Loubresse N, Prokhorova I, Holtkamp W, Rodnina MV, Yusupova G, Yusupov M. Structural basis for the inhibition of the eukaryotic ribosome. Nature. 2014 Sept 25;513(7519):517–22.

22. Fleming A. On the antibacterial action of cultures of a penicillium, with special reference to their use in the isolation of *B. influenzae*. Br J Exp Pathol. 1929;10(3):226.

23. Chain E, Florey HW, Gardner AD, Heatley NG, Jennings MA, Orr-Ewing J, et al. Penicillin as a chemotherapeutic agent. The lancet. 1940;236(6104):226–8.

24. Florey HW, Abraham E. The work on penicillin at Oxford. J Hist Med Allied Sci. 1951;302–17.

25. Waksman SA, Starkey RL. Partial sterilization of soil, microbiological activities and soil fertility: II. Soil Sci. 1923;16(4):247–68.

26. Waksman SA. Associative and antagonistic effects of microorganisms: I. Historical review of antagonistic relationships. Soil Sci. 1937;43(1):51–68.

27. Woodruff HB. Selman A. Waksman, winner of the 1952 Nobel Prize for physiology or medicine. Appl Environ Microbiol. 2014;80(1):2–8.

28. Hutchings MI, Truman AW, Wilkinson B. Antibiotics: past, present and future. Curr Opin Microbiol. 2019;51:72–80.

29. Waksman SA, Woodruff HB. Streptothricin, a new selective bacteriostatic and bactericidal agent, particularly active against Gram-negative bacteria. Proc Soc Exp Biol Med. 1942;49(2):207–10.

30. Waksman SA, Tishler M. The chemical nature of actinomycin, an antimicrobial substance produced by *Actinomyces antibloticus*. 1942;

31. Waksman SA, Horning ES, Spencer EL. Two antagonistic fungi, *Aspergillus fumigatus* and *Aspergillus clavatus*, and their antibiotic substances. J Bacteriol. 1943;45(3):233–48.

32. Schatz A, Bugle E, Waksman SA. Streptomycin, a Substance Exhibiting Antibiotic Activity Against Gram-Positive and Gram-Negative Bacteria.*. Exp Biol Med. 1944 Jan 1;55(1):66–9.

33. Feldman W, Hinshaw H. Effects of streptomycin on experimental tuberculosis in guinea pigs: Preliminary report. 1944;

34. Ekemezie CL, Melnikov SV. Hibernating ribosomes as drug targets? Front Microbiol. 2024;15:1436579.

35. Lin J, Zhou D, Steitz TA, Polikanov YS, Gagnon MG. Ribosome-targeting antibiotics: modes of action, mechanisms of resistance, and implications for drug design. Annu Rev Biochem. 2018;87(1):451–78.

36. Polikanov YS, Aleksashin NA, Beckert B, Wilson DN. The mechanisms of action of ribosome-targeting peptide antibiotics. Front Mol Biosci [Internet]. 2018 [cited 2023 June 7];5. Available from: https://www.frontiersin.org/articles/10.3389/fmolb.2018.00048

37. Dinos G, Wilson DN, Teraoka Y, Szaflarski W, Fucini P, Kalpaxis D, et al. Dissecting the ribosomal inhibition mechanisms of edeine and pactamycin: the universally conserved residues G693 and C795 regulate P-Site RNA binding. Mol Cell. 2004 Jan 16;13(1):113–24.

38. Okuyama A, Machiyama N, Kinoshita T, Tanaka N. Inhibition by kasugamycin of initiation complex formation on 30S ribosomes. Biochem Biophys Res Commun. 1971;43(1):196–9.

39. Schuwirth BS, Day JM, Hau CW, Janssen GR, Dahlberg AE, Cate JHD, et al. Structural analysis of kasugamycin inhibition of translation. Nat Struct Mol Biol. 2006;13(10):879–86.

40. Schluenzen F, Takemoto C, Wilson DN, Kaminishi T, Harms JM, Hanawa-Suetsugu K, et al. The antibiotic kasugamycin mimics mRNA nucleotides to destabilize tRNA binding and inhibit canonical translation initiation. Nat Struct Mol Biol. 2006;13(10):871–8.

41. Zhang Y, Aleksashin NA, Klepacki D, Anderson C, Vázquez-Laslop N, Gross CA, et al. The context of the ribosome binding site in mRNAs defines specificity of action of kasugamycin, an inhibitor of translation initiation. Proc Natl Acad Sci. 2022;119(4):e2118553119.

42. Pioletti M, Schlünzen F, Harms J, Zarivach R, Glühmann M, Avila H, et al. Crystal structures of complexes of the small ribosomal subunit with tetracycline, edeine and IF3. EMBO J. 2001;

43. Wilson DN, Schluenzen F, Harms JM, Starosta AL, Connell SR, Fucini P. The oxazolidinone antibiotics perturb the ribosomal peptidyl-transferase center and effect tRNA positioning. Proc Natl Acad Sci. 2008;105(36):13339–44.

44. Paranjpe MN, Marina VI, Grachev AA, Maviza TP, Tolicheva OA, Paleskava A, et al. Insights into the molecular mechanism of translation inhibition by the ribosome-targeting antibiotic thermorubin. Nucleic Acids Res. 2023;51(1):449–62.

45. Bulkley D, Johnson F, Steitz TA. The antibiotic thermorubin inhibits protein synthesis by binding to inter-subunit bridge B2a of the ribosome. J Mol Biol. 2012;416(4):571–8.

46. Savelsbergh A, Rodnina MV, Wintermeyer W. Distinct functions of elongation factor G in ribosome recycling and translocation. Rna. 2009;15(5):772–80.

47. Peske F, Rodnina MV, Wintermeyer W. Sequence of steps in ribosome recycling as defined by kinetic analysis. Mol Cell. 2005;18(4):403–12.

48. Svetlov MS, Koller TO, Meydan S, Shankar V, Klepacki D, Polacek N, et al. Context-specific action of macrolide antibiotics on the eukaryotic ribosome. Nat Commun. 2021;12(1):2803.

49. Syroegin EA, Flemmich L, Klepacki D, Vazquez-Laslop N, Micura R, Polikanov YS. Structural basis for the context-specific action of the classic peptidyl transferase inhibitor chloramphenicol. Nat Struct Mol Biol. 2022;29(2):152–61.

50. Syroegin EA, Aleksandrova EV, Polikanov YS. Structural basis for the inability of chloramphenicol to inhibit peptide bond formation in the presence of A-site glycine. Nucleic Acids Res. 2022;50(13):7669–79.

51. Tsai K, Stojković V, Lee DJ, Young ID, Szal T, Klepacki D, et al. Structural basis for context-specific inhibition of translation by oxazolidinone antibiotics. Nat Struct Mol Biol. 2022;29(2):162–71.

52. Recht MI, Douthwaite S, Puglisi JD. Basis for prokaryotic specificity of action of aminoglycoside antibiotics. EMBO J. 1999;

53. Berdy J. Bioactive microbial metabolites. J Antibiot (Tokyo). 2005;58(1):1–26.

54. McDonald BR, Currie CR. Lateral gene transfer dynamics in the ancient bacterial genus Streptomyces. MBio. 2017;8(3):10–1128.

55. Nikolaidis M, Hesketh A, Frangou N, Mossialos D, Van de Peer Y, Oliver SG, et al. A panoramic view of the genomic landscape of the genus *Streptomyces*. Microb Genomics. 2023;9(6):001028.

56. Mayfield C, Williams S, Ruddick S, Hatfield H. Studies on the ecology of actinomycetes in soil IV. Observations on the form and growth of streptomycetes in soil. Soil Biol Biochem. 1972;4(1):79–91.

57. Hopwood DA. *Streptomyces* in nature and medicine: the antibiotic makers. Oxford University Press; 2007.

58. Zacharia VM, Traxler MF. Exploring new horizons. Elife. 2017;6:e23624.

59. Law JWF, Pusparajah P, Ab Mutalib NS, Wong SH, Goh BH, Lee LH. A review on mangrove actinobacterial diversity: the roles of *Streptomyces* and novel species discovery. Prog Microbes Mol Biol. 2019;2(1).

60. Procópio RE de L, Silva IR da, Martins MK, Azevedo JL de, Araújo JM de. Antibiotics produced by *Streptomyces*. Braz J Infect Dis. 2012;16:466–71.

61. Barka EA, Vatsa P, Sanchez L, Gaveau-Vaillant N, Jacquard C, Klenk HP, et al. Taxonomy, physiology, and natural products of Actinobacteria. Microbiol Mol Biol Rev. 2016 Mar;80(1):1–43.

62. Westhoff S, Otto SB, Swinkels A, Bode B, van Wezel GP, Rozen DE. Spatial structure increases the benefits of antibiotic production in *Streptomyces*. Evolution. 2020;74(1):179–87.

63. Dulmage HT. The production of neomycin by *Streptomyces fradiae* in synthetic media. Appl Microbiol. 1953;1(2):103–6.

64. Sugiyama M, Mochizuki H, Nimi O, Nomi R. Mechanism of protection of protein synthesis against streptomycin inhibition in a producing strain. J Antibiot (Tokyo). 1981;34(9):1183–8.

65. Distler J, Braun C, Ebert A, Piepersberg W. Gene cluster for streptomycin biosynthesis in *Streptomyces griseus*: analysis of a central region including the major resistance gene. Mol Gen Genet MGG. 1987;208(1):204–10.

66. Thompson CJ, Gray GS. Nucleotide sequence of a streptomycete aminoglycoside phosphotransferase gene and its relationship to phosphotransferases encoded by resistance plasmids. Proc Natl Acad Sci. 1983;80(17):5190–4.

67. Salauze D, Perez-Gonzalez J, Piepersberg W, Davies J. Characterisation of aminoglycoside acetyltransferase-encoding genes of neomycin-producing *Micromonospora chalcea* and *Streptomyces fradiae*. Gene. 1991;101(1):143–8.

68. Huang F, Haydock SF, Mironenko T, Spiteller D, Li Y, Spencer JB. The neomycin biosynthetic gene cluster of *Streptomyces fradiae* NCIMB 8233: characterisation of an aminotransferase involved in the formation of 2-deoxystreptamine. Org Biomol Chem. 2005;3(8):1410–8.

69. Akshay S, Bertea M, Hobbie SN, Oettinghaus B, Shcherbakov D, Böttger EC, et al. Phylogenetic sequence variations in bacterial rRNA affect species-specific susceptibility to drugs targeting protein synthesis. Antimicrob Agents Chemother. 2011 Aug 17;55(9):4096–102.

70. Kumar S, Stecher G, Suleski M, Hedges SB. TimeTree: a resource for timelines, timetrees, and divergence times. Mol Biol Evol. 2017;34(7):1812–9.

71. McGuire AM, Weiner B, Park ST, Wapinski I, Raman S, Dolganov G, et al. Comparative analysis of *Mycobacterium* and related Actinomycetes yields insight into the evolution of Mycobacterium tuberculosis pathogenesis. BMC Genomics. 2012;13:1–27.

72. Scherr N, Nguyen L. *Mycobacterium* versus *Streptomyces*—we are different, we are the same. Curr Opin Microbiol. 2009;12(6):699–707.

73. Qin MH, Madiraju MV, Rajagopalan M. Characterization of the functional replication origin of *Mycobacterium tuberculosis*. Gene. 1999;233(1–2):121–30.

74. Armstrong DT, Eisemann E, Parrish N. A brief update on mycobacterial taxonomy, 2020 to 2022. J Clin Microbiol. 2023;61(4):e00331-22.

75. Hobbie SN, Pfister P, Bruell C, Sander P, François B, Westhof E, et al. Binding of neomycin-class aminoglycoside antibiotics to mutant ribosomes with alterations in the A site of 16S rRNA. Antimicrob Agents Chemother. 2006;50(4):1489–96.

76. Akshay S, Bertea M, Hobbie SN, Oettinghaus B, Shcherbakov D, Böttger EC, et al. Phylogenetic Sequence Variations in Bacterial rRNA Affect Species-Specific Susceptibility to Drugs Targeting Protein Synthesis. Antimicrob Agents Chemother. 2011 Aug 17;55(9):4096–102.

77. Hentschel J, Burnside C, Mignot I, Leibundgut M, Boehringer D, Ban N. The complete structure of the *Mycobacterium smegmatis* 70S ribosome. Cell Rep. 2017;20(1):149–60.

78. Mishra S, Ahmed T, Tyagi A, Shi J, Bhushan S. Structures of *Mycobacterium smegmatis* 70S ribosomes in complex with HPF, tmRNA, and P-tRNA. Sci Rep. 2018;8(1):13587.

79. Shasmal M, Sengupta J. Structural diversity in bacterial ribosomes: mycobacterial 70S ribosome structure reveals novel features. PloS One. 2012;7(2):e31742.

80. Yang K, Chang JY, Cui Z, Li X, Meng R, Duan L, et al. Structural insights into species-specific features of the ribosome from the human pathogen *Mycobacterium tuberculosis*. Nucleic Acids Res. 2017;45(18):10884–94.

81. Kushwaha AK, Bhushan S. Unique structural features of the *Mycobacterium* ribosome. Prog Biophys Mol Biol. 2020;152:15–24.

82. Li Y, Sharma MR, Koripella RK, Yang Y, Kaushal PS, Lin Q, et al. Zinc depletion induces ribosome hibernation in mycobacteria. Proc Natl Acad Sci. 2018;115(32):8191–6.

83. Majumdar S, Li Y, Manjari SR, Gamper HB, Hou YM, Banavali NK, et al. A novel Actinobacteria-specific ribosome hibernation factor in *Mycobacterium tuberculosis*. bioRxiv. 2024;2024–11.

84. Nicholson D, Salamina M, Panek J, Helena-Bueno K, Brown CR, Hirt RP, et al. Adaptation to genome decay in the structure of the smallest eukaryotic ribosome. Nat Commun. 2022;13(1):591.

85. Shalev M, Kondo J, Kopelyanskiy D, Jaffe CL, Adir N, Baasov T. Identification of the molecular attributes required for aminoglycoside activity against *Leishmania*. Proc Natl Acad Sci. 2013;110(33):13333–8.

86. Berman HM, Westbrook J, Feng Z, Gilliland G, Bhat TN, Weissig H, et al. The protein data bank. Nucleic Acids Res. 2000;28(1):235–42.

87. Pettersen EF, Goddard TD, Huang CC, Meng EC, Couch GS, Croll TI, et al. UCSF ChimeraX: Structure visualization for researchers, educators, and developers. Protein Sci. 2021;30(1):70–82.

88. Quast C, Pruesse E, Yilmaz P, Gerken J, Schweer T, Yarza P, et al. The SILVA ribosomal RNA gene database project: improved data processing and web-based tools. Nucleic Acids Res. 2012;41(D1):D590–6.

89. Katoh K, Standley DM. MAFFT multiple sequence alignment software version 7: improvements in performance and usability. Mol Biol Evol. 2013;30(4):772–80.

90. Tamura K, Stecher G, Kumar S. MEGA11: Molecular evolutionary genetics analysis version 11. Mol Biol Evol. 2021;38(7):3022–7.

91. Kumar S, Suleski M, Craig JM, Kasprowicz AE, Sanderford M, Li M, et al. TimeTree 5: an expanded resource for species divergence times. Mol Biol Evol. 2022 Aug 1;39(8):msac174.

92. Borovinskaya MA, Shoji S, Holton JM, Fredrick K, Cate JHD. A steric block in translation caused by the antibiotic spectinomycin. ACS Chem Biol. 2007 Aug 1;2(8):545–52.

93. Demirci H, Murphy F, Murphy E, Gregory ST, Dahlberg AE, Jogl G. A structural basis for streptomycin-induced misreading of the genetic code. Nat Commun. 2013 Jan 15;4(1):1355.

94. Polikanov YS, Osterman IA, Szal T, Tashlitsky VN, Serebryakova MV, Kusochek P, et al. Amicoumacin A inhibits translation by stabilizing mRNA interaction with the ribosome. Mol Cell. 2014;56(4):531–40.

95. Shalev-Benami M, Zhang Y, Rozenberg H, Nobe Y, Taoka M, Matzov D, et al. Atomic resolution snapshot of *Leishmania* ribosome inhibition by the aminoglycoside paromomycin. Nat Commun. 2017 Nov 17;8(1):1589.

96. Svidritskiy E, Ling C, Ermolenko DN, Korostelev AA. Blasticidin S inhibits translation by trapping deformed tRNA on the ribosome. Proc Natl Acad Sci. 2013;110(30):12283–8.

97. Davidovich C, Bashan A, Auerbach-Nevo T, Yaggie RD, Gontarek RR, Yonath A. Induced-fit tightens pleuromutilins binding to ribosomes and remote interactions enable their selectivity. Proc Natl Acad Sci. 2007;104(11):4291–6.

98. Olivier NB, Altman RB, Noeske J, Basarab GS, Code E, Ferguson AD, et al. Negamycin induces translational stalling and miscoding by binding to the small subunit head domain of the *Escherichia coli* ribosome. Proc Natl Acad Sci. 2014 Nov 18;111(46):16274–9.

99. Cocozaki AI, Altman RB, Huang J, Buurman ET, Kazmirski SL, Doig P, et al. Resistance mutations generate divergent antibiotic susceptibility profiles against translation inhibitors. Proc Natl Acad Sci. 2016 July 19;113(29):8188–93.

100. Borovinskaya MA, Pai RD, Zhang W, Schuwirth BS, Holton JM, Hirokawa G, et al. Structural basis for aminoglycoside inhibition of bacterial ribosome recycling. Nat Struct Mol Biol. 2007;14(8):727–32.

101. Tsai K, Stojković V, Lee DJ, Young ID, Szal T, Klepacki D, et al. Structural basis for context-specific inhibition of translation by oxazolidinone antibiotics. Nat Struct Mol Biol. 2022;29(2):162–71.

102. Borovinskaya MA, Shoji S, Fredrick K, Cate JH. Structural basis for hygromycin B inhibition of protein biosynthesis. RNA. 2008;14(8):1590–9.

103. Schedlbauer A, Kaminishi T, Ochoa-Lizarralde B, Dhimole N, Zhou S, López-Alonso JP, et al. Structural characterization of an alternative mode of tigecycline binding to the bacterial ribosome. Antimicrob Agents Chemother. 2015;59(5):2849–54.

104. Hansen JL, Schmeing TM, Moore PB, Steitz TA. Structural insights into peptide bond formation. Proc Natl Acad Sci. 2002;99(18):11670–5.

105. Schmeing TM, Huang KS, Kitchen DE, Strobel SA, Steitz TA. Structural insights into the roles of water and the 2′ hydroxyl of the P site tRNA in the peptidyl transferase reaction. Mol Cell. 2005;20(3):437–48.

106. Nicholson D, Edwards TA, O'Neill AJ, Ranson NA. Structure of the 70S ribosome from the human pathogen *Acinetobacter baumannii* in complex with clinically relevant antibiotics. Structure. 2020;28(10):1087–100.

107. Dunkle JA, Xiong L, Mankin AS, Cate JHD. Structures of the *Escherichia coli* ribosome with antibiotics bound near the peptidyl transferase center explain spectra of drug action. Proc Natl Acad Sci. 2010 Oct 5;107(40):17152–7.

108. Arenz S, Juette MF, Graf M, Nguyen F, Huter P, Polikanov YS, et al. Structures of the orthosomycin antibiotics avilamycin and evernimicin in complex with the bacterial 70S ribosome. Proc Natl Acad Sci. 2016;113(27):7527–32.

109. Noeske J, Huang J, Olivier NB, Giacobbe RA, Zambrowski M, Cate JH. Synergy of streptogramin antibiotics occurs independently of their effects on translation. Antimicrob Agents Chemother. 2014;58(9):5269–79.

110. Bulkley D, Johnson F, Steitz TA. The antibiotic thermorubin inhibits protein synthesis by binding to inter-subunit bridge B2a of the ribosome. J Mol Biol. 2012;416(4):571–8.

111. Zhang L, Wang YH, Zhang X, Lancaster L, Zhou J, Noller HF. The structural basis for inhibition of ribosomal translocation by viomycin. Proc Natl Acad Sci. 2020;117(19):10271–7.

112. Hansen JL, Ippolito JA, Ban N, Nissen P, Moore PB, Steitz TA. The structures of four macrolide antibiotics bound to the large ribosomal subunit. Mol Cell. 2002;10(1):117–28.

113. Stanley RE, Blaha G, Grodzicki RL, Strickler MD, Steitz TA. The structures of the anti-tuberculosis antibiotics viomycin and capreomycin bound to the 70S ribosome. Nat Struct Mol Biol. 2010 Mar;17(3):289–93.

114. Harms JM, Wilson DN, Schluenzen F, Connell SR, Stachelhaus T, Zaborowska Z, et al. Translational regulation via L11: molecular switches on the ribosome turned on and off by thiostrepton and micrococcin. Mol Cell. 2008;30(1):26–38.

115. Gürel G, Blaha G, Moore PB, Steitz TA. U2504 determines the species specificity of the a-site cleft antibiotics: The structures of tiamulin, homoharringtonine, and bruceantin bound to the ribosome. J Mol Biol. 2009;389(1):146–56.

116. Schrodinger. The PyMOL molecular graphics system, Version 1.8 [Internet]. 2015. Available from: http://www.pymol.org/pymol

117. Klappenbach JA, Saxman PR, Cole JR, Schmidt TM. rrndb: the ribosomal RNA operon copy number database. Nucleic Acids Res. 2001;29(1):181–4.

118. Coleman GA, Davín AA, Mahendrarajah TA, Szánthó LL, Spang A, Hugenholtz P, et al. A rooted phylogeny resolves early bacterial evolution. Science. 2021 May 7;372(6542):eabe0511.

119. Davín AA, Woodcroft BJ, Soo RM, Morel B, Murali R, Schrempf D, et al. A geological timescale for bacterial evolution and oxygen adaptation. Science. 2025;388:eadp1853.

120. Fraser CM, Gocayne JD, White O, Adams MD, Clayton RA, Fleischmann RD, et al. The Minimal Gene Complement of *Mycoplasma genitalium*. Science. 1995 Oct 20;270(5235):397–404.

121. Glass JI, Lefkowitz EJ, Glass JS, Heiner CR, Chen EY, Cassell GH. The complete sequence of the mucosal pathogen *Ureaplasma urealyticum*. Nature. 2000;407(6805):757–62.

122. Tomb JF, White O, Kerlavage AR, Clayton RA, Sutton GG, Fleischmann RD, et al. The complete genome sequence of the gastric pathogen *Helicobacter pylori*. Nature. 1997;388(6642):539–47.

123. Prada CF, Casadiego MA, Freire CC. Evolution of *Helicobacter* spp: variability of virulence factors and their relationship to pathogenicity. PeerJ. 2022;10:e13120.

124. Liu B, Ren YS, Su CY, Abe Y, Zhu DH. Pangenomic analysis of *Wolbachia* provides insight into the evolution of host adaptation and cytoplasmic incompatibility factor genes. Front Microbiol. 2023;14:1084839.

125. Burt A, Toader B, Warshamanage R, von Kügelgen A, Pyle E, Zivanov J, et al. An image processing pipeline for electron cryo-tomography in RELION-5. FEBS Open Bio. 2024;14(11):1788–804.

126. Scheres SH. Semi-automated selection of cryo-EM particles in RELION-1.3. J Struct Biol. 2015;189(2):114–22.

127. Zivanov J, Nakane T, Scheres SH. Estimation of high-order aberrations and anisotropic magnification from cryo-EM data sets in RELION-3.1. IUCrJ. 2020;7(2):253–67.

128. Punjani A, Rubinstein JL, Fleet DJ, Brubaker MA. cryoSPARC: algorithms for rapid unsupervised cryo-EM structure determination. Nat Methods. 2017;14(3):290–6.

129. Varadi M, Bertoni D, Magana P, Paramval U, Pidruchna I, Radhakrishnan M, et al. AlphaFold Protein Structure Database in 2024: providing structure coverage for over 214 million protein sequences. Nucleic Acids Res. 2024;52(D1):D368–75.

130. Jumper J, Evans R, Pritzel A, Green T, Figurnov M, Ronneberger O, et al. Highly accurate protein structure prediction with AlphaFold. nature. 2021;596(7873):583–9.

131. Casañal A, Lohkamp B, Emsley P. Current developments in Coot for macromolecular model building of Electron Cryo-microscopy and Crystallographic Data. Protein Sci. 2020;29(4):1055–64.

132. Eddy SR. Accelerated profile HMM searches. PLoS Comput Biol. 2011;7(10):e1002195.

133. Garreau De Loubresse N, Prokhorova I, Holtkamp W, Rodnina MV, Yusupova G, Yusupov M. Structural basis for the inhibition of the eukaryotic ribosome. Nature. 2014 Sept 25;513(7519):517–22.

134. Myasnikov AG, Kundhavai Natchiar S, Nebout M, Hazemann I, Imbert V, Khatter H, et al. Structure–function insights reveal the human ribosome as a cancer target for antibiotics. Nat Commun. 2016;7(1):12856.

135. Xing H, Taniguchi R, Khusainov I, Kreysing JP, Welsch S, Turoňová B, et al. Translation dynamics in human cells visualized at high resolution reveal cancer drug action. Science. 2023 July 7;381(6653):70–5.

136. Dmitriev SE, Vladimirov DO, Lashkevich KA. A quick guide to small-molecule inhibitors of eukaryotic protein synthesis. Biochem Mosc. 2020 Nov 1;85(11):1389–421.

137. Olombrada M, Lázaro-Gorines R, López-Rodríguez JC, Martínez-del-Pozo Á, Oñaderra M, Maestro-López M, et al. Fungal ribotoxins: a review of potential biotechnological applications. Toxins. 2017;9(2):71.

138. Brar GA, Weissman JS. Ribosome profiling reveals the what, when, where and how of protein synthesis. Nat Rev Mol Cell Biol. 2015;16(11):651–64.

139. Zhou DC, Zittoun R, Marie JP. Homoharringtonine: an effective new natural product in cancer chemotherapy. Bull Cancer (Paris). 1995;82(12):987–95.

140. Peltz SW, Morsy M, Welch EM, Jacobson A. Ataluren as an agent for therapeutic nonsense suppression. Annu Rev Med. 2013 Jan 14;64(1):407–25.

141. Ryan NJ. Ataluren: First global approval. Drugs. 2014 Sept;74(14):1709–14.

142. Flexner LB, Gambetti P, Flexner JB, Roberts RB. Studies on memory: distribution of peptidyl-puromycin in subcellular fractions of mouse brain. Proc Natl Acad Sci. 1971 Jan;68(1):26–8.

143. Eberwine J, Miyashiro K, Kacharmina JE, Job C. Local translation of classes of mRNAs that are targeted to neuronal dendrites. Proc Natl Acad Sci U S A. 2001 June 19;98(13):7080–5.

144. Ko T, Oliveira MM, Alapin JM, Morstein J, Klann E, Trauner D. Optical control of translation with a puromycin photoswitch. J Am Chem Soc. 2022 Nov 30;144(47):21494–501.

145. Melnikov S, Ben-Shem A, Garreau de Loubresse N, Jenner L, Yusupova G, Yusupov M. One core, two shells: bacterial and eukaryotic ribosomes. Nat Struct Mol Biol. 2012 June;19(6):560–7.

146. Shalev M, Kondo J, Kopelyanskiy D, Jaffe CL, Adir N, Baasov T. Identification of the molecular attributes required for aminoglycoside activity against Leishmania. Proc Natl Acad Sci. 2013 Aug 13;110(33):13333–8.

147. Hashem Y, Des Georges A, Fu J, Buss SN, Jossinet F, Jobe A, et al. High-resolution cryo-electron microscopy structure of the *Trypanosoma brucei* ribosome. Nature. 2013;494(7437):385–9.

148. Fan-Minogue H, Bedwell DM. Eukaryotic ribosomal RNA determinants of aminoglycoside resistance and their role in translational fidelity. RNA. 2008 Jan 1;14(1):148–57.

149. Hobbie SN, Kaiser M, Schmidt S, Shcherbakov D, Janusic T, Brun R, et al. Genetic Reconstruction of Protozoan rRNA Decoding Sites Provides a Rationale for Paromomycin Activity against Leishmania and Trypanosoma. PLoS Negl Trop Dis. 2011 May 24;5(5):e1161.

150. Ashelford KE, Chuzhanova NA, Fry JC, Jones AJ, Weightman AJ. At least 1 in 20 16S rRNA sequence records currently held in public repositories is estimated to contain substantial anomalies. Appl Environ Microbiol. 2005 Dec;71(12):7724–36.

151. Edgar RC. Accuracy of taxonomy prediction for 16S rRNA and fungal ITS sequences. PeerJ. 2018;6:e4652.

152. Lawrence JG, Hendrix RW, Casjens S. Where are the pseudogenes in bacterial genomes? Trends Microbiol. 2001;9(11):535–40.

153. Torrents D, Suyama M, Zdobnov E, Bork P. A genome-wide survey of human pseudogenes. Genome Res. 2003;13(12):2559–67.

154. Prade VM, Gundlach H, Twardziok S, Chapman B, Tan C, Langridge P, et al. The pseudogenes of barley. Plant J. 2018 Feb;93(3):502–14.

155. David-Eden H, Mankin AS, Mandel-Gutfreund Y. Structural signatures of antibiotic binding sites on the ribosome. Nucleic Acids Res. 2010 Oct 1;38(18):5982–94.

156. Petrov AS, Bernier CR, Hsiao C, Norris AM, Kovacs NA, Waterbury CC, et al. Evolution of the ribosome at atomic resolution. Proc Natl Acad Sci. 2014 July 15;111(28):10251–6.

157. Petrov AS, Gulen B, Norris AM, Kovacs NA, Bernier CR, Lanier KA, et al. History of the ribosome and the origin of translation. Proc Natl Acad Sci. 2015 Dec 15;112(50):15396–401.

158. Parks MM, Kurylo CM, Dass RA, Bojmar L, Lyden D, Vincent CT, et al. Variant ribosomal RNA alleles are conserved and exhibit tissue-specific expression. Sci Adv. 2018 Feb 2;4(2):eaao0665.

159. Melnikov S, Manakongtreecheep K, Söll D. Revising the structural diversity of ribosomal proteins across the three domains of life. Mol Biol Evol. 2018;35(7):1588–98.

160. Ekemezie CL, Chan LI, Brown CR, Helena-Bueno K, Williams TA, Melnikov SV. Natural variation in the drug-binding residues of bacterial ribosomes. bioRxiv. 2024;2024–10.

161. Velegraki A, Cafarchia C, Gaitanis G, Iatta R, Boekhout T. Malassezia infections in humans and animals: pathophysiology, detection, and treatment. PLoS Pathog. 2015;11(1):e1004523.

162. Strassert JF, Irisarri I, Williams TA, Burki F. A molecular timescale for eukaryote evolution with implications for the origin of red algal-derived plastids. Nat Commun. 2021;12(1):1879.

163. Mahendrarajah TA, Moody ER, Schrempf D, Szánthó LL, Dombrowski N, Davín AA, et al. ATP synthase evolution on a cross-braced dated tree of life. Nat Commun. 2023;14(1):7456.

164. Weiss LM. Microsporidiosis. Hunt Trop Med Emerg Infect Dis. 2020;825–31.

165. Prokhorova I, Altman RB, Djumagulov M, Shrestha JP, Urzhumtsev A, Ferguson A, et al. Aminoglycoside interactions and impacts on the eukaryotic ribosome. Proc Natl Acad Sci. 2017;114(51):E10899–908.

166. McDonald BR, Currie CR. Lateral gene transfer dynamics in the ancient bacterial genus *Streptomyces*. mBio. 2017 June 6;8(3):10.1128/mbio.00644-17.

167. Blaha GM, Polikanov YS, Steitz TA. Elements of ribosomal drug resistance and specificity. Curr Opin Struct Biol. 2012 Dec;22(6):750–8.

168. Vila-Sanjurjo A, Squires CL, Dahlberg AE. Isolation of kasugamycin resistant mutants in the 16 S ribosomal RNA of Escherichia coli. J Mol Biol. 1999;293(1):1–8.

169. Fredrick K, Noller HF. Catalysis of ribosomal translocation by sparsomycin. Science. 2003;300(5622):1159–62.

170. Schuwirth BS, Day JM, Hau CW, Janssen GR, Dahlberg AE, Cate JHD, et al. Structural analysis of kasugamycin inhibition of translation. Nat Struct Mol Biol. 2006;13(10):879–86.

171. Paternoga H, Crowe-McAuliffe C, Bock LV, Koller TO, Morici M, Beckert B, et al. Structural conservation of antibiotic interaction with ribosomes. Nat Struct Mol Biol. 2023 Aug 7;30:1380–92.

172. Brodersen DE, Clemons WM, Carter AP, Morgan-Warren RJ, Wimberly BT, Ramakrishnan V. The structural basis for the action of the antibiotics tetracycline, pactamycin, and hygromycin B on the 30S ribosomal subunit. Cell. 2000;103(7):1143–54.

173. Harms J, Schluenzen F, Zarivach R, Bashan A, Gat S, Agmon I, et al. High resolution structure of the large ribosomal subunit from a mesophilic eubacterium. Cell. 2001;107(5):679–88.

174. Schlünzen F, Zarivach R, Harms J, Bashan A, Tocilj A, Albrecht R, et al. Structural basis for the interaction of antibiotics with the peptidyl transferase centre in eubacteria. Nature. 2001;413(6858):814–21.

175. Tu D, Blaha G, Moore PB, Steitz TA. Structures of MLSBK antibiotics bound to mutated large ribosomal subunits provide a structural explanation for resistance. Cell. 2005;121(2):257–70.

176. Osterman IA, Wieland M, Maviza TP, Lashkevich KA, Lukianov DA, Komarova ES, et al. Tetracenomycin X inhibits translation by binding within the ribosomal exit tunnel. Nat Chem Biol. 2020;16(10):1071–7.

177. Hoeffler U, Ko HL, Pulverer G. Antimicrobial susceptibility of *Propionibacterium acnes* and related microbial species. Antimicrob Agents Chemother. 1976 Sept;10(3):387–94.

178. Pereyre S, Gonzalez P, De Barbeyrac B, Darnige A, Renaudin H, Charron A, et al. Mutations in 23S rRNA account for intrinsic resistance to macrolides in *Mycoplasma hominis* and *Mycoplasma fermentans* and for acquired resistance to macrolides in *M. hominis*. Antimicrob Agents Chemother. 2002;46(10):3142–50.

179. UniProt Consortium. UniProt: a worldwide hub of protein knowledge. Nucleic Acids Res. 2019;47(D1):D506–15.

180. Johnson JS, Spakowicz DJ, Hong BY, Petersen LM, Demkowicz P, Chen L, et al. Evaluation of 16S rRNA gene sequencing for species and strain-level microbiome analysis. Nat Commun. 2019;10(1):5029.

181. Mankin AS. Pactamycin resistance mutations in functional sites of 16 S rRNA. J Mol Biol. 1997;274(1):8–15.

182. Andersson JO, Andersson SG. Genome degradation is an ongoing process in Rickettsia. Mol Biol Evol. 1999;16(9):1178–91.

183. McCutcheon JP, Moran NA. Extreme genome reduction in symbiotic bacteria. Nat Rev Microbiol. 2012;10(1):13–26.

184. Woese CR, Fox GE, Zablen L, Uchida T, Bonen L, Pechman K, et al. Conservation of primary structure in 16S ribosomal RNA. Nature. 1975;254(5495):83–6.

185. Smit S, Widmann J, Knight R. Evolutionary rates vary among rRNA structural elements. Nucleic Acids Res. 2007;35(10):3339–54.

186. Kehrenberg C, Schwarz S. Mutations in 16S rRNA and ribosomal protein S5 associated with high-level spectinomycin resistance in *Pasteurella multocida*. Antimicrob Agents Chemother. 2007;51(6):2244–6.

187. O'Connor M, Dahlberg AE. Isolation of spectinomycin resistance mutations in the 16S rRNA of *Salmonella enterica* serovar Typhimurium and expression in *Escherichia coli* and *Salmonella*. Curr Microbiol. 2002;45:0429–33.

188. Brink MF, Brink G, Verbeet M, de Boer HA. Spectinomycin interacts specifically with the residues G 1064 and C 1192 in 16S rRNA, thereby potentially freezing this molecule into an inactive conformation. Nucleic Acids Res. 1994;22(3):325–31.

189. Mankin AS. Pactamycin resistance mutations in functional sites of 16 S rRNA11Edited by D. E. Draper. J Mol Biol. 1997 Nov 21;274(1):8–15.

190. To KY, Chen CC, Lai YK. Isolation and characterization of streptomycin-resistant mutants in Nicotiana plumbaginifolia. Theor Appl Genet. 1989 July 1;78(1):81–6.

191. Yeh KC, To KY, Sun S, Wu M, Lin T, Chen C. Point mutations in the chloroplast 16S rRNA gene confer streptomycin resistance in *Nicotiana plumbaginifolia*. Curr Genet. 1994 Sept 1;26:132–5.

192. Montandon PE, Nicolas P, Schürmann P, Stutz E. Streptomycin-resistance of *Euglena gracilis* chloroplasts: identification of a point mutation in the 16S rRNA gene in an invariant position. Nucleic Acids Res. 1985 June 25;13(12):4299–310.

193. Harris EH, Burkhart BD, Gillham NW, Boynton JE. Antibiotic resistance mutations in the chloroplast 16S and 23S rRNA genes of *Chlamydomonas Reinhardtii*: Correlation of genetic and physical Maps of the chloroplast genome. Genetics. 1989 Oct;123(2):281–92.

194. Fromm H, Edelman M, Aviv D, Galun E. The molecular basis for rRNA-dependent spectinomycin resistance in *Nicotiana* chloroplasts. EMBO J. 1987 Nov;6(11):3233–7.

195. Etzold T, Fritz CC, Schell J, Schreier PH. A point mutation in the chloroplast 16S rRNA gene of a streptomycin resistant *Nicotiana tabacum*. Febs Lett. 1987;219(2):343–6.

196. Frattali AL, Flynn MK, De Stasio EA, Dahĺberg AE. Effects of mutagenesis of C912 in the streptomycin binding region of *Escherichia coli* 16S ribosomal RNA. Biochim Biophys Acta BBA-Gene Struct Expr. 1990;1050(1–3):27–33.

197. Leclerc D, Melancon P, Brakier-Gingras L. Mutations in the 915 region of *Escherichia coli* 16S ribosomal RNA reduce the binding of streptomycin to the ribosome. Nucleic Acids Res. 1991;19(14):3973–7.

198. Demirci H, Murphy FV, Murphy EL, Connetti JL, Dahlberg AE, Jogl G, et al. Structural analysis of base Substitutions in *Thermus thermophilus* 16S rRNA conferring streptomycin resistance. Antimicrob Agents Chemother. 2014 Aug;58(8):4308–17.

199. Bonny C, Montandon PE, Marc-Martin S, Stutz E. Analysis of streptomycin-resistance of *Escherichia coli* mutants. Biochim Biophys Acta BBA-Gene Struct Expr. 1991;1089(2):213–9.

200. Dailidiene D, Bertoli MT, Miciuleviciene J, Mukhopadhyay AK, Dailide G, Pascasio MA, et al. Emergence of tetracycline resistance in *Helicobacter pylori*: multiple mutational changes in 16S ribosomal DNA and other genetic loci. Antimicrob Agents Chemother. 2002;46(12):3940–6.

201. Polikanov YS, Szal T, Jiang F, Gupta P, Matsuda R, Shiozuka M, et al. Negamycin interferes with decoding and translocation by simultaneous interaction with rRNA and tRNA. Mol Cell. 2014;56(4):541–50.

202. Bauer G, Berens C, Projan SJ, Hillen W. Comparison of tetracycline and tigecycline binding to ribosomes mapped by dimethylsulphate and drug-directed Fe2+ cleavage of 16S rRNA. J Antimicrob Chemother. 2004;53(4):592–9.

203. Miyazaki K, Kitahara K. Functional metagenomic approach to identify overlooked antibiotic resistance mutations in bacterial rRNA. Sci Rep. 2018 Apr 3;8(1):5179.

204. Galimand M, Gerbaud G, Courvalin P. Spectinomycin resistance in *Neisseria* spp. due to mutations in 16S rRNA. Antimicrob Agents Chemother. 2000 May;44(5):1365–6.

205. Criswell D, Tobiason VL, Lodmell JS, Samuels DS. Mutations conferring aminoglycoside and spectinomycin resistance in *Borrelia burgdorferi*. Antimicrob Agents Chemother. 2006 Feb;50(2):445–52.

206. Binet R, Maurelli AT. Fitness cost due to mutations in the 16S rRNA associated with spectinomycin resistance in *Chlamydia psittaci* 6BC. Antimicrob Agents Chemother. 2005 Nov;49(11):4455–64.

207. Sigmund CD, Ettayebi M, Morgan EA. Antibiotic resistance mutations in 16S and 23S ribosomal RNA genes of Escherichia coli. Nucleic Acids Res. 1984;12(11):4653–64.

208. Sander P, Prammananan T, Bo¨ttger EC. Introducing mutations into a chromosomal rRNA gene using a genetically modified eubacterial host with a single rRNA operon. Mol Microbiol. 1996 Dec;22(5):841–8.

209. Binet R, Maurelli AT. Frequency of spontaneous mutations that confer antibiotic resistance in *Chlamydia* spp. Antimicrob Agents Chemother. 2005 July;49(7):2865–73.

210. Svab Z, Maliga P. Mutation proximal to the tRNA binding region of the *Nicotiana plastid* 16S rRNA confers resistance to spectinomycin. Mol Gen Genet MGG. 1991 Aug;228(1–2):316–9.

211. Pfister P, Risch M, Brodersen DE, Böttger EC. Role of 16S rRNA helix 44 in ribosomal resistance to hygromycin B. Antimicrob Agents Chemother. 2003 May;47(5):1496–502.

212. Gregory ST, Carr JF, Rodriguez-Correa D, Dahlberg AE. Mutational analysis of 16S and 23S rRNA genes of *Thermus thermophilus*. J Bacteriol. 2005;187(14):4804–12.

213. Recht MI, Puglisi JD. Aminoglycoside resistance with homogeneous and heterogeneous populations of antibiotic-resistant ribosomes. Antimicrob Agents Chemother. 2001 Sept;45(9):2414–9.

214. Miyaguchi H, Narita H, Sakamoto K, Yokoyama S. An antibiotic-binding motif of an RNA fragment derived from the A-site-related region of *Escherichia coli* 16S rRNA. Nucleic Acids Res. 1996;24(19):3700–6.

215. Kalapala SK, Hobbie SN, Böttger EC, Shcherbakov D. Mutation K42R in ribosomal protein S12 does not affect susceptibility of *Mycobacterium smegmatis* 16S rRNA A-site mutants to 2-deoxystreptamines. Plos One. 2010;5(8):e11960.

216. Pfister P, Hobbie S, Brüll C, Corti N, Vasella A, Westhof E, et al. Mutagenesis of 16S rRNA C1409-G1491 base-pair differentiates between 6′OH and 6′NH3+ aminoglycosides. J Mol Biol. 2005 Feb 18;346(2):467–75.

217. Kim SY, Kim DH, Moon SM, Song JY, Huh HJ, Lee NY, et al. Association between 16S rRNA gene mutations and susceptibility to amikacin in *Mycobacterium avium* Complex and *Mycobacterium abscessus* clinical isolates. Sci Rep. 2021 Mar 17;11(1):6108.

218. Brown-Elliott BA, Iakhiaeva E, Griffith DE, Woods GL, Stout JE, Wolfe CR, et al. *In Vitro* Activity of amikacin against Isolates of *Mycobacterium avium* complex with proposed MIC breakpoints and finding of a 16S rRNA gene mutation in treated isolates. J Clin Microbiol. 2013 Oct;51(10):3389–94.

219. Sato T, Higuchi H, Yokota S, Tamura Y. *Mycoplasma bovis* isolates from dairy calves in Japan have less susceptibility than a reference strain to all approved macrolides associated with a point mutation (G748A) combined with multiple species-specific nucleotide alterations in 23S rRNA. Microbiol Immunol. 2017;61(6):215–24.

220. Kinnear A, McAllister TA, Zaheer R, Waldner M, Ruzzini AC, Andrés-Lasheras S, et al. Investigation of macrolide resistance genotypes in *Mycoplasma bovis* isolates from Canadian feedlot cattle. Pathogens. 2020;9(8):622.

221. Thompson J, Cundliffe E, Dahlberg AE. Site-directed mutagenesis of *Escherichia coli* 23S ribosomal RNA at position 1067 within the GTP hydrolysis centre. J Mol Biol. 1988;203(2):457–65.

222. Xu W, Pagel FT, Murgola EJ. Mutations in the GTPase center of *Escherichia coli* 23S rRNA indicate release factor 2-interactive sites. J Bacteriol. 2002;184(4):1200–3.

223. Ross J, Snelling A, Eady E, Cove J, Cunliffe W, Leyden J, et al. Phenotypic and genotypic characterization of antibiotic-resistant *Propionibacterium acnes* isolated from acne patients attending dermatology clinics in Europe, the USA, Japan and Australia. Br J Dermatol. 2001;144(2):339–46.

224. Ettayebi M, Prasad SM, Morgan EA. Chloramphenicol-erythromycin resistance mutations in a 23S rRNA gene of *Escherichia coli*. J Bacteriol. 1985;162(2):551–7.

225. Perez-Trallero E, Marimon JM, Iglesias L, Larruskain J. Fluoroquinolone and macrolide treatment failure in pneumococcal pneumonia and selection of multidrug-resistant isolates. Emerg Infect Dis. 2003;9(9):1159.

226. Douthwaite S, Hansen LH, Mauvais P. Macrolide–ketolide inhibition of MLS-resistant ribosomes is improved by alternative drug interaction with domain II of 23S rRNA. Mol Microbiol. 2000;36(1):183–93.

227. Lee SY, Ning Y, Fenno JC. 23S rRNA point mutation associated with erythromycin resistance in *Treponema denticola*. FEMS Microbiol Lett. 2002;207(1):39–42.

228. Berisio R, Corti N, Pfister P, Yonath A, Bottger EC. 23S rRNA 2058A→ G alteration mediates ketolide resistance in combination with deletion in L22. Antimicrob Agents Chemother. 2006;50(11):3816–23.

229. Bébéar C, Pereyre S. Mechanisms of drug resistance in *Mycoplasma pneumoniae*. Curr Drug Targets-Infect Disord. 2005;5(3):263–71.

230. Tait-Kamradt A, Davies T, Cronan M, Jacobs M, Appelbaum P, Sutcliffe J. Mutations in 23S rRNA and ribosomal protein L4 account for resistance in pneumococcal strains selected in vitro by macrolide passage. Antimicrob Agents Chemother. 2000;44(8):2118–25.

231. Long KS, Munck C, Andersen TMB, Schaub MA, Hobbie SN, Böttger EC, et al. Mutations in 23S rRNA at the peptidyl transferase center and their relationship to linezolid binding and cross-resistance. Antimicrob Agents Chemother. 2010 Nov;54(11):4705–13.

232. Li BB, Wu CM, Wang Y, Shen JZ. Single and dual mutations at positions 2058, 2503 and 2504 of 23S rRNA and their relationship to resistance to antibiotics that target the large ribosomal subunit. J Antimicrob Chemother. 2011;66(9):1983–6.

233. Sergiev PV, Lesnyak DV, Burakovsky DE, Svetlov M, Kolb VA, Serebryakova MV, et al. Non-stressful death of 23S rRNA mutant G2061C defective in puromycin reaction. J Mol Biol. 2012;416(5):656–67.

234. Killeavy EE, Jogl G, Gregory ST. Tiamulin-resistant mutants of the thermophilic bacterium *Thermus thermophilus*. Antibiotics. 2020;9(6):313.

235. Furneri PM, Rappazzo G, Musumarra MP, Di Pietro P, Catania LS, Roccasalva LS. Two new point mutations at A2062 associated with resistance to 16-membered macrolide antibiotics in mutant strains of *Mycoplasma hominis*. Antimicrob Agents Chemother. 2001;45(10):2958–60.

236. Wilson DN, Schluenzen F, Harms JM, Starosta AL, Connell SR, Fucini P. The oxazolidinone antibiotics perturb the ribosomal peptidyl-transferase center and effect tRNA positioning. Proc Natl Acad Sci. 2008;105(36):13339–44.

237. Depardieu F, Courvalin P. Mutation in 23S rRNA responsible for resistance to 16-membered macrolides and streptogramins in *Streptococcus pneumoniae*. Antimicrob Agents Chemother. 2001;45(1):319–23.

238. Kloss P, Xiong L, Shinabarger DL, Mankin AS. Resistance mutations in 23 S rRNA identify the site of action of the protein synthesis inhibitor linezolid in the ribosomal peptidyl transferase center. J Mol Biol. 1999;294(1):93–101.

239. Khaitovich P, Tenson T, Kloss P, Mankin AS. Reconstitution of functionally active *Thermus aquaticus* large ribosomal subunits with in vitro-transcribed rRNA. Biochemistry. 1999;38(6):1780–8.

240. Leviev I, Rodriguez-Fonseca C, Phan H, Garrett R, Heilek G, Noller H, et al. A conserved secondary structural motif in 23S rRNA defines the site of interaction of amicetin, a universal inhibitor of peptide bond formation. EMBO J. 1994;13(7):1682–6.

241. Blaha G, Gürel G, Schroeder SJ, Moore PB, Steitz TA. Mutations outside the anisomycin-binding site can make ribosomes drug-resistant. J Mol Biol. 2008;379(3):505–19.

242. Aagaard C, Phan H, Trevisanato S, Garrett RA. A spontaneous point mutation in the single 23S rRNA gene of the thermophilic arachaeon *Sulfolobus acidocaldarius* confers multiple drug resistance. J Bacteriol. 1994;176(24):7744–7.

243. Adrian PV, Mendrick C, Loebenberg D, McNicholas P, Shaw KJ, Klugman KP, et al. Evernimicin (SCH27899) inhibits a novel ribosome target site: analysis of 23S ribosomal DNA mutants. Antimicrob Agents Chemother. 2000;44(11):3101–6.

244. Kofoed CB, Vester B. Interaction of avilamycin with ribosomes and resistance caused by mutations in 23S rRNA. Antimicrob Agents Chemother. 2002;46(11):3339–42.

245. Belova L, Tenson T, Xiong L, McNicholas PM, Mankin AS. A novel site of antibiotic action in the ribosome: Interaction of evernimicin with the large ribosomal subunit. Proc Natl Acad Sci. 2001 Mar 27;98(7):3726–31.

246. Pringle M, Poehlsgaard J, Vester B, Long KS. Mutations in ribosomal protein L3 and 23S ribosomal RNA at the peptidyl transferase centre are associated with reduced susceptibility to tiamulin in Brachyspira spp. isolates. Mol Microbiol. 2004;54(5):1295–306.

247. Farrell DJ, Mendes RE, Ross JE, Jones RN. Linezolid surveillance program results for 2008 (LEADER Program for 2008). Diagn Microbiol Infect Dis. 2009;65(4):392–403.

248. Toh SM, Mankin AS. An indigenous posttranscriptional modification in the ribosomal peptidyl transferase center confers resistance to an array of protein synthesis inhibitors. J Mol Biol. 2008;380(4):593–7.

249. Prystowsky J, Siddiqui F, Chosay J, Shinabarger DL, Millichap J, Peterson LR, et al. Resistance to linezolid: characterization of mutations in rRNA and comparison of their occurrences in vancomycin-resistant enterococci. Antimicrob Agents Chemother. 2001;45(7):2154–6.

250. Papadimitriou-Olivgeris M, Giormezis N, Fligou F, Liakopoulos A, Marangos M, Anastassiou ED, et al. Factors influencing linezolid-nonsusceptible coagulase-negative staphylococci dissemination among patients in the intensive care unit: a retrospective cohort study. Chemotherapy. 2014;59(6):420–6.

251. Zarazaga M, Tenorio C, Del Campo R, Ruiz-Larrea F, Torres C. Mutations in ribosomal protein L16 and in 23S rRNA in *Enterococcus* strains for which evernimicin MICs differ. Antimicrob Agents Chemother. 2002;46(11):3657–9.

252. Kim DF, Green R. Base-pairing between 23S rRNA and tRNA in the ribosomal A site. Mol Cell. 1999;4(5):859–64.

253. Vannuffel P, Di Giambattista M, Morgan EA, Cocito C. Identification of a single base change in ribosomal RNA leading to erythromycin resistance. J Biol Chem. 1992;267(12):8377–82.

254. Carter AP, Clemons WM, Brodersen DE, Morgan-Warren RJ, Wimberly BT, Ramakrishnan V. Functional insights from the structure of the 30S ribosomal subunit and its interactions with antibiotics. Nature. 2000;407(6802):340–8.

255. Furneri PM, Rappazzo G, Musumarra MP, Tempera G, Roccasalva LS. Genetic basis of natural resistance to erythromycin in *Mycoplasma hominis*. J Antimicrob Chemother. 2000;45(4):547–8.

256. Van Drie JH, Tong L. Cryo-EM as a powerful tool for drug discovery. Bioorg Med Chem Lett. 2020;30(22):127524.

257. Ito T, Roongsawang N, Shirasaka N, Lu W, Flatt PM, Kasanah N, et al. Deciphering pactamycin biosynthesis and engineered production of new pactamycin analogues. ChemBioChem. 2009;10(13):2253–65.

258. Gao W, Wu Z, Sun J, Ni X, Xia H. Modulation of kanamycin B and kanamycin A biosynthesis in *Streptomyces kanamyceticus* via metabolic engineering. PLoS One. 2017;12(7):e0181971.

259. Ibrahim AA, El-Housseiny GS, Aboshanab KM, Yassien MA, Hassouna NA. Paromomycin production from *Streptomyces rimosus* NRRL 2455: statistical optimization and new synergistic antibiotic combinations against multidrug resistant pathogens. BMC Microbiol. 2019;19:1–15.

260. Finlay AC, Hobby G, Hochstein F, Lees T, Lenert T, Means J, et al. Viomycin, a new antibiotic active against mycobacteria. Am Rev Tuberc. 1951;63(1):1–3.

261. Skinner RH, Cundliffe E. Resistance to the antibiotics viomycin and capreomycin in the *Streptomyces* species which produce them. Microbiology. 1980;120(1):95–104.

262. Olivier NB, Altman RB, Noeske J, Basarab GS, Code E, Ferguson AD, et al. Negamycin induces translational stalling and miscoding by binding to the small subunit head domain of the *Escherichia coli* ribosome. Proc Natl Acad Sci. 2014;111(46):16274–9.

263. Grossman TH. Tetracycline antibiotics and resistance. Cold Spring Harb Perspect Med. 2016 Apr 1;6(4):a025387.

264. Sokolski WT. Spectinomycin. In: Analytical Microbiology. Elsevier; 1972. p. 339–41.

265. Kasuga K, Sasaki A, Matsuo T, Yamamoto C, Minato Y, Kuwahara N, et al. Heterologous production of kasugamycin, an aminoglycoside antibiotic from *Streptomyces kasugaensis*,

in *Streptomyces lividans* and *Rhodococcus erythropolis* L-88 by constitutive expression of the biosynthetic gene cluster. Appl Microbiol Biotechnol. 2017;101:4259–68.

266. Davison JR, Lohith KM, Wang X, Bobyk K, Mandadapu SR, Lee SL, et al. A new natural product analog of blasticidin S reveals cellular uptake facilitated by the NorA multidrug transporter. Antimicrob Agents Chemother. 2017;61(6):10–1128.

267. Li C, Zhang F, Kelly WL. Heterologous production of thiostrepton A and biosynthetic engineering of thiostrepton analogs. Mol Biosyst. 2011;7(1):82–90.

268. Cundliffe E. Mechanism of resistance to thiostrepton in the producing-organism *Streptomyces azureus*. Nature. 1978;272(5656).

269. Ashy MA, Abd-El-Galil MK, Abou-Zeid AZA. Carbomycin, a macrolide antibiotic. Zentralblatt Für Bakteriol Parasitenkd Infekt Hyg Zweite Naturwissenschaftliche Abt Mikrobiol Landwirtsch Technol Umweltschutzes. 1980;135(6):541–51.

270. Lázaro E, Sanz E, Remacha M, Ballesta J. Characterization of sparsomycin resistance in *Streptomyces sparsogenes*. Antimicrob Agents Chemother. 2002;46(9):2914–9.

271. Tercero JA, Espinosa JC, Lacalle RA, Jiménez A. The biosynthetic pathway of the aminonucleoside antibiotic puromycin, as deduced from the molecular analysis of the pur cluster of *Streptomyces alboniger* (∗). J Biol Chem. 1996;271(3):1579–90.

272. Pulsawat N, Kitani S, Nihira T. Characterization of biosynthetic gene cluster for the production of virginiamycin M, a streptogramin type A antibiotic, in *Streptomyces virginiae*. Gene. 2007;393(1–2):31–42.

273. Weitnauer G, Mühlenweg A, Trefzer A, Hoffmeister D, Süssmuth R, Jung G, et al. Biosynthesis of the orthosomycin antibiotic avilamycin A: deductions from the molecular analysis of the avi biosynthetic gene cluster of *Streptomyces viridochromogenes* Tü57 and production of new antibiotics. Chem Biol. 2001;8(6):569–81.

274. Ehrlich J, Bartz QR, Smith RM, Joslyn DA, Burkholder PR. Chloromycetin, a new antibiotic from a soil actinomycete. Science. 1947;106(2757):417–417.

275. Shepherd MD, Kharel MK, Bosserman MA, Rohr J. Laboratory maintenance of Streptomyces species. Curr Protoc Microbiol. 2010;18(1):10E – 1.

276. National Research Council. Correlates of smallest sizes for microorganisms. In National Academies Press (US); 1999.

277. Erath J, Kemper D, Mugo E, Jacoby A, Valenzuela E, Jungers CF, et al. A rapid, facile, and economical method for the isolation of ribosomes and translational machinery for structural and functional studies. bioRxiv. 2024;

278. Ben-Shem A, Garreau de Loubresse N, Melnikov S, Jenner L, Yusupova G, Yusupov M. The structure of the eukaryotic ribosome at 3.0 Å resolution. Science. 2011;334(6062):1524–9.

279. Ingham KC. [20] Protein precipitation with polyethylene glycol. In: Methods in enzymology. Elsevier; 1984. p. 351–6.

280. Khatter H, Myasnikov AG, Mastio L, Billas IM, Birck C, Stella S, et al. Purification, characterization and crystallization of the human 80S ribosome. Nucleic Acids Res. 2014;42(6):e49–e49.

281. Costa TR, Ignatiou A, Orlova EV. Structural analysis of protein complexes by cryo electron microscopy. Bact Protein Secret Syst Methods Protoc. 2017;377–413.

282. Thompson RF, Walker M, Siebert CA, Muench SP, Ranson NA. An introduction to sample preparation and imaging by cryo-electron microscopy for structural biology. Methods. 2016;100:3–15.

283. Russo CJ, Passmore LA. Specimen preparation for high-resolution cryo-EM. Methods Enzymol. 2016;579.

284. Cabra V, Samsó M. Do's and don'ts of cryo-electron microscopy: a primer on sample preparation and high quality data collection for macromolecular 3D reconstruction. J Vis Exp JoVE. 2015;(95):52311.

285. Helena-Bueno K, Rybak MY, Ekemezie CL, Sullivan R, Brown CR, Dingwall C, et al. A new family of bacterial ribosome hibernation factors. Nature. 2024 Feb;626(8001):1125–32.

286. Arenz S, Juette MF, Graf M, Nguyen F, Huter P, Polikanov YS, et al. Structures of the orthosomycin antibiotics avilamycin and evernimicin in complex with the bacterial 70S ribosome. Proc Natl Acad Sci. 2016;113(27):7527–32.

287. Mangano K, Marks J, Klepacki D, Saha CK, Atkinson GC, Vázquez-Laslop N, et al. Context-based sensing of orthosomycin antibiotics by the translating ribosome. Nat Chem Biol. 2022;18(11):1277–86.

288. Majumdar S, Deep A, Sharma MR, Canestrari J, Stone M, Smith C, et al. The small mycobacterial ribosomal protein, bS22, modulates aminoglycoside accessibility to its 16S rRNA helix-44 binding site. bioRxiv. 2023;

289. Shan C, Yue Q, Ding X. Knockout of ribosomal genes bS22 and bL37 increases the sensitivity of mycobacteria to antibiotics. Sheng Wu Gong Cheng Xue Bao Chin J Biotechnol. 2022;38(3):1061–73.

Appendix

Appendix 1. Supplementary Information Chapter 3.

The supplementary data and tables listed in this appendix section can be assessed here: https://drive.google.com/drive/folders/128B7g9xy2ZZknyNBJLcfLomyRs_Iauqw?usp=drive_link

Supplementary Data S3

Data S3.1 | Aligned full length 18S rRNA

Data S3.2 | Aligned full length 25S rRNA

Data S3.3 | Aligned drug-binding residues 18S rRNA

Data S3.4 | Aligned drug-binding residues 25S rRNA

Data S3.5 | Eukaryotic species analysed in this work

Data S3.6 | Scripts

Appendix 2. Supplementary Information Chapter 4.

Supplementary Data S4

Data S4.1| High quality library of 16S rRNA sequences

Data S4.2 | High quality library of 23S rRNA sequences

Data S4.3 | Aligned drug-binding residues 16S rRNA

Data S4.4 | Aligned drug-binding residues 23S rRNA

Data S4.5 | Full sequences of 16S rRNA analysed in this study

Data S4.6 | Full sequences of 2sS rRNA analysed in this study

Data S4.7 | Bacterial phyla profile sequence of drug-binding residues 16S rRNA

Data S4.8 | Bacterial phyla profile sequence of drug-binding residues 23S rRNA

Data S4.9 | List of bacterial species analysed in this study

Data S4.10 | Collection of python scripts used for this study

Supplementary Figure Chapter 4

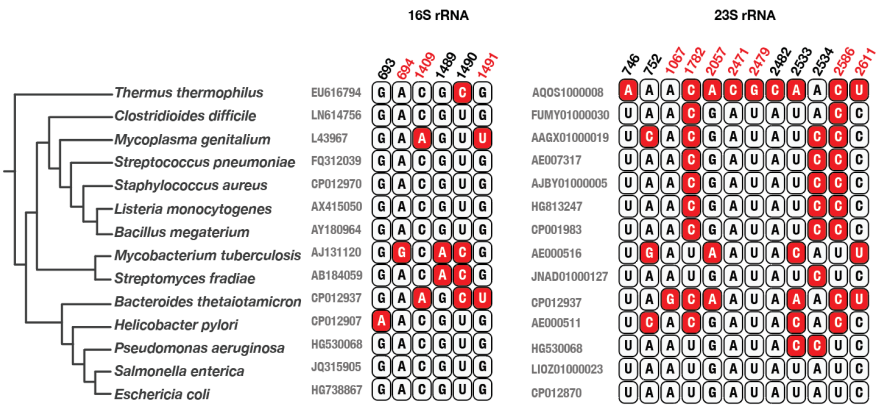

Figure S4.1 | Common model bacteria bear many variable drug-binding residues. Ribosome structures show the position of ribosomal drug-binding sites and highlight the location of variable rRNA drug-binding residues among some common model bacterial species (these rRNA residues are highlighted in red). Residue numbers highlighted in red indicate rRNA bases where mutations have been shown to confer drug resistance. The panel illustrates that certain drug-binding residues of the ribosome are not conserved between many commonly studied bacteria.

Appendix 3. Supplementary Information Chapter 5

Supplementary information Calculations S5.1

Q1. What is the concentration of 1 $0D_{260}$ (A_{260}) unit of ribosome?

Formula for estimating concentration from absorbance measure is:

$A = \varepsilon \times c \times l$ equation (1)

Where:

A: Absorbance

ε: Molar extinction (L/mol·cm)

c: Concentration (M)

l: path length (cm)

This implies that concentration (c) = A/ε/l. equation (2)

Note: molar extinction (ε) of 70S ribosome at 260 nm = ~ 4.2×10^7 L/mol·cm

Path length of curvette = 1 cm

Substituting the corresponding values in equation:

c = 1/ ~ 4.2×10^7 L/mol·cm/1

c = 2.38 x 10^{-8} M = ~24 nM

Therefore, the concentration of 1 A_{260} unit of ribosome is **~24 nM.**

Q2. How many ribosome particles are present in 24 nM of 1 µL ribosome sample?

1 mole of any substance contains 6.022 x 10^{23} Avogadro's particles

Number of particles = number of moles x Avogadro's particles

Number of moles = Concentration (M) x Volume (L)

Therefore, number of particles = Concentration x Volume x Avogadro's particles equation (3)

Concentration = 24 nM =

Volume = 1 µL = 1x 10^{-12}

Number of particles = 2.4 x 10^{-8} M x 1 x 10^{-6} L x 6.022 x 10^{23}

Number of particles = 1.445×10^{10}

Therefore 1 µL of 24 nM ribosome sample contains **1.445×10^{10} particles.**

Supplementary Figure Chapter 5

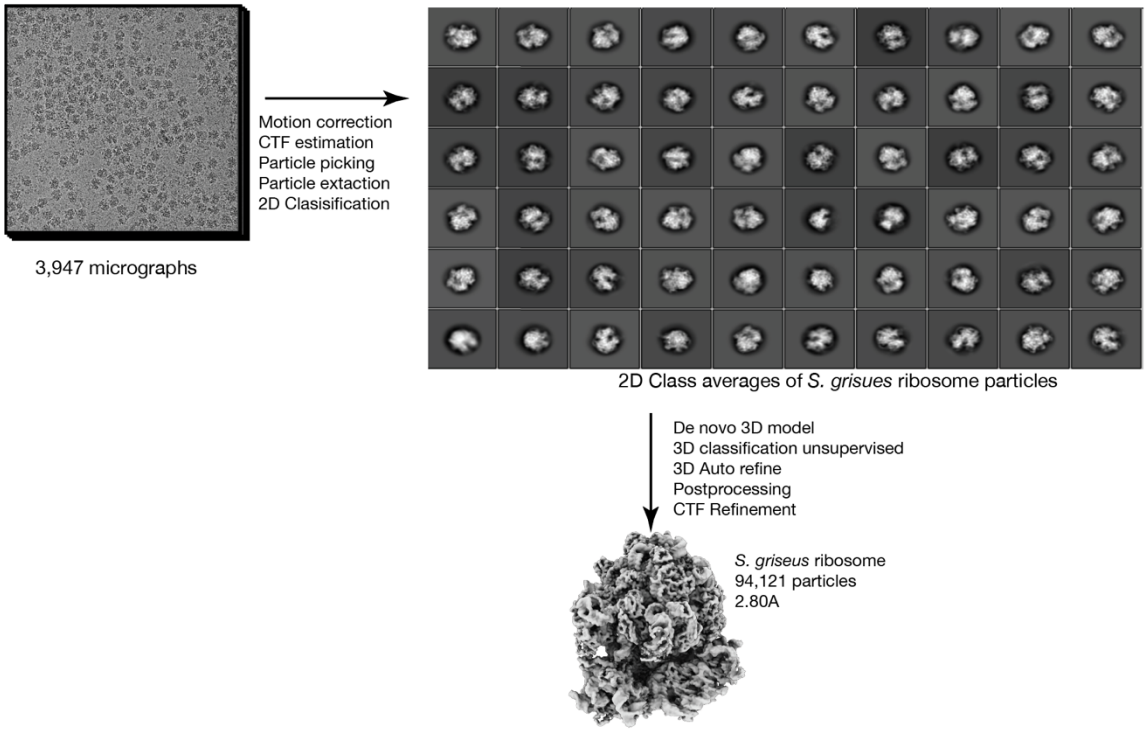

Figure S5.1 | Workflow for processing *S. griseus* cryo-EM dataset on Relion.

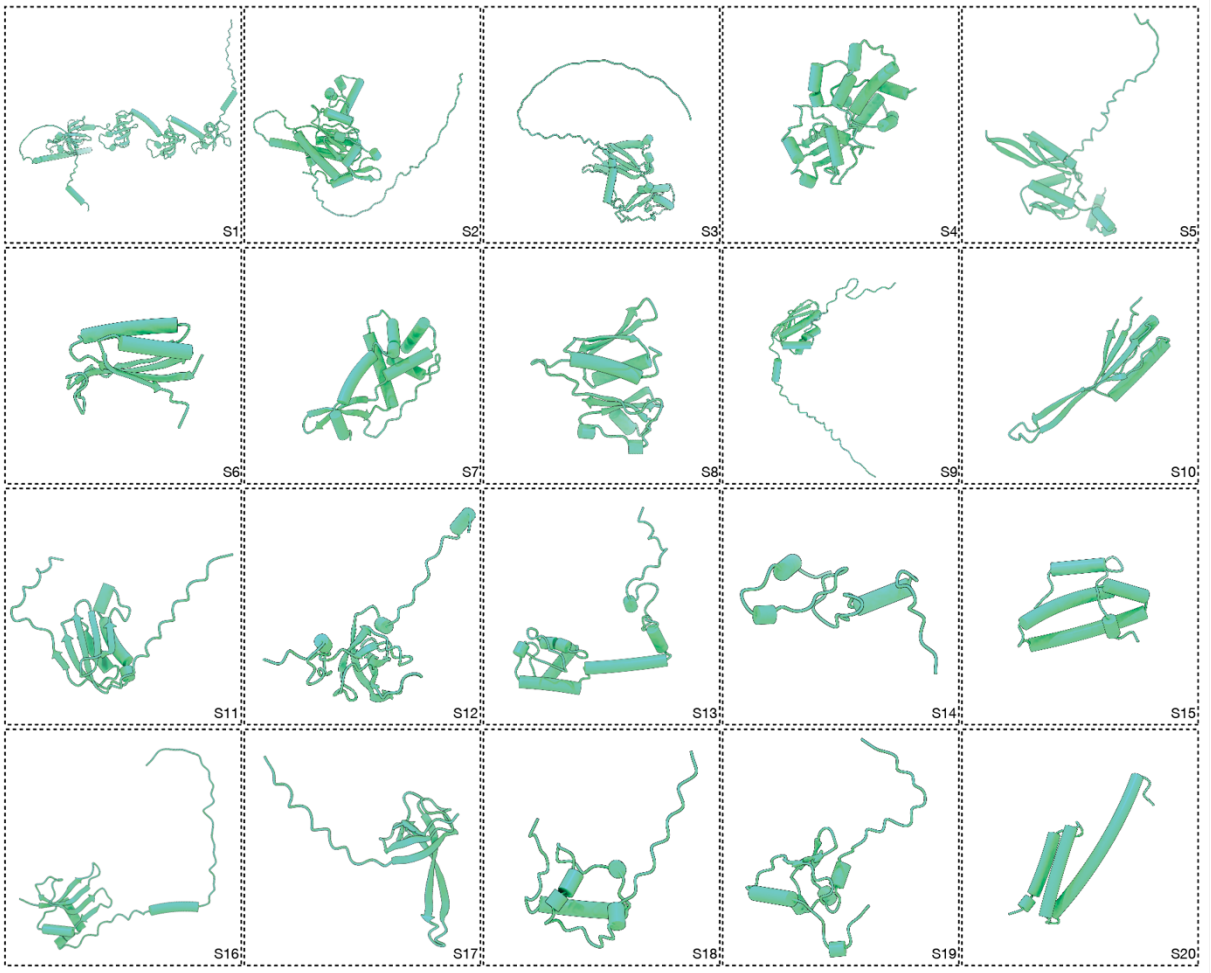

Figure S5.2 | AlphaFold predicted structures of *S. griseus* 30S ribosomal proteins.

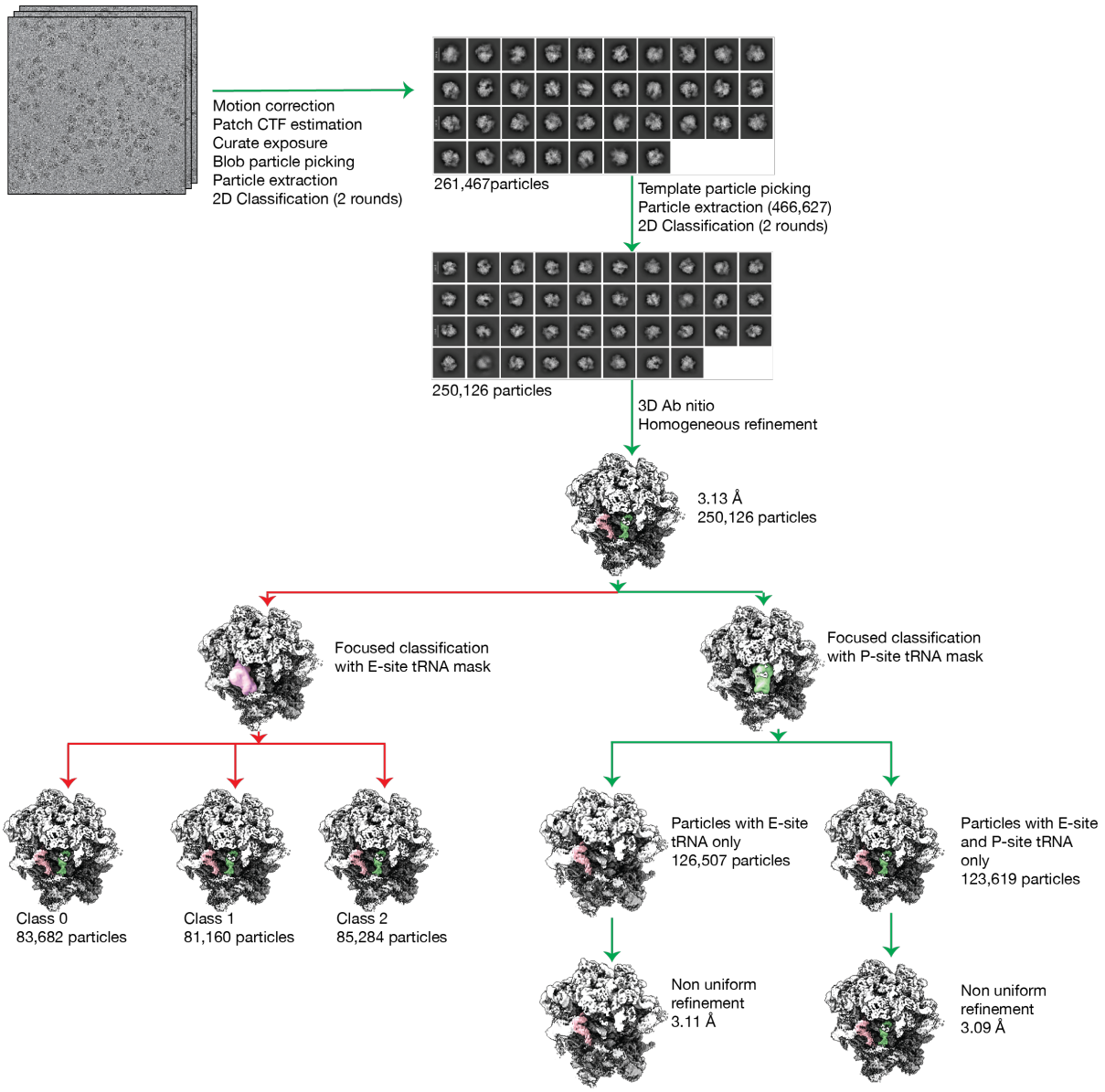

Figure S5.3 | Workflow for processing *S. fradiae* cryo-EM dataset on cryoSPARC.

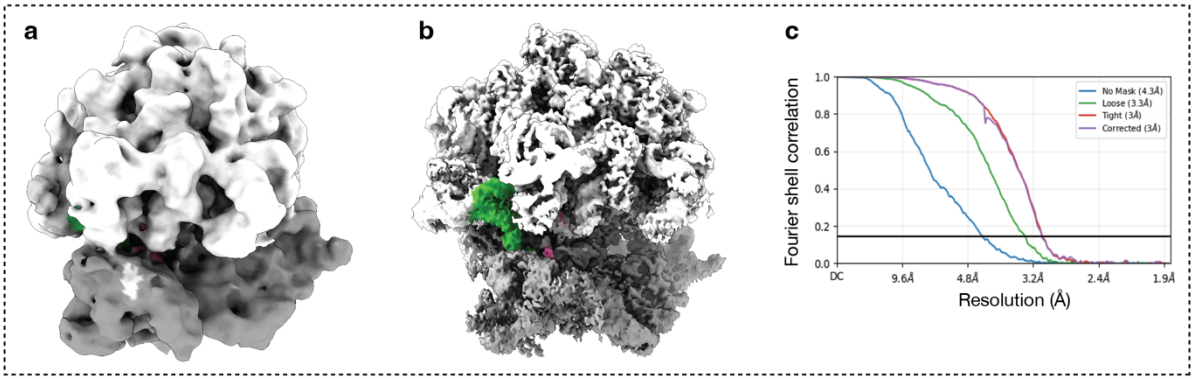

Figure S5.4 | 3D reconstruction of *S. fradiae* ribosome cryo-EM map. (a) 3D initial map of *S. fradiae* ribosome (not sharpened). (b) Homogenous refined map of *S. fradiae* ribosome showing distinct features. (c) FSC plot of the refined map in (b).

Supplementary Table Chapter 5

Table S5.1 | HHMER homolog search for bS22 ribosomal protein. Prior to assessing the taxonomic distributions of bS22 homologs, I implement quality control steps to remove records that are either poorly characterized or those with no taxonomic assignment. This result in a 77% reduction in the number of bacterial phyla bearing apparent homologs of bS22.

Table S5.2 | HHMER homolog search for bL37 ribosomal protein. Prior to assessing the taxonomic distributions of bL37 homologs, I implement quality control steps to remove records that are either poorly characterized or those with no taxonomic assignment. Unlike bS22, bL37 is found only in a few clades in the Actinomycetota phylum thereby suggesting that this ribosomal protein may be an Actinomycetota specific ribosomal protein.

Appendix 4. Publications.

Publication 1. Extensive natural variation in bacterial ribosomal drug-binding sites.

Cell Reports

CellPress
OPEN ACCESS

Article

Extensive natural variation in bacterial ribosomal drug-binding sites

Chinenye L. Ekemezie,[1,3] Lewis I. Chan,[1,3] Charlotte R. Brown,[1] Karla Helena-Bueno,[1] Tom A. Williams,[2,*] and Sergey V. Melnikov[1,4,*]

[1]Biosciences Institute, Newcastle University, Newcastle upon Tyne NE2 4HH, UK
[2]School of Biological Sciences, University of Bristol, Bristol BS8 1TQ, UK
[3]These authors contributed equally
[4]Lead contact
*Correspondence: tom.a.williams@bristol.ac.uk (T.A.W.), sergey.melnikov@newcastle.ac.uk (S.V.M.)
https://doi.org/10.1016/j.celrep.2025.115878

SUMMARY

Ribosomes from certain bacteria possess divergent drug-binding sites compared to those of *Escherichia coli*, leading to natural evasion or hypersensitivity to antibiotics. However, in the absence of systematic studies, it is unknown whether this divergence is rare or common among bacterial species. Here, we address this by reconstructing the evolutionary history of drug-binding residues in bacterial ribosomes. We find that many rRNA residues that are currently viewed as bacterial-specific features of ribosomal drug-binding sites are in fact conserved only in a subset of bacteria. Conversely, species with divergent drug-binding sites are widespread in nature, arising from ancient rRNA polymorphisms at the direct ribosome-drug interface. Using a few bacterial species harboring divergent drug-binding sites, we identify their intrinsic resistance to corresponding ribosome-targeting antibiotics. Overall, we reveal the extensive lineage-specific diversity of ribosomal drug-binding sites, offering a resource for developing more targeted antibiotics and enabling personalized drug selection for specific pathogens.

Publication 2. Evolution of drug-binding residues in eukaryotic ribosomes.

TITLE

Evolution of drug-binding residues in eukaryotic ribosomes

AUTHORS

Lewis I. Chan[1,&], Chinenye L. Ekemezie[1,&], Karla Helena-Bueno[1], Charlotte R. Brown[1], Tom A. Williams[2,*] Sergey V. Melnikov[1,*]

AFFILIATIONS

[1] Biosciences Institute, Newcastle University, Newcastle upon Tyne, NE2 4HH, UK
[2] School of Biological Sciences, University of Bristol, Bristol, BS8 1TQ, UK
[&] Contributed equally

CORRESPONDENCE

* To whom correspondence should be addressed:
tom.a.williams@bristol.ac.uk and sergey.melnikov@newcastle.ac.uk

ABSTRACT

Drugs that target eukaryotic ribosomes are becoming increasingly important as research tools and potential therapies against cancer and pathogenic eukaryotes. However, in the absence of comparative studies, we currently do not know how many eukaryotes possess ribosomal drug-binding sites identical to those in humans, and how many significantly differ from humans. To address this, we traced the evolutionary history of individual ribosomal drug-binding residues from the emergence of eukaryotes to the present day. We found that ribosomal drug-binding sites are divergent across eukaryotic clades, with some of the clades exhibiting more substitutions in their ribosomal drug-binding sites compared to humans than humans do compared to bacteria. Overall, our work provides a resource for understanding the evolutionary divergence of drug-binding sites in eukaryotic ribosomes, which may inform the use of ribosome inhibitors as research tools and lineage-specific drugs against eukaryotic parasites.

frontiers | Frontiers in Microbiology

TYPE Mini Review
PUBLISHED 29 July 2024
DOI 10.3389/fmicb.2024.1436579

OPEN ACCESS

EDITED BY
Jiqiang Ling,
University of Maryland, United States

REVIEWED BY
Michael Benedik,
Texas A and M University, United States

*CORRESPONDENCE
Chinenye L. Ekemezie
✉ c.l.ekemezie2@ncl.ac.uk
Sergey V. Melnikov
✉ sergey.melnikov@ncl.ac.uk

RECEIVED 22 May 2024
ACCEPTED 24 June 2024
PUBLISHED 29 July 2024

CITATION
Ekemezie CL and Melnikov SV (2024) Hibernating ribosomes as drug targets? *Front. Microbiol.* 15:1436579. doi: 10.3389/fmicb.2024.1436579

Hibernating ribosomes as drug targets?

Chinenye L. Ekemezie[1]* and Sergey V. Melnikov[1,2]*

[1]Biosciences Institute, Newcastle University, Newcastle upon Tyne, United Kingdom, [2]Medical School of Newcastle University, Newcastle upon Tyne, United Kingdom

When ribosome-targeting antibiotics attack actively growing bacteria, they occupy ribosomal active centers, causing the ribosomes to stall or make errors that either halt cellular growth or cause bacterial death. However, emerging research indicates that bacterial ribosomes spend a considerable amount of time in an inactive state known as ribosome hibernation, in which they dissociate from their substrates and bind to specialized proteins called ribosome hibernation factors. Since 60% of microbial biomass exists in a dormant state at any given time, these hibernation factors are likely the most common partners of ribosomes in bacterial cells. Furthermore, some hibernation factors occupy ribosomal drug-binding sites – leading to the question of how ribosome hibernation influences antibiotic efficacy, and vice versa. In this review, we summarize the current state of knowledge on physical and functional interactions between hibernation factors and ribosome-targeting antibiotics and explore the possibility of using antibiotics to target not only active but also hibernating ribosomes. Because ribosome hibernation empowers bacteria to withstand harsh conditions such as starvation, stress, and host immunity, this line of research holds promise for medicine, agriculture, and biotechnology: by learning to regulate ribosome hibernation, we could enhance our capacity to manage the survival of microorganisms in dormancy.

KEYWORDS

hibernation, ribosome, ribosome-targeting drugs, dormancy, antimicrobial resistance

Article

A new family of bacterial ribosome hibernation factors

https://doi.org/10.1038/s41586-024-07041-8

Received: 17 February 2023

Accepted: 8 January 2024

Published online: 14 February 2024

Open access

Check for updates

Karla Helena-Bueno[1,12], Mariia Yu. Rybak[2,12], Chinenye L. Ekemezie[1], Rudi Sullivan[3], Charlotte R. Brown[1], Charlotte Dingwall[1], Arnaud Baslé[1], Claudia Schneider[1], James P. R. Connolly[1], James N. Blaza[4,5,6], Bálint Csörgő[7], Patrick J. Moynihan[3], Matthieu G. Gagnon[2,8,9,10]✉, Chris H. Hill[5,6,11]✉ & Sergey V. Melnikov[1]✉

To conserve energy during starvation and stress, many organisms use hibernation factor proteins to inhibit protein synthesis and protect their ribosomes from damage[1,2]. In bacteria, two families of hibernation factors have been described, but the low conservation of these proteins and the huge diversity of species, habitats and environmental stressors have confounded their discovery[3–6]. Here, by combining cryogenic electron microscopy, genetics and biochemistry, we identify Balon, a new hibernation factor in the cold-adapted bacterium *Psychrobacter urativorans*. We show that Balon is a distant homologue of the archaeo-eukaryotic translation factor aeRF1 and is found in 20% of representative bacteria. During cold shock or stationary phase, Balon occupies the ribosomal A site in both vacant and actively translating ribosomes in complex with EF-Tu, highlighting an unexpected role for EF-Tu in the cellular stress response. Unlike typical A-site substrates, Balon binds to ribosomes in an mRNA-independent manner, initiating a new mode of ribosome hibernation that can commence while ribosomes are still engaged in protein synthesis. Our work suggests that Balon–EF-Tu-regulated ribosome hibernation is a ubiquitous bacterial stress-response mechanism, and we demonstrate that putative Balon homologues in *Mycobacteria* bind to ribosomes in a similar fashion. This finding calls for a revision of the current model of ribosome hibernation inferred from common model organisms and holds numerous implications for how we understand and study ribosome hibernation.